SPATIAL AND TEMPORAL PATTERNS OF NITROUS OXIDE AND THEIR RELATIONSHIP TO SOIL WATER AND SOIL PROPERTIES

A Thesis
Submitted to the College of
Graduate Studies and Research
in Partial Fulfillment of the Requirements
for the Degree of Doctor of Philosophy
in the Department of Soil Science
University of Saskatchewan
Saskatoon

By
Thomas Trent Yates

PERMISSION TO USE

In presenting this thesis in partial fulfillment of the requirements for Postgraduate degree from the University of Saskatchewan, I agree that the Libraries of this University may make it freely available for inspection. I further agree that permission for copying of this thesis in any manner, in whole or in part, for scholarly purposes may be granted by the professor or professors who supervised my thesis work or, in their absence, by the head of the department or the Dean of the College within which my thesis work was done. It is understood that any copying or publication or use of this thesis or parts thereof for financial gain shall not be allowed without my written permission. It is also understood that due recognition shall be given to me and to the University of Saskatchewan in any scholarly use that may be made of any material in my thesis.

Requests for permission to copy or to make other use of material in this thesis in whole or part should be addressed to:

Head of the Department of Soil Science
University of Saskatchewan
Saskatoon, Saskatchewan, S7N 5A8

ABSTRACT

Soil N_2O flux is sensitive to soil moisture content and soil temperature, which are in turn sensitive to changes in climate and topography. Thus, N_2O flux measurements exhibit a high degree of spatial and temporal variability. Knowing how the spatial distribution of soil N_2O flux changes over time in a hummocky, agricultural landscape will identify measurement scales appropriate for estimates of N_2O emissions from these types of terrains. As well, little is known about N_2O emissions from uncultivated, ephemeral wetlands in agricultural landscapes, but this information is needed for accurate inventories of N_2O emissions. The objectives of this study were to describe the spatial and temporal distribution of soil N_2O flux in a hummocky agricultural landscape, and to understand how soil water and soil temperature control the spatial and temporal patterns of N_2O flux. For a hummocky, agricultural landscape in the Dark Brown soil zone of Saskatchewan, N_2O flux and related soil variables were measured along a 128-point transect multiple times over two years and concurrently from a 50 point, stratified design over three years. The spatial and temporal variation in N_2O flux followed an event-based / background emission pattern. High flux events were triggered by precipitation events and recession of water from wetlands following spring snowmelt. Days with high mean flux were characterized by highly skewed (reverse J-shaped) distributions. High variance and coherency was observed at cultivated wetland elements during emission events. Strong location-dependent positive relationships were found between soil N_2O flux and water-filled pore space or soil temperature, related to specific landscape elements. Background emissions were characterized by random variation or cyclic behavior that ranged in scale from 20 to 60 m. Cumulative emissions were highest from cultivated wetlands and basin centers of uncultivated wetlands, although emissions from cultivated wetlands were much more important to total cumulative emissions on an area basis. The results indicate that models intended to estimate N_2O flux from these landscapes cannot rely on a single predictive relationship, but will have to incorporate predictive relationships localized at specific landscape elements depending on the time of year. At certain times predictive relationships cannot be used and up-scaled estimates will have to rely on direct measurement of emissions.

ACKNOWLEDGMENTS

It would simply not have been possible to undertake and complete the research required to write this manuscript without the unlimited emotional and financial support of my partner, Colleen, and my son, Rowan and my daughter, Eleanor. I would also like to recognize the unqualified support of my parents, Ed and Ileen Yates and Colleen's parents Gordon and Florence Glen. To all my family I cannot say enough thanks.

I am also very grateful to my advisors Dr. Dan Pennock and Dr. Bing Si. As good friends and mentors they made this experience enjoyable, yet challenging. I would also like to recognize the members of my committee: Dr. Garth van der Kamp, Dr. Richard Farrell, Dr. Reynald Lemke, Dr. Glen Padbury, and Dr. Murray Bentham. The Graduate Chair, Dr. Diane Knight did an excellent job of keeping meetings on track and ensuring that I had the support that I needed to do my work.

Dr. Jeff Braidek and Dr. Angela Bedard-Haughn worked hard to ensure the intensive field program behind the data collection went smoothly. I thank them and the nearly countless technicians and summer students who had to shoulder much of the labour and often in undesirable weather conditions. Of those I would like to mention Angela Taylor, Neil Webb, Darin Richman, Sam Corbett, Wai Ma, Rachel Buhler, Murray Lungal, and Kim Phipps.

Direct financial support for this research was provided by the Biological Greenhouse Gas Sources and Sinks (BGSS) program administered by Agriculture and Agri-Food Canada (AAFC), and by Ducks Unlimited Canada (DUC). Support in the form of in kind contributions and use of the St. Denis site was provided by the Canadian Wildlife Service (CWS). I would like to personally recognize Dr. Rhonda McDougal (DUC) and Dr. Bob Clark (CWS).

TABLE OF CONTENTS

LIST OF TABLES

LIST OF FIGURES

LIST OF ABBREVIATIONS

BC	basin center
BMP	best management practice
CV	concave
CW	cultivated wetland
CX	convex
DF	film thickness
DNDC	DeNitrification and Decompostion
F	flux
GC	gas chromatograph
h	distance between sample locations
HPE	Harr's point estimate
k_t	time constant
LHS	latin hypercube simulation
MCS	monte carlo simulation
MDCD	minimum detectable concentration difference
pdf	probability distribution function
RG	riparian grass
RPE	Rosenblueth's point estimate
RT	riparian trees
S	smooting operator
SP	spherical model
SSE	sum of squared errors
t_0	time zero
TDR	time domain reflectometry
UW	uncultivated wetland
V	chamber volume
W	Kendall's coefficient
W	Wavelet coefficient
W	mean wavelet coefficient
WFPS	water-filled pore space
x	location
z_k	threshold value
Γ	gamma function
γ	indicator semivariogram
η	scaling parameter
μ_p	mean of differences between paired values
π	rectangle function
σ_p	standard deviation of differences between paired values
τ	spatial translation
Ψ	wavelet function

1.0 INTRODUCTION

It has been documented that the content of atmospheric nitrous oxide (N_2O) is increasing (FAO and IFA, 2001; Khalil and Rasmussen, 1992). In addition to contributing to the greenhouse effect, nitrous oxide in the atmosphere is converted to nitric oxide (NO) and NO destroys ozone (Agriculture and Agrifood Canada, 1998a; Rodhe, 1990; Cicerone, 1987). For these reasons there has been considerable concern and research regarding the flux, sources and factors relating to N_2O production.

Soils naturally produce N_2O. Agriculturally managed soils, especially those that receive N fertilizers, produce a significant portion of global N_2O (FAO and IFA, 2001). N_2O emissions also represent an economic loss to the producer in terms of inputs and productivity.

The primary soil processes that produce N_2O are denitrification and nitrification. Nitrous oxide is a by-product of the oxidation of ammonium during nitrification. Denitrification is the reduction of nitrogenous oxides to N_2O and N_2 when the supply of oxygen (O_2) is limited (Tiedje, 1994). A third process of importance is nitrifier denitrification (Wrage et al. 2001; Poth and Focht, 1985).

Many soil characteristics have been identified as factors influencing the process of denitrification and the proportion of N_2O to N_2. Such factors include landscape position (Ambus, 1998; Pennock et al., 1992), water-filled pore space (WFPS) (Davidson and Verchot, 2000; Linn and Doran, 1984), sediment type, land-use and vegetation, N and C availability (Corre et al., 1996), soil moisture (Corre et al., 1996; Parton et al., 1988; Parkin, 1987), inorganic N (Davidson and Verchot, 2000; Skiba et al., 1993), availability of O_2 (Del Grosso et al., 2000; Parkin, 1987; Firestone et al., 1979), soil temperature (Maag and Vinther, 1999; Kliewer and Gilliam, 1995; Parton et al., 1988), particulate organic C (Parkin, 1987), and pH (Tiedje, 1982; Van Cleemput et al., 1976; Yoshida and Alexander, 1970).

This list of factors can be grouped into three categories that represent the most important controls on the production of N_2O from soil: availability of O_2, availability of

N and C, and climate. These controls, and the soil properties that we measure to describe them, interact at different temporal and spatial scales. For example, according to Corre et al. (1996) soil water is a micro-scale control on available O_2, C and N. The distribution of soil water is in turn controlled by topographic redistribution at a landscape scale. Soil texture (geomorphology), land use and climate control topographical-soil relationships at a regional scale (Corre et al., 1996).

Nitrous oxide emissions have high spatial and temporal variability (Groffman et al., 2000; Brumme et al., 1999; Corre et al., 1996). As a result, measurement of N_2O flux at the micro- or landscape scale has been very difficult to extrapolate to the regional scale or from daily to annual periods (Groffman et al., 2000).

Models or algorithms are used to interpolate from micro-scale data to regional-scale estimates of N_2O fluxes (Schimel and Potter, 1995). Because models are used to extrapolate and predict, they are abstractions of reality and prone to error (Schimel and Potter, 1995). Assumptions that are made to facilitate the model may be incorrect and uncertainty may exist in the parameters used (Clausnitzer et al., 1998). Errors may also exist in mathematical functions and computer code (Smith et al., 2002). Hence, it is important to evaluate the uncertainty that surround the use of models (Clausnitzer et al., 1998; Veldkamp and Weitz, 1994).

The objectives of this research were to: a) describe the spatial and temporal distribution of soil N_2O flux in a hummocky agricultural landscape, and b) understand how soil water and soil temperature control the spatial and temporal patterns N_2O flux. Both spatial statistics and landscape segmentation techniques were used to describe the spatial and temporal patterns. Spatial statistics are well suited to describing the relationship between soil N_2O flux and controls such as soil water or temperature. Landscape segmentation techniques are appropriate for making annual estimates of flux and describing the contribution of specific landscape elements to the annual flux.

The highly variable nature of N_2O flux data make the application of spatial statistics challenging. An understanding of the nature of the distribution of N_2O flux data is important to successfully apply the appropriate statistical technique. This issue is dealt with in Yates et al. (2006a) (Chapter 3) of the dissertation. The shapes of the probability distribution functions for the N_2O flux at the site are described, the

relationship between these shapes and the broad environmental controls are established, and the implication of these shapes for spatial statistical analysis is discussed. In Yates et al. (2006b) (Chapter 4) the most appropriate spatial statistical technique, wavelet analysis, was applied to the N_2O data set and the relationship between flux and landscape elements was assessed by wavelets. Wavelet, cross-wavelet and wavelet coherency analysis was used in Chapter 5 to assess the relationship between flux and soil water or soil temperature. Using an alternative sampling design, Chapter 6 presents annual estimates of flux developed for the site, with special emphasis on the contribution of ephemeral ponds to annual emissions.

Although the objectives of the research are addressed in totality by Chapters 3 to 6, and the line of research running through them is coherent, these chapters have been written as stand alone research papers. Each paper contains the appropriate literature review required to set a context for the work and to interpret the results within the paper. Each paper also contains a complete methods and materials section. Thus, there will be a degree of redundancy of information, which is unavoidable when using this format. Steps have been taken to reduce redundancy, such as a combined lists for references and abbreviations and coherency through the thesis is provided by a general literature review in Chapter 2 and a synthesis of results and implications for future research is given in Chapter 7.

The format of the thesis has facilitated the submission and acceptance of Chapters 3 and 4 for publication in a peer-reviewed journal. It is intended that Chapters 5 and 6 follow in the same manner. The advantage of having peer reviewed work in the thesis outweighs any disadvantages this format may present to the reader.

2.0 LITERATURE REVIEW

2.1 Nitrous Oxide as an Environmental Concern

Nitrous oxide (N_2O) is a greenhouse gas with a warming potential that is approximately 296 times that of carbon dioxide (CO_2) over 100 years (IPCC, 2001). It is very effective at trapping radiant energy reflected from the earth's surface, causing the atmosphere to warm and, in turn, the planet (Agriculture and Agrifood Canada, 1998a). Research has demonstrated that the content of atmospheric N_2O is increasing at an approximate rate of 0.8 ppbv yr^{-1} (Khalil and Rasmussen, 1992) and estimates of the atmospheric lifetime of N_2O are in the order of 150 years (Agriculture and Agrifood Canada, 1998a). In addition to contributing to the greenhouse effect, N_2O is a natural regulator of the production of ozone. Nitrous oxide is photo-oxidized in the stratosphere to NO, which consumes ozone in a catalytic reaction (Cicerone, 1987).

The anthropogenic sources of N_2O include the burning of fossil fuels, industrial processes and agriculture, but it is agriculture, particularly the use of mineral fertilizers that is considered the most important of these (FAO and IFA, 2001). Up to 70% of N_2O emissions due to human activity come from agriculture (Agriculture and Agrifood Canada, 1998a). Globally, natural soils are the chief source of N_2O (FAO and IFA, 2001). It is estimated that soils were responsible for emitting 69.7 Gg of N_2O in 1996, or approximately 50% of the N_2O emissions due to agricultural practices in Canada. The majority of this soil N_2O production came from the Prairie Provinces with Saskatchewan producing the most (Agriculture and Agrifood Canada, 1998a).

An increase in the atmospheric greenhouse gas content is believed to drive radiative forcing, creating an imbalance in the climate system of which one result is an increase in surface and lower-atmosphere temperatures (IPCC, 2001). For this reason alone, N_2O is an environmental concern. Globally, not enough is known about the distribution and magnitude of N_2O sources (FAO and IFA, 2001). It is especially important to collect information on N_2O emissions from Saskatchewan soils because of

the concentration of agricultural land in this province. Overall, such information is lacking (Corre et al., 1999).

2.2 Soil Processes Important to the Production of Nitrous Oxide

Nitrification and denitrification are two microbially mediated processes that are responsible for the production of N_2O in soil. Nitrous oxide is also produced through the abiotic process of chemodenitrification (Broadbent and Clark, 1965) and through nitrifier denitrification (Wrage et al., 2001; Poth and Focht, 1985; Castignetti and Hollocher, 1982). Biotic denitrification can be sub-divided into respiratory denitrification and non-respiratory denitrification although the bulk of N_2O produced by denitrification is respiratory (Tiedje, 1988). There are also two forms of nitrate reduction to ammonium that influence the availability of NO_3^- for denitrification.

2.2.1 Denitrification

Denitrification is any process that reduces nitrogenous oxides such as NO_3^- and NO_2^- to N_2O or N_2 (Knowles, 1981; Tiedje, 1988). Respiratory denitrification is the biological process that is usually referred to when the term denitrification is used (Tiedje, 1988). When O_2 is not available, nitrogenous oxides (Reaction 2.1) are used as electron acceptors and reduced in an energy conservation process known as electron transport phosphorylation (Tiedje, 1982).

$$NO_3^- \rightarrow NO_2^- \rightarrow NO \rightarrow N_2O \rightarrow N_2 \qquad [2.1]$$

Such a process allows aerobic microorganisms to function in an anaerobic environment (Knowles, 1981). From equation 2.1 the level of NO_3^- would be expected to be rate limiting and an important control on denitrification (Knowles, 1981).

Non-respiratory denitrification is the reduction of NO_3^- or NO_2^- to N_2O but not N_2 by processes that are not yet understood (Tiedje, 1988). A variety of organisms, including both aerobes and anaerobes, appear to possess this ability. The process can occur in drier soils than respiratory denitrification (Tiedje, 1994). However, this process is not considered to be significant as a source of N_2O (Tiedje, 1988).

Assimilatory and dissimilatory nitrate reductions are microbial processes that reduce NO_3^- to NH_4^+. This process provides a higher capacity for electron acceptance

per molecule than does the reduction of NO_3^- to N_2O. This may be an advantage in an environment that is poor in electron acceptors (low NO_3^-). Both processes produce $NH_4^+$and minimize the production of N_2O by conserving N (Tiedje, 1988); however assimilatory reduction is regulated by the supply of NH_4^+, whereas dissimilatory reduction is regulated by the supply of O_2.

2.2.2 Nitrification

Nitrification is the oxidation of ammonium (NH_4^+) and is a process carried out by chemoautotrophic bacteria for the purpose of obtaining energy (Schmidt and Belser, 1994). Nitrification is a two-step process whereby NH_4^+ is oxidized to nitrite (NO_2^-) by one group of nitrifying bacteria, and NO_2^- is oxidized to nitrate (NO_3^-) by a second group (Schmidt and Belser, 1994). Nitrous oxide is a byproduct of the first step (Reaction 2.2).

$$\begin{array}{ccccc} NH_4^+ & \rightarrow & NH_2OH & \rightarrow & NO_2^- \rightarrow NO_3^- \\ & & \downarrow & & \\ & & N_2O & & \end{array} \qquad [2.2]$$

The supply of available N and C, as well as O_2 is considered limiting to the activity of nitrifiers (Schmidt and Belser, 1994). Skiba et al. (1993) found that low soil water content (18% dry wt.) favored production of N_2O by nitrification and that an increase to a water content of 20.4% dry wt. favored production of N_2O by denitrification.

2.2.3 Nitrifier Denitrification

Although some studies have concluded that nitrification can produce a significant portion of the total N_2O measured (Ambus, 1998; Koops et al., 1997), other researchers have felt that most of the N_2O attributed to nitrification is actually produced by nitrifier denitrification (Wrage et al., 2001; Poth and Focht, 1985). Nitrite produced during the oxidation of NH_4^+ may be reduced rather than being further oxidized to NO_3^-. This reduction may proceed to the formation of both N_2O and nitrogen gas (N_2) as occurs during denitrification (Reaction 2.3).

$$NH_4^+ \rightarrow NH_2OH \rightarrow NO_2^- \rightarrow NO \rightarrow N_2O \rightarrow N_2$$
$$\downarrow \qquad [2.3]$$
$$N_2O$$

Castignetti and Hollocher (1982) recognized the production of denitrification enzymes by a heterotrophic nitrifier. However, unlike nitrification, this process occurs under low O_2 conditions (Wrage et al., 2001). Koops et al. (1997) felt that in addition to low O_2, nitrifier denitrification also becomes important under low available NO_3^-. Poth and Focht (1985) rejected nitrification as a significant source of N_2O, and attributed N_2O production to nitrifiers performing denitrification.

2.2.4 Chemodenitrification

Chemodenitrification is the generation of nitrogen gas products through reactions that are mediated non-biologically (Knowles, 1981). Chemodenitrification involves the chemical decomposition of nitrous acid (HNO_2) or reaction of HNO_2 with amino acids, ammonia, urea and other soil constituents such as metal ions. The process occurs primarily, but not necessarily, at low pH values (5 or less). NO, N_2O and N_2 have been reported as products of chemodenitrification and of these NO is most abundant (van Cleemput et al., 1976). Overall, chemodenitrification is not considered to be an important form of denitrification (Tiedje, 1988; Robertson and Tiedje, 1987), and hence not an important source of N_2O. However, fertilizer or urine inputs in grazed areas may lower soil pH and cause significant chemodenitrification in the short term.

2.3 Proximal Controls on the Production of Soil Nitrous Oxide

Factors that control the production of soil N_2O can be thought of as either proximal (local) or distal (non-local) (Robertson, 1989). A proximal factor controls N_2O production at a process level. Proximal controls are in turn regulated by factors that operate at a broader scale. These are distal controls.

The previous section indicates that the level of available O_2, mineral N, and available C are strong proximal controls on the microbial processes responsible for soil N_2O emissions. Soil moisture and soil temperature are factors that act as direct controls

on microbial activity, and indirectly on O_2 supply and C & N dynamics. Microbial activity is also influenced by pH and pH is also a control on chemodenitrification.

2.3.1 Oxygen and Soil Water Content

Considering that O_2 is the preferred electron acceptor in the process of electron transport phosphorylation, the level of O_2 in the soil should determine how readily nitrogenous oxides are selected and reduced as electron acceptors in the process of denitrification. Studies have found that increases in soil O_2 result in a decline in total denitrification (Letey et al., 1980; Firestone et al., 1979) or that limited O_2 corresponds to increased N_2O production or denitrification activity (McKenney et al., 2001; Renault and Stengel, 1994; Broadbent and Stojanovic, 1951). Where O_2 is not limiting, denitrification is suppressed and any N_2O produced is related to nitrification (Parton et al., 1988; Robertson and Tiedje, 1987).

The availability of O_2 at a particular point in the soil is determined by the rate at which O_2 can diffuse to that point and the rate at which the O_2 is consumed by microbial activity (Tiedje, 1988). The O_2 status of a soil is difficult to measure in the field so availability of O_2 has usually been assessed by surrogate measurements such as water-filled pore space (WFPS) (Maag and Vinther, 1999; Linn and Doran, 1984), soil moisture content (Koops et al., 1997; Skiba et al., 1993), or air-filled porosity (Letey et al., 1980). Presence of water in pore spaces or as films on soil aggregates slows diffusion of O_2 (Renault and Stengel, 1994). Microbial activity will increase with soil water content until diffusion of O_2 is restricted and the environment becomes anaerobic (Linn and Doran, 1984). Thus, soil water content is a control on denitrification and nitrification.

Davidson and Verchot (2000) observed that nitrification occurs up to a WFPS of 60%. At WFPS greater than 60% denitrification becomes dominant (Lemke et al., 1998). At high values of WFPS (>80%) O_2 diffusion may be restricted to the point where the product of denitrification is primarily N_2 (Veldkamp et al., 1998). Under these conditions, N_2O is itself used as an electron acceptor and reduced to N_2. Robertson and Tiedje (1987) concluded that denitrification can act as a sink as well as a

source of N_2O because they also observed that when the level of O_2 was low, N_2O was denitrified to N_2.

2.3.2 Soil Temperature

A positive correlation between soil temperature and N_2O evolution has been observed (Maag and Vinther, 1999; Kliewer and Gilliam, 1995). Anderson and Boswell (1964) found that nitrification was limited until the soil temperature reached 4 °C. Soil temperature directly controls denitrification through its control on activity of denitrifiers. It is also indirect in that an increase in soil temperature and an accompanied increase in microbial activity will, in turn, increase the consumption of O_2, creating anaerobic micro-sites and spurring denitrification (Maag and Vinther, 1999). Temperature also influences the solubility of O_2 in water and the diffusion of O_2 to micro-sites of denitrification activity (Renault and Sierra, 1994).

The interaction of soil temperature and N_2O production is not widely studied and detailed field measurements are rare. The influence of temperature is often assessed by monitoring seasonal changes in emissions and air temperature (Groffman et al., 2000; Corre et al., 1996). Indirectly, soil temperature can be related to an increase in N_2O emissions during spring thaw from saturated soil layers (Nyborg et al., 1997). The saturated soil layer develops from the inability of the unfrozen soil water to infiltrate the frozen soil layer below (Hayashi et al., 2003).

2.3.3 Available C and N

Although C is an electron donor and nitrogenous compounds are electron acceptors in the process of denitrification, the relationship between available C and N, and N_2O emission is complicated. This is borne out by numerous studies that have been undertaken to clarify this relationship and the range of conclusions that are drawn, sometimes contradictory. For example, Bowman and Focht (1974) found denitrification rates to be dependent upon NO_3^- concentration; however, Linn and Doran (1984) did not observe any relationship between NO_3^- levels and N_2O emissions, although they did find a relationship between soluble organic C and N_2O emissions as did Stanford et al. (1975). Tiedje (1988) and Myrold and Tiedje (1985) suggest that N supply will have an

effect on emissions in a soil that has a low concentration of NO_3^-. Thus NO_3^- concentration exerts a control on N_2O emissions where it is limiting and less or no control where NO_3^- is not limiting. Corre et al. (1996) found that C and N availability became important to N_2O emissions only when soil moisture conditions were favorable for denitrification (i.e., availability of O_2 was restricted).

Availability of N is commonly assessed by measurement of soil mineral N levels (Del Grosso et al., 2000; Drury et al., 1998; Firestone et al., 1979). The importance of C has been assessed through a measure of bio-available C such as soluble organic carbon (Drury et al., 1998; Burford and Bremner, 1975), extractable (glucose equivalent) C (Stanford et al., 1975) and total organic C (Burford and Bremner, 1975; Stanford et al., 1975). Measurements of available N and C typically access discrete nutrient pools and fail to account for N and C cycling. A better understanding of N and C cycling in agricultural and natural systems may improve our understanding of N and C available for N_2O processes.

2.3.4 Soil pH

Soil pH has been occasionally cited as an influencing factor on N_2O production or denitrification (Knowles, 1981; Firestone et al., 1980; Stevens and Laughlin, 1998). It is also linked to chemodenitrification, which occurs at a pH below 5 (Tiedje, 1994). Firestone et al. (1980) observed that pH did not influence N_2O production until NO_3^- levels were not limiting. Stevens and Laughlin (1998) noted that the influence of pH was small compared to WFPS, but it did have an effect on the mole fraction of N_2O. The mole fraction of N_2O decreased with an increase in pH. Van Cleemput and Patrick (1974) found that the reduction of NO_3^- increased with increasing pH.

2.4 Distal Controls on the Production of Soil Nitrous Oxide

A landscape includes both the topography and geomorphology (landform), and the human activity within the landscape (land use) (D.J. Pennock, personal communication, 2004). Geomorphology includes soil characteristics such as soil texture, which in turn influences soil structure. Landscapes are an indirect control on

soil N_2O emissions through the control landscapes have on soil water distribution, C and N dynamics, soil mineralogy, and soil texture and structure.

2.4.1 Landform

A landform pattern of N_2O emissions has been observed by many authors in different regions for example, Ambus (1998), Corre et al. (1996), Ambus and Christensen (1994), and Pennock et al. (1992). Ambus and Christensen (1994) observed that production of N_2O from a depression was four fold that of the upland area associated with the depression. This was also noted by Ambus (1998) and in both studies the increased production of N_2O in depressional areas was attributed to the presence of wetter soils due to slower drainage. Pennock et al. (1992) noted that topography indirectly influenced the spatial distribution of denitrification by its direct control on the redistribution of water and its concentration in low areas. Corre et al. (1996) observed that foot-slope elements had a proportionally higher (72%) number of N_2O producing micro-sites (hotspots) compared to shoulder elements (28%). Corre et al. (1996) concluded that the spatial distribution of N_2O emissions was closely related to landscape and its control on the micro-scale distribution of moisture.

2.4.2 Land-use

Land-use can be broadly divided into non-agricultural (natural systems) and agricultural activities, and the latter can be broken into numerous categories based on tillage system, applied fertilizers, and crop rotation. Numerous research studies have addressed the N_2O production from these various land-uses finding differences generally explained by the affect the land-use has on the moisture, C and N status of the soil (Izaurralde et al., 2004; Rozas et al., 2001; Corre et al., 1999; Lemke et al., 1999; Drury et al., 1998; Mackenzie et al., 1997; Groffman, 1984; Linn and Doran, 1984).

Pasture and hay land, that is unfertilized, has been found to contribute significantly less N_2O to regional fluxes, when compared to fertilized cropped land (Corre et al., 1999). Izaurralde et al. (2004) found natural areas to have low emissions compared to agricultural areas. Mackenzie et al. (1997) and Linn and Doran (1984) found no- or zero-till systems to have higher N_2O production conventional tillage

systems. In contrast, Lemke et al. (1999) found that conventional tillage produce equal or higher emissions, compared to zero-till, especially during the spring snowmelt period.

Application of N fertilizer generally increases N_2O emissions compared to a non-fertilized soil (Drury et al., 1998). The increase in N_2O emissions arising from the use of N fertilizer is more of a function of the excess N (after crop uptake) than it is of the rate of N applied (Drury et al., 1998). Groffman (1984) found differences in nitrification and denitrification activity to be related to the distribution of crop residue in the soil profile between conventional tillage and no-till systems. Rozas et al. (2001) found that the denitrification rate was higher when fertilizer was applied at planting than if applied at the six-leaf stage. Greater evapotranspiration by the advanced crop maintained a lower soil moisture content and limited denitrification, in addition to reducing excess N.

2.4.3 Hydrology of Ephemeral Wetlands

A hummocky terrain is characterized by the absence of a well developed drainage system due to the presence of numerous closed basins (van der Kamp and Hayashi, 1998). The wetlands and their catchments are considered to be hydrologically closed in that they do not have permanent inflow or outflow (Parsons et al., 2004). The temporary pooling of water in these basins is responsible for the development of the semi-permanent or ephemeral wetlands. The source of water that collects in these depressions is primarily derived from the melting of snow that accumulates over winter in the uplands (catchment) and wetland areas of the basin.

Lissey (1968) referred to water movement in these closed basins or potholes as depression-focused recharge. Such descriptions refer to a general hydrological model whereby water is gained through run off from snow melt and summer precipitaion, and lost by evapotranspiration and seepage (van der Kamp et al., 1999; Lakshman, 1971). Basins in the Prairie Pothole Region have been classed as recharge, discharge or flow-through on the basis of the net movement of groundwater (Richardson et al., 2001). The majority of wetlands at the St. Denis site can be classed as recharge wetlands with small vertical and large lateral infiltration components. It is rare that water is lost as runoff from these basins (van der Kamp et al., 1999).

The basic water balance for the closed recharge basin is based on snowmelt and summer precipitation as the water sources. Early spring snowmelt runs off into the depressions and is the primary source of water for the wetland. Summer precipitation extends the life of the ephemeral ponds. Water loss from the closed basins is almost entirely by evapotranspiration and net evaporation declines over the summer months with the reduction in evaporative surface area as water level declines (Laksham, 1971). Some water infiltrates beneath the pond as vertical recharge to groundwater and aquifers at depth. However, most infiltration occurs through the soils at the margins of the pond as lateral recharge where it discharges and is evapotranspired by the vegetation surrounding the pond and in the upland soils surrounding the pond (Hayashi et al., 1998a). Parsons et al. (2004) found that infiltration (lateral and vertical) accounted for 70% of water loss from the pond, with the lateral infiltration dominant over the vertical recharge. Most of this appears to be driven by root uptake as infiltration in the ponds was observed to be highest during the afternoon when plants are transpiring (Hayashi et al., 1998b).

Groundwater beneath ponds has been observed to rise dramatically during May due to input of spring snow melt (Laksham, 1971). Groundwater beneath the wetland rises and forms a groundwater mound with the pond as the surface representation of this mound (Parsons et al., 2004; Miller et al., 1985; Meyboom, 1966). Later in season, the groundwater mound flattens due to the lateral as well as the vertical flow (Miller et al., 1985). This lateral flow has been observed to occur to a maximum of 5 m depth; below this the flow is basically vertical (Zebarth et al., 1989).

Shjeflo (1968), Laksham (1971) and Hayashi et al. (2003) observed similar patterns in groundwater and pond water level changes. Increases in pond water level in the spring are generally rapid as a result of the snow melt runoff. Declines in pond levels are comparatively slower and result from evaporation and seepage. The storage capacity of some depressions was exceeded only in years of excessive snowmelt runoff and in these years the majority of the depressions still retained all the water without overflowing. Rise in groundwater level and recession of pond water level in spring probably coincides with the disappearance of the frost layer.

Hayashi et al. (2003) observed that overland flow during summer only occurred during unusually intense storms with heavy precipitation. These only occur every few years at the St. Denis research site. van der Kamp et al. (2002) noted that precipitation in the fall (Sep. – Nov.) is generally too light and the soil too dry to generate runoff.

Evapotranspiration in summer depresses the water table directly below the tree ring creating a trough in the water table. This is thought to cause a reversal in the flow such that it moves towards the pond center instead of away from it (Meyboom, 1966). However, this flow to pond center does not actually act as recharge to the wetland because the water table trough beneath the pond margin intercepts this water and it is evapotranspired (Rosenberry and Winter, 1997). Meyboom (1966) also observed that a second trough or cone of depression forms later in summer after the pond has dried and plants populate the pond area. The evapotranspiration in the pond area effectively shuts down the already diminished recharge from the wetland and it is not until the following spring that a new groundwater mound forms and recharge to the groundwater is again significant.

2.4.4 Soil Texture and Structure

Soil texture and structure determines the pore system, and this is important for water movement (Fitzpatrick, 1986) and hence the changes in WFPS. Thus, size, connectivity or tortuosity of pores is a control of the occurrence and duration of saturated soils, and this controls periods of restricted O_2 diffusion. The % of WFPS that is required to restrict diffusion of O_2 and trigger denitrification will vary depending on the texture of the soil. For example, Del Grosso et al. (2000) found that an intact clay soil became anoxic at a lower % WFPS than an intact loam soil.

Aggregate size is a factor in the aerobic status of sites of microbial activity. Renault and Stengel (1994) modeled aggregate size and found that for a given microbial respiration rate, the aerobic volume fraction of an aggregate decreases as the radius of the aggregate increases. This is also exacerbated by the presence of water. Renault and Stengel (1994) found that small aggregates remained aerobic until saturated, but large unsaturated aggregates tended to have an anaerobic center.

2.4.5 Climate and Weather

Seasonal changes in precipitation and temperature is a control on the input of water into the landscape and its loss through evapotranspiration. In this manner, climate is a control on the soil moisture status and availability of C and N (Groffman et al., 2000). An example of this would be the increase in soil organic matter across the prairie region as mean annual precipitation increases. Groffmann et al. (2000) observed that N_2O flux patterns across ecosystems were similar to patterns of C and N across the same areas.

Local changes in precipitation, i.e., weather, can cause short-term changes in N_2O flux. Mosier et al. (1981) observed that N_2O flux increased after precipitation events that cause short-term increases in soil water content. Mosier et al. (1981) felt that the changes in soil water that they observed were not enough to trigger denitrification. Thus the magnitude of a precipitation event can be a determining factor in what process will produce the N_2O and the magnitude of the flux.

2.5 Spatial Scales of Soil Nitrous Oxide Emission

Blöschl and Sivapalan (1995) discuss the concept of scale and state that there is more than one definition depending on if one is referring to the scale of the process, the scale of the observation (measurement), or the scale of the model (estimate). The scale is the time or distance that is characteristic to the process, observation or model. Spatial variability in trace gases such as soil N_2O is expressed over a range of spatial scales.

Schimel and Potter (1995) state that N_2O forming processes occur at a scale less than one centimeter (i.e., micro- or process scale). So, we tend to measure N_2O emissions at scales that are larger than the micro scale, such as over several cm's to 100's of meters (Schimel and Potter, 1995). For example, a measurement at a single point (point scale) could be a chamber measurement with a footprint of 12 cm or a micrometerological measurement with a footprint of 12 m. The intent is to make point-scale measurements that are reflective of the micro-scale process and extrapolate these measurements to a regional or global scale. Even so, variability at the point scale has been observed to be high (Foloronso and Rolston, 1984) and has been attributed to the patchy distribution of denitrification activity or hotspots in soil (Ambus and Christensen,

1994; Parkin, 1987). The result is that soil N_2O flux at the scale of the observation displays a high degree of spatial and temporal variability (Parton et al., 1988; Parkin, 1987; Folorunso and Rolston, 1984). Coefficients of variation have been observed to be as high as 500% (Folorunso and Rolston, 1985). Thus, predictive relationships between N_2O flux and controlling variables have been difficult to define (Corre et al., 1996).

Up-scaling of N_2O emission data to local (1 to 100 km) or regional scale (100 to 1000 km) from the point scale may be best achieved using an intermediary scale, such as the field scale (100 to 1000 m). Thinking in terms of landscape offers the ability to partition the field into units defined by landform (topographic attributes) and land-use. Corre et al. (1996) considered topography to directly control the distribution of hydrological or pedological factors that affect the N_2O forming processes at the micro-scale (O_2, C and N status). The uncertainty that exists at the landscape, i.e., field scale, can be further defined because the landscape can be broken into elements that are appropriate to the variability of the controlling factors. Meaningful selection of the sampling units (landforms) will allow the up-scaling of flux measurements collected at points within the units (Corre et al., 1996).

2.6 Temporal Variation of Soil Nitrous Oxide Emission

Variation in soil N_2O emission can also be expressed over range of temporal scales. Emissions vary over minutes, hours, days, seasons, and years. Derwent et al. (1999) relates specific temporal scales and spatial scales; for example, point-scale measurements would be expected to have small-scale temporal variation (e.g., minutes, or hours) compared to temporal variation in global scales (e.g., years or decades).

Brumme et al. (1999) observed distinct temporal patterns at different scales. They viewed overall N_2O flux as the combination of a steady background flux due to factors that do not change over the long term (such as soil acidity, nutrient status or mean annual climate) and short-term, peak fluxes due to events such as rainfall or freeze/thaw cycles. Short-term precipitation events can quickly increase soil water content to the threshold required for denitrification to occur (Sexstone et al., 1985). An increase in emissions associated with these short-term events usually occurred after a lag time of one or two hours and return to normal after approximately 12 h (Sexstone et al.,

1985). The lag time appeared to be controlled by soil texture, as soils with more clay content had comparatively poor infiltration compared to lighter soils and took longer to initiate N_2O emissions.

Corre et al. (1996) observed a correlation between N_2O emissions and the pattern of seasonal precipitation. High N_2O fluxes occurred in spring and early summer, when rainfall was more frequent. As summer progressed into fall, precipitation decreased as did N_2O emissions. Clearly, more frequent rainfall events leads to more occurrences of the conditions that are responsible for increases in N_2O flux, such as saturated soils and denitrification.

Both Lemke et al. (1998) and Corre et al. (1996) observed a strong pulse of N_2O during spring thaw even though soil temperatures were near freezing. This may have been due to the release of N_2O that accumulated beneath the frozen soil during winter or the combination of saturated soils and high available N in thawed soil immediately above the frozen layer. Saturated soil with a ready source of available N would lead to high microbial activity in an O_2 limited environment, and these are good conditions for denitrification. Lemke et al. (1998) also noted that the period from spring thaw until mid July was most active in terms of N_2O emissions. Reduced precipitation after mid-July and low NO_3^- lead to lower emissions. Spring thaw and early summer appear to be the most critical periods regarding detection of N_2O emissions in the Western Canadian Prairie region.

2.7 Soil Nitrous Oxide Emission Models and Uncertainty Analysis

Up-scaling of fluxes of N_2O requires that we interpolate the results from the scale at which the data is collected to the scale at which we want to interpret it (Schimel and Potter, 1995). In other words a regional estimate of N_2O emission requires measurements made at a point scale, possibly stratified or aggregated using landscape or field-scale units and extrapolated or up-scaled to the regional scale. Up-scaling of emission measurements can be achieved in a number of ways such as the measure and multiply approach (Schimel and Potter, 1995) used for spatial up-scaling and interpolation between sampling dates for temporal up-scaling (Pennock et al., 2005). More sophisticated methods of up-scaling include the use of models or sets of

algorithms that mathematically simulate the soil processes that produce N_2O emissions using the data collected at the micro-scale. Models for trace gas flux estimations are primarily empirical or mechanistic or some combination of the two types (Schimel and Panikov, 1999). Empirical models rely on regression equations using climatic parameters. Mechanistic models try to simulate real soil and atmospheric processes. Linking models to a GIS database has been used to up-scale model estimates from both types of models (Butterbach-Bahl et al., 2004).

Uncertainty in soil nitrous oxide emission measurements or estimates involves an objective, quantitative analysis of the variability in those values (Derwent et al., 1999). There are many sources of uncertainty. Spatial and temporal variability in soil N_2O emissions coupled with measurement and sampling errors results in substantial uncertainty in regional or global estimates (Lapitan et al., 1999). As well, models and algorithms typically rely on assumptions. These assumptions and variability in input data leads to uncertainty in model output (Veldkamp and Weitz, 1994).

Up-scaling results in increased uncertainty (Derwent et al., 1999). Uncertainty is considered lowest at the point scale because the measurement unit and the measurement itself are at the same scale. As the scale of measurement unit increases uncertainty increases because the spatial variation becomes more complex. This uncertainty can be reduced by including additional information at each scale (Derwent et al., 1999) such as increasing the density of point measurements to capture the increased spatial or temporal variability. An alternative would be to stratify spatial or temporal units at a scale that represents discrete ranges of variability. O'Neill (1988) refers to this as the coherent level where predictive power is maximized.

Methods used for uncertainty analysis involve the creation of a probability density function (pdf) for each input variable. The models are run repeatedly using input data sampled at random from the pdfs. Confidence intervals about the flux estimates serve as the measure of uncertainty. Yu et al. (2001) evaluated four methods of uncertainty analysis: Monte Carlo Simulation (MCS), Latin Hypercube Simulation (LHS), Rosenblueth's Point Estimation (RPE) and Harr's Point Estimation (HPE). The difference between these methods is in the sampling mechanism for drawing values from the pdf's and the sample size required to obtain the range of variance in the model

output (Yu et al., 2001). Yu et al. (2001) used MCS as the standard in their study and found MCS and LHS to produce similar results but LHS required fewer samplings, and thus was considered more efficient. RPE and HPE had wider confidence intervals around the estimated mean N_2O flux compared to MCS and LHS.

Understanding the uncertainty surrounding both measurements and estimates will aid in their reduction and improve our ability to validate model predictions. Currently, comprehensive data on N_2O emissions that includes a wide variety of regions over extensive time periods is not available to adequately validate model estimates (Butterbach-Bahl et al., 2004).

3.0 PROBABILITY DISTRIBUTION AND SPATIAL DEPENDENCE OF NITROUS OXIDE EMISSION: TEMPORAL CHANGE IN HUMMOCKY TERRAIN

3.1 Preface

The most common observation regarding soil N_2O flux is that it is highly variable in space and time, and that soil N_2O data is characterized by skewed probability distributions. What is seldom investigated or reported is the actual shape of these distributions. Does the distribution change over time? What factors are responsible for this change? It is generally agreed that soil N_2O flux is sensitive to environmental factors such as soil moisture and soil temperature that change constantly, yet few have speculated on what changes in these factors will mean to the distribution shape of soil N_2O data over time. The data collected at the St Denis Wildlife Area is an excellent opportunity to explore such data at its basic level and fill in this knowledge gap.

3.2 Introduction

Nitrous oxide (N_2O) is a greenhouse gas with a 100-year global warming potential of approximately 296 times that of carbon dioxide (CO_2) and the level of atmospheric N_2O is estimated to be increasing at a rate of 0.8 ($\pm$ 0.2) ppb yr^{-1} (IPCC, 2001). It is estimated that up to 70% of anthropogenic emissions come from agricultural activities (Agriculture and Agri-Food Canada, 1998a) with the soil identified as the chief source (FAO and IFA, 2001).

Respiratory denitrification is considered the dominant source of soil N_2O emissions (Tiedje, 1988). However, soil N_2O emissions are also produced as a by product of nitrification (Skiba et al., 1993). The availability of oxygen (O_2), carbon (C) and nitrogen (N) are important process-level controls on the production of N_2O in the soil (Robertson, 1989). Oxygen has a major influence on the synthesis and activity of reductive enzymes (Tiedje, 1988) and denitrification occurs in anaerobic soil microsites

or hotspots (Parkin, 1987). Anaerobic conditions depend on the rates of O_2 diffusion versus consumption (Tiedje, 1988). The diffusion of O_2 is slowed by the presence of water in soil pores and as films on soil aggregates (Renault and Stengel, 1994), and denitrification becomes the dominant process producing N_2O when water-filled pore space (WFPS) exceeds approximately 60% (Lemke et al., 1998; Davidson and Verchot, 2000). Beyond a WFPS of 80%, production of N_2O drops as denitrification consumes N_2O and produces N_2 (Veldkamp et al., 1998). Below a WFPS of 60%, increased diffusion of O_2 limits denitrification and N_2O production is attributed to nitrification (Robertson and Tiedje, 1987).

The probability distribution of soil N_2O data is commonly described as approximately log normal or highly skewed (Corre et al., 1996; Parkin, 1987). Parkin (1987) attributes this to the patchy distribution of denitrification in anaerobic microsites. High values of N_2O flux occur only when all conditions are non-limiting. Hence, measurements of N_2O emissions from the soil are typically characterized by high degrees of spatial and temporal variability (Groffman et al., 2000). The large uncertainty associated with soil N_2O emission data makes the definition of predictive relationships between N_2O flux and controlling variables difficult (Corre et al., 1996). In turn, up-scaled measurements and model predictions of soil N_2O flux are also highly uncertain (Derwent et al., 1999). Validation of model estimates of soil N_2O flux should include reproduction of the probability distribution of measured soil N_2O data. Parkin (1987) modeled denitrification activity and produced a highly skewed data set of denitrification rates with a similar probability distribution as the original denitrification measurements. He speculated that the probability distribution of soil denitrification data would change temporally as controlling factors, such as soil moisture, changed. However, little information is available on how the probability distribution of soil N_2O data changes with time as state variables such as soil moisture and temperature change.

The probability distribution can give us information about the variability in N_2O emission data, but cannot tell us anything about the spatial dependency of the data. Information is available on the spatial dependence of N_2O emissions at a moment in time (Ambus and Christensen, 1994), but there is little information on how spatial dependency changes over time. The first objective of this chapter was to examine the

shape and temporal stability of the probability distribution for successive samplings of soil N_2O flux data collected from the same set of locations across two growing seasons. The second objective was to estimate the range of spatial dependence for each of these data sets and also assess its change over time.

3.3 Method and Materials

3.3.1 Field Site and Sampling Design

The research site was located in the St. Denis National Wildlife Area, 52° 12' N latitude, 106° 5'W longitude, approximately 40 km east of Saskatoon, Saskatchewan, Canada. The site was on a hummocky, till terrain. Slopes were 10-15% and the parent material was a combination of unsorted calcareous till and glacio-lacustrine sediments. The glacio-lacustrine sediments blanket the till in a thin mantle, leaving the till very close to the surface or exposed on topographically high positions and some convergent areas that lead into lower slope positions. Soil types ranged from thin Chernozemic Rego Dark Brown (Typic Calciborolls) on the tops of knolls through the thicker Chernozemic Orthic Dark Brown (Typic Haploborolls) in the mid-slope and toe-slope positions, to Chernozemic Eluviated Dark Brown (Albic Argiborolls) and Gleysolic Humic Luvic (Argic Cryaquolls) in depressional positions. Chernozemic Calcareous Dark Brown (Haplic Calciborolls) were found in shoulder and back-slope positions as well as some foot-slope positions. Overall, soil textures range from a loam at topographically high positions to a silt loam in depressions. The hydrological pattern on the site is depression focused where the bulk of infiltrating water moves laterally through the depression margins where it is recycled through evaporative and transpiration processes (Hayashi et al., 1998a).

A detailed topographic survey of the site was completed using a Sokkisha Set 5 Electronic Total Station, (Sokkisha Co. Ltd. Tokyo, Japan) and a Trimble^{TR} Pro XRS, Global Positioning System (Trimble Navigation, Sunnyvale, CA). In June of 2003 a 128-point, linear transect was established at the site on cultivated land that had been fallow since 2002. The previous crop was *Hordeum vulgare*. Locations were evenly spaced (4.5 m) and represented numerous landform cycles including three vegetated depressions (Figure 3.1).

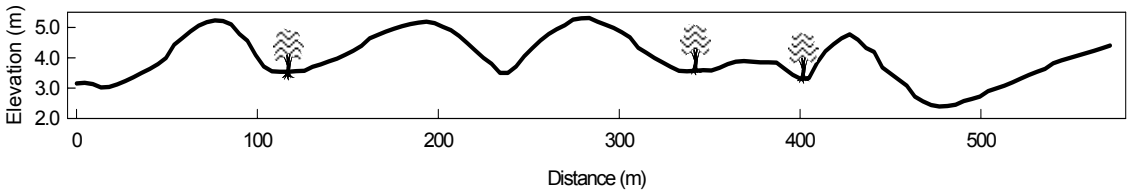

Figure 3.1: Profile of relative elevation (m) along the sample transect at the St. Denis Site. Tree symbol denotes location of vegetated depression.

In May of 2004 the east side of the site, including the transect area, was seeded to grass by Ducks Unlimited Canada. The mix consisted of *Agropyron elongatum*, *Agropyron intermedium*, *Bromus biebersteinii*, *Elymus dauricus*, *Festuca rubra*, *Onobrychis viciifolia*, *Elymus canadensis*, *Agropyron trachycaulum* and *Medicago sativa*.

3.3.2 Soil N_2O Flux Measurements

At each location along the 128-point transect soil N_2O flux was measured using a two piece, closed, vented chamber (International Atomic Energy Agency, 1992) consisting of a polyvinyl chloride (PVC) ring base and vented cap with sampling port similar to Hutchinson and Mosier (1981). The chamber, when placed for sample collection, had a head space of 2.25 L and covered a soil surface area of 0.02 m^2. Prior to the start of data collection, the bases were pressed into the soil and secured using 20 cm spikes where they remained for the duration of the field season. At each sampling event, the chamber was placed onto the base and sealed by a rubber ring within the cap. Samples of the headspace gas were drawn from the chamber with a 20-mL syringe and injected into 12-mL evacuated tubes for transport back to the laboratory. Samples of the headspace gas were drawn at three equally spaced time intervals of 8 min. In 2003 the N_2O concentration in ambient air was used as the initial (time zero; t_0) concentration after Anthony et al. (1995). In 2004, individual time zero samples were collected from each chamber. Sampling of the 128 points was executed by four people each sampling a complete time interval and moving from location to location every 45 s. This allowed for a complete transect sampling in less than 2 h. Gas sampling was timed to begin at midday. Samples were returned to the lab, placed in cold storage, and analyzed within 1 to 2 wks.

Nitrous oxide concentrations were determined using a Varian CP3800 GC (Varian Canada Inc., Mississauga, ON) equipped with dual electron capture detectors (ECD). Operating conditions for the GC were as follows: injector temperature = 100°C, column temperature = 35°C, detector temperature = 370°C; separations were carried out using Poraplot Q columns (12.5-m × 0.32-mm i.d. fused silica capillary column, DF (film thickness) = 8 μm; includes a 2.5-m particle trap) with ultra high purity He (14.4 mL min^{-1}) as the carrier gas and P5 (95:5 v/v Ar:CH_4 mix) as the make-up gas (12.0 mL min^{-1}). Samples (300 μL) were introduced using a CombiPAL™ auto-sampler (CTC Analytics AG, Switzerland) with on-column injection and a split ratio of 10:1. The system was calibrated using standard gases (N_2O in N_2) obtained from PraxAir (Mississauga, ON). Data processing was performed using the Varian *Star Chromatography Workstation* (ver. 6.2) software. Internal calibration curves were obtained by applying linear least squares regression to the gas concentration (ppbv N_2O) *versus* peak area data; N_2O concentrations in the headspace samples were then calculated automatically from the regression equations.

Ambient air samples were included as reference samples in each analytical run to check the 'within run' precision, calculate the minimum detectable concentration difference (MDCD), and correct for detector drift. The MDCD was calculated by (i) analyzing matched pairs of the reference gas samples at regular intervals during each analytical run; (ii) calculating the average difference between sample pairs (μ_p) as well as the standard deviation (σ_p); and (iii) calculating the MDCD using Eq. [3.1].

$$\text{MDCD} = \mu_p + (2\sigma_p) \qquad [3.1]$$

The MDCD was used to filter the raw data when calculating the actual N_2O flux; i.e., concentration differences between t_0 and each subsequent time step that were <MDCD were not considered to be significantly different from the t_0 concentration. Anthony et al. (1995) arbitrarily chose to use an MDCD that was twice the mean absolute difference between pairs of ambient air samples. The form of MDCD presented in this study has a statistical basis in that it is a value that is within the upper bound of the 95% confidence interval for the mean paired difference. The variability in our data is such that the

method employed here to calculate the MDCD is slightly more rigorous than that used by Anthony et al. (1995).

Although some studies assume that the change in N_2O concentration within the chamber over time is linear it has been demonstrated that the concentration (ng L^{-1}) *vs.* time (min) relationship is not linear due to the decreasing concentration gradient between the chamber air and the soil air (Hutchinson and Mosier, 1981). Measuring N_2O concentration at t_0 and for each of the three 8 min time intervals produces 4 points for the concentration *vs.* time curve and allows its description using a polynomial relationship. The vertical flux of N_2O at the soil–atmosphere interface (ng N_2O-N m^{-2} s^{-1}) was then calculated as the slope of the line tangent to the concentration *vs*. time curve at t_0. That is, the flux at t_0 was calculated as the 1st derivative of the 2nd-order polynomial equation ($y = ax^2 + bx + c$) used to describe the concentration *vs*. time relationship. The flux (ng N L^{-1} min^{-1}) was then converted to an area-second basis by multiplying by 1.87 L min m^{-2} s^{-1} [i.e., the chamber volume ÷ (surface area × 60 s min^{-1})]. In cases where 'rogue' data points prevented the use of the 2nd-order polynomial model (i.e., only 3 points available instead of 4) the flux was calculated as the slope of the linear model that best described the concentration *vs*. time relationship (Hutchinson and Mosier, 1981) (Eq. [3.2]).

$$F_{N_2O} = \frac{V}{k_t A} m \qquad [3.2]$$

Where F_{N_2O} is the flux at t_0, V = chamber volume (L), A = cross-sectional area of soil covered by the chamber (m^2), k_t = time constant (60 s min^{-1}), and m = slope of the linear, regression equation (ng L^{-1} min^{-1}).

3.3.3 Measurement of Soil Moisture, Soil Temperature and Climate Data

At each location, volumetric soil moisture over a 15-cm depth was measured at the time of gas sampling using time domain reflectometry (TDR) after Topp and Ferre (2002). Readings were obtained manually from a Tektronix 1502 B cable tester (Tektronix, Wilsonville, OR). Also at each location, soil temperature was measured at 5- and 20-cm depths using buried type T thermocouples constructed of twisted copper

and constantan (45% Ni and 55% Cu) wire pairs and read using a Barnant DuaLogR™ thermocouple reader (Barnant Company, Barrington, IL). A meteorological station on site recorded hourly averages of precipitation, air temperature and wind speed.

3.3.4 Statistical Analysis

Summary statistics and histograms were generated using MINITAB® Release 14 (Minitab Inc. 2003). Probability distributions of soil N_2O emission data sets were assessed by making individual, pair-wise comparisons of the shape and peak locations of their histograms using the Chi-square test (Eq. [3.3]). The histogram is a common exploratory tool for data analysis and the Chi-square test is based on, and looks at, the actual shape of the histogram. A common criticism of the use of the Chi-square test is the subjectivity associated with the binning of data (Press et al., 1992). However, by using 15 bins (15 to 20 is recommended) and keeping the number of bins consistent between histograms (a requirement of the Chi-square test) we minimize the subjectivity. Si (2002) used this technique to compare histograms of soil water flux. Alternative methods for comparison of distributions include the K-S test and its variants. The K-S as it is based on the cumulative probability distribution has no subjectivity. However, it is generally considered non-sensitive, especially when the median values of the distributions being compared are similar (Press et al., 1992). Our data sets have large numbers of zero values and as a result the majority of median values are at or near zero. As well, the K-S test and its variants are not sensitive because of presence of "notches" in the data (Press et al., 1992). Notches are a lack of data points at certain probabilities. Essentially, the K-S test and its variants require many data points at all probabilities, a feature absent in some of our data sets. For these reasons we chose the Chi-square test.

Histograms were consistently constructed using 15 bins or frequency classes.

$$\chi^2 = \sum_{i=1}^{N_B} \frac{(R_i - S_i)^2}{R_i + S_i} \qquad [3.3]$$

Where N_B is the number of bins, R_i is the frequency of N_2O values that fall within a specific i^{th} bin for data from a specific sampling day and S_i is the frequency of N_2O values that fall within a specific i^{th} bin for data from another sampling day. The null hypothesis that there is no significant difference between probability distributions of

data sets for any two sampling days was rejected if the Chi statistic was greater than the critical value (23.68) determined using a pre-selected significance level of 95% and 14 degrees of freedom (N-1). Conversely, if the Chi statistic was less than the critical value, the null hypothesis was not rejected and the two distributions were said to be similar. Chi square determinations—as well as comparisons between data sets from different sampling days—were made using Mathcad® 11 (Mathsoft Engineering and Education Inc., 2002).

To present and organize the histograms of the N_2O flux data, a visual classification was used that grouped each of the 15 distributions into one of four classes: Reverse J-shaped, semi-reverse J-shaped, log normal and symmetrical. The reverse J-shaped distribution is described in Williams (1984) and represents an extremely skewed data set. The semi reverse J-shaped class was created for the purpose of describing highly skewed distributions that did not fit the definition of the reverse J-shaped distribution, and appeared transitional to the log normal shaped distributions. The symmetrical distribution class recognized that, although exhibiting some skew, there were distributions that were very close in shape to a normal distribution.

Trangmar et al. (1985) provides a comprehensive explanation of spatial dependence and its application to soil properties. Briefly, the range of spatial dependence is the maximum separation distance between two locations over which these locations can be said to be spatially related in regards to the soil property of interest. Locations separated by distances greater than this maximum are spatially independent. The range is derived by determining the change in semi-variance of the soil property as distance between measurement locations increase. Spatial independence is achieved when the semi-variance no longer increases and is constant (sill). The distance required to reach the sill is the range. Theoretically when the separation distance is zero, the sill should be zero. This is often not the case and the level of semi-variance when the separation distance is zero is called the nugget variance or nugget. The nugget is a measure of unexplained variability. A high nugget-to-sill ratio would indicate large variation over short distances or little spatial correlation.

The spatial dependence for the N_2O flux on each sampling day was determined using the indicator semivariogram and a nested semivariogram model (Goovaerts,

1997). The semivariogram is sensitive to extreme values that are common in N_2O flux data. Preliminary data analysis indicated that a robust estimator, such as Cressie (1993) was insufficient to overcome the effect of extreme values and that a transformation of the data was required. The indicator transform or semivariogram is the use of the semivariogram on data that has been characterized by cut-off or threshold values. The thresholds can be chosen based on cumulative probability levels. The 1st, 2nd and 3rd quartile of the distribution of N_2O flux measurements for each sampling date were chosen as threshold values for this analysis. For the data from each sampling date, each of the 128 values was coded as an indicator datum, $i(u_\alpha;z_k)$, of either 1 or 0 depending on whether the flux value (u_α) was less than or equal to, or greater than the threshold value(z_k), respectively (Goovaerts, 1997). In this way only the position of the data point in relation to the threshold value is considered. By using more than one threshold value one can look at the spatial pattern of small values separate from large values and vice versa. This allows spatial patterns to emerge that might have been masked by the extreme values. Following Goovaerts (1997) (Eq. [3.4]) the indicator semivariogram was written as

$$\gamma_I(h;z_k)=\frac{1}{2N(h)}\sum_{\alpha=1}^{N(h)}\left[i(u_\alpha;z_k)-i(u_\alpha+h;z_k)^2\right] \qquad [3.4]$$

where z_k is the threshold value, h is the distance between sample locations, N is number of sample locations, and $i(u_\alpha; z_k)$ *and* $i(u_\alpha + h\ ; z_k)$ are indicator data separated by h. This is the regular semivariogram applied to the indicator data. The semivariogram was calculated over a lag spacing of 4.5 m and a distance of 288 m which is half the total lag distance.

Visual inspection of the empirical semivariogram (Fig. 3.2) indicated more than one basic model may be necessary to fit the semivariogram rather than a blind fit with a single spherical model. After Goovaerts (1997) a linear combination of four models were nested and fitted to the semivariograms produced for each threshold value on each sampling date. A nugget model and three spherical models, each representing a different range of spatial dependency, was used. These ranges of spatial dependency were 15, 50 and 125 m. The nested model was designed to fit these three ranges and the nugget

model to each semivariogram and indicate which spatial scale was dominant on each date and at what threshold value. The nested model (Eq. [3.5]) was written as

$$gSP(h,a,b,c,d) = a \cdot g(h) + b \cdot SP(h,15) + c \cdot SP(h,50) + d \cdot SP(h,125) \quad [3.5]$$

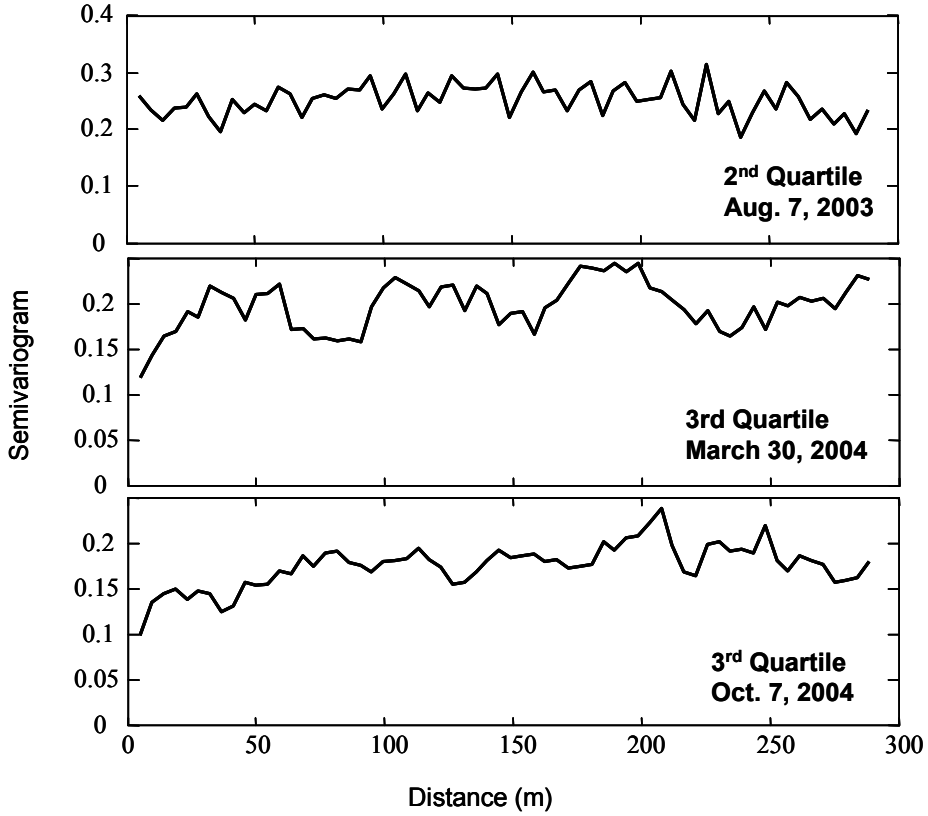

Figure 3.2: Semivariogram for three sampling dates at the St. Denis site. High nugget effect and range of spatial dependency of approximately 125 m for 7 Aug. 2003. Range of approximately 50 m for 30 Mar. 2004. Range of approximately 15 and 125 m for 7 Oct. 2004.

where a, b, c, and d are parameters representing the relative contribution of each model to the total semivariance or sill. The nugget model was represented by $g(h) = 0 \; if \; h = 0, otherwise \; 1$ and the spherical model for each range of spatial dependence (Eq. [3.6]) was

$$SP(h,\tau) = \left[1.5 \cdot \frac{h}{\tau} - 0.5 \cdot \left(\frac{h}{\tau} \right)^3 \right] if \; h < \tau, otherwise \; 1 \quad [3.6]$$

with τ as the range of spatial dependence. The estimates of parameters a, b, c, and d were used in an iterative function which minimized the sums of squared error (SSE) and

gave the best fit to the curve and best estimates of the parameters (Eq. [3.7]) (Cressie, 1985).

$$SSE(a,b,c,d) = \sum_{i=1}^{m} \frac{N(h)}{gSP(h_i,a,b,c,d)^2} (\gamma_I(h;z_k) - gSP(h_i,a,b,c,d))^2 \qquad [3.7]$$

where m is the number of lags, gSP(h_i,a,b,c,d) is the model semivariogram and $\gamma_I(h;z_k)$ is the sample semivariogram. The model fit was weighted toward the initial values in the curve by dividing *N(h)* by the model semivariogram.

3.4 Results

3.4.1 Precipitation and Air Temperature

Daily precipitation for the 2003 and 2004 field seasons is shown in Figure 3.3. The collection of rainfall and air temperature data for the St. Denis site began on 18 June 2003. During the period of sample collection in 2003 (19 June to 15 Oct.) cumulative precipitation totaled 164 mm. The mean daily air temperature for this period was 15 ºC with a mean daily peak of 26 °C (16 Aug.) and a mean daily low of -2 °C (15 Oct.) (data not shown). In 2004, the cumulative rainfall during the period of sample collection (30 Mar. to 7 Oct.) was 270 mm. The mean air temperature for this period was 13 °C with a mean daily peak of 22 °C (18 July) and a mean daily low of 0 °C (1 Oct.) (data not shown).

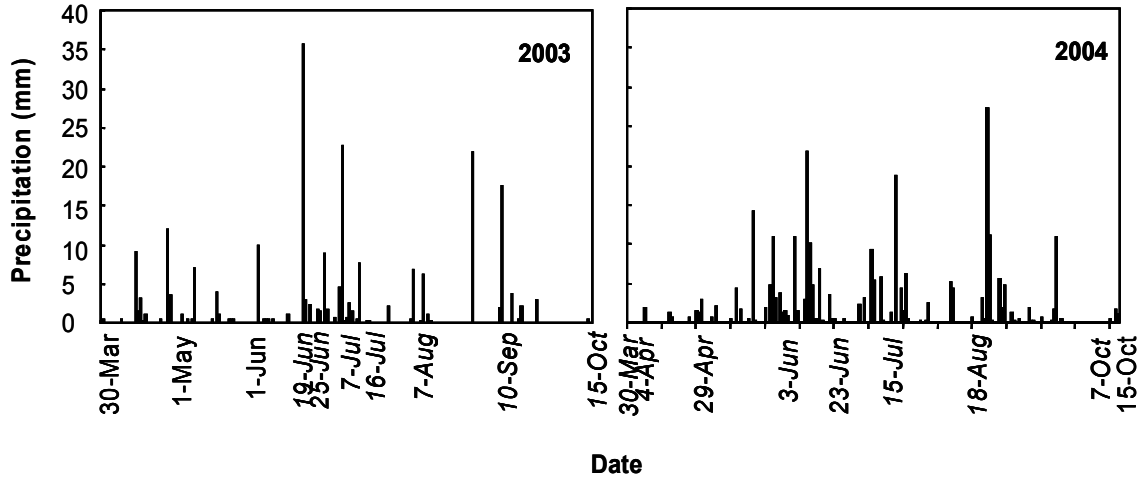

Figure 3.3: Daily precipitation (mm) at the St. Denis site for the field seasons of 2003 and 2004. Nitrous oxide flux measurements occurred on italicized sampling dates.

Rainfall recorded at the Saskatoon Airport for the period from 30 Mar. 2003 - 18 June 2003 was 61 mm (Environment Canada, 2005a). Thus, total the rainfall recorded in 2003 for a period equivalent to the 2004 field season was 225 mm. In 2003, 61% of precipitation fell between 20 June and 13 July, and 28 Aug. and 9 Sep. (Fig. 3.3), whereas the majority of precipitation in 2004 was more evenly distributed over a much longer period, between approximately 12 May and 24 Aug. (Fig. 3.3). Rainfall from Apr. 2003 to Sep. 2003, inclusive, was below the 30-year average of 250 mm for the Saskatoon Airport (Environment Canada, 2005b), whereas rainfall in 2004 was above average. Mean air temperature reported for this same 30 year period was 13 °C.

3.4.2 Soil Moisture and Soil Temperature

The soil moisture data for each sampling day is presented as mean WFPS (%) ranked according to mean N_2O flux (Fig. 3.4). The mean WFPS in 2003 was at or near 60% on seven dates including the four dates on which the mean flux was highest as well as the date on which the lowest mean flux was recorded. There is no value for 30 Mar. because the soil was frozen at the time of sampling and the TDR could not be used. Mean soil temperature for sampling dates in Mar., Apr. and Oct. was < 10 °C, and on most dates was less than 5 °C (Fig. 3.4). Mean soil temperature on all other sampling dates was consistently > 10 °C.

3.4.3 Nitrous Oxide Flux

The N_2O flux data had a range of mean values and standard deviations with the largest fluxes also having the largest ranges and standard deviations. On three dates the mean flux was greater than 15 ng N_2O-N m^{-2} s^{-1}. Fluxes on the remaining dates were <9.0 ng N_2O-N m^{-2} s^{-1}, with fluxes <1.0 ng N_2O-N m^{-2} s^{-1} on four sampling dates (Table 3.1). The lowest mean flux dates were also associated with the lowest range in values and standard deviation. On only one date (23 June 2004) was the mean flux negative.

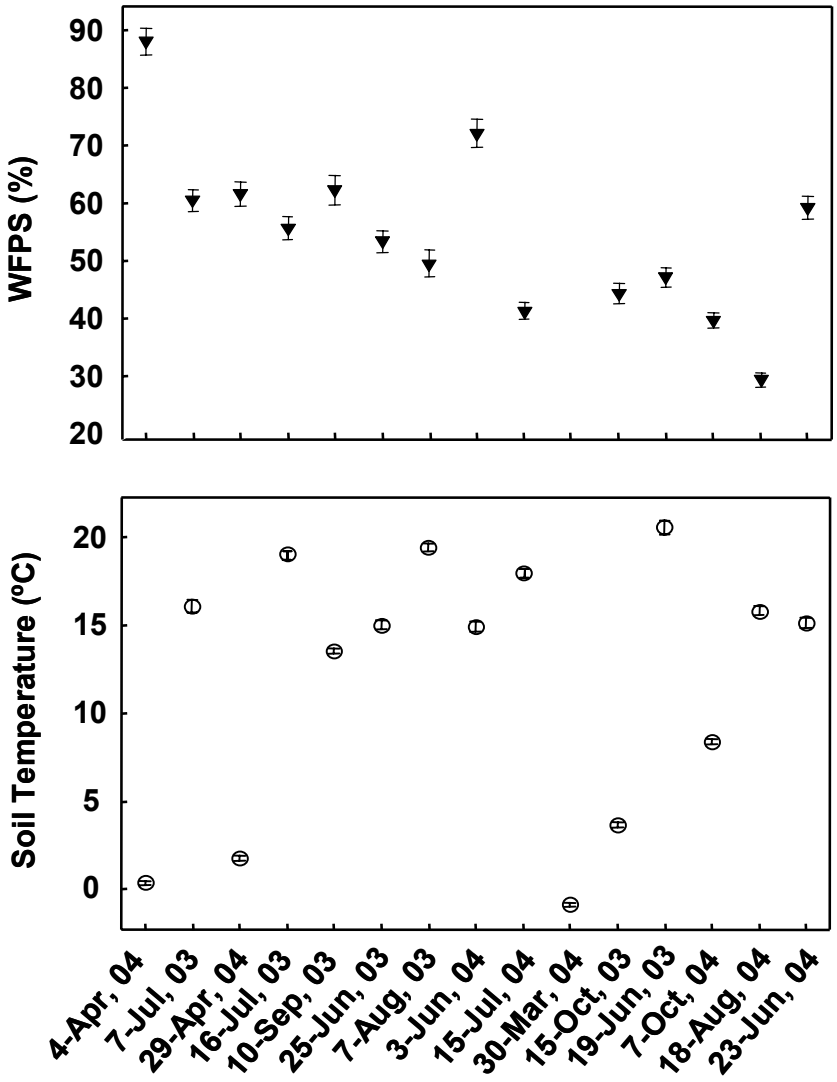

Figure 3.4: Mean water-filled pore space (WFPS) (0 to15 cm), and soil temperature (0- to 20- cm) at the St. Denis site for 2003 and 2004. Error bars indicate 95% confidence interval. Water-filled pore space absent for 30 Mar. due to frozen soil. Data is presented in order of decreasing mean N_2O flux.

3.4.4 Probability Distributions and Chi Square Comparison

Probability distributions for the N_2O data from the 15 sampling days in 2003 and 2004 (Fig. 3.5) all exhibited some degree of skewness and kurtosis (Table 3.1), and ranged in shape from symmetrical through log normal to reverse J-shaped (Williams, 1984). The majority of dates had skewness values <5, though the four dates with the largest mean fluxes exhibited skewness values >5 and the highest values of kurtosis. High frequency in the bin centered on zero (Table 3.1) is associated with both reverse J-shaped and symmetrical distributions. On 19 June 2003 (Fig. 3.5) and 10 Sep. 2003

there were what appeared to be reverse J-shaped distributions except for a single, very low frequency bin to the left of the peak and the distributions for these two dates have been called semi-reverse J-shaped.

Results of the Chi-square testing demonstrate that the majority of distributions were significantly different from each other (Fig. 3.6). That is, of 105 possible comparisons, only 8 pairs of distributions did not show a significant difference. In both 2003 and 2004 consecutive sampling dates were similar in distribution shape, specifically the two dates in July of 2003 and the two dates in Apr. of 2004.

Table 3.1: Mean N_2O flux, standard deviation, range (ng N_2O-N m^{-2} s^{-1}), skewness, kurtosis, zero bin frequency, and distribution shape for the 15 sampling dates at the St. Denis transect during 2003 and 2004. Data is in order of decreasing mean N_2O flux. N=128

Sampling Date	Mean	Std. Dev.†	Range	Skewness	Kurtosis	Zero Bin Frequency‡	Distribution Shape
4 Apr. 2004	25.3	50.5	510.9	7.7	69.9	76	Reverse J-shaped
7 July 2003	21.6	40.2	354.5	5.8	41.0	67	Reverse J-shaped
29 Apr. 2004	17.3	92.7	884.3	7.7	64.0	123	Reverse J-shaped
16 July 2003	8.5	31.8	346.9	9.7	103.5	102	Reverse J-shaped
10 Sep. 2003	7.2	12.3	84.9	2.6	8.5	72	Semi-reverse J-shaped
25 June 2003	4.6	7.9	36.4	2.3	5.2	74	Reverse J-shaped
7 Aug. 2003	4.5	10.0	50.2	1.0	1.0	45	Symmetrical
3 June 2004	4.3	5.8	37.4	1.4	2.5	54	Log normal
15 July 2004	3.6	3.2	19.3	2.0	6.5	24	Log normal
30 Mar. 2004	2.3	4.8	30.0	1.8	5.2	58	Log normal
15 Oct. 2004	1.3	4.0	35.8	1.7	7.8	95	Symmetrical
19 June 2003	0.6	1.6	11.2	3.2	11.8	99	Semi-reverse J-shaped
7 Oct. 2004	0.4	2.5	13.8	0.6	1.1	43	Symmetrical
18 Aug. 2004	0.2	1.8	13.4	2.4	9.3	103	Symmetrical
23 June 2004	-0.2	1.9	15.4	-2.1	10.3	102	Symmetrical

†Standard Deviation

‡ Number of values in frequency interval centered on zero flux prior to standardization of distributions.

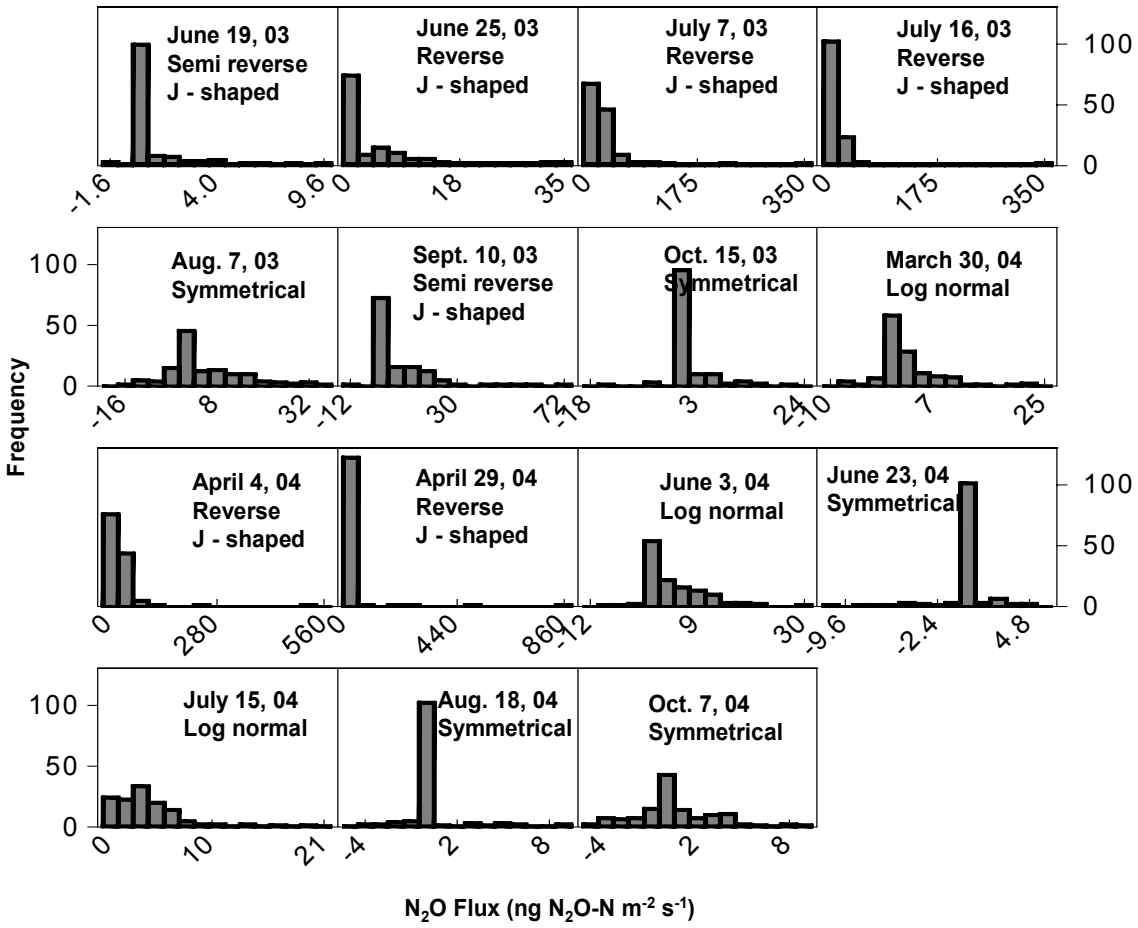

Figure 3.5: Histograms of N_2O data from the St. Denis transect. Each histogram has 15 bins. N_2O. Data is in order of decreasing mean N_2O flux.

	April 4, 2004	July 7, 2003	April 29, 2004	July 16, 2003	September 10, 2003	June 25, 2003	August 7, 2003	June 3, 2004	July 15, 2004	March 30, 2004	October 15, 2003	June 19, 2003	October 7, 2004	August 18, 2004	June 23, 2004
April 4, 2004	X														
July 7, 2003		X													
April 29, 2004			X												
July 16, 2003				X											
September 10, 2003					X										
June 25, 2003						X									
August 7, 2003							X								
June 3, 2004								X							
July 15, 2004									X						
March 30, 2004										X					
October 15, 2003											X				
June 19. 2003												X			
October 7, 2004													X		
August 18, 2004														X	
June 23, 2004															X

Figure 3.6: Results of a Chi square test of similarity between probability distributions for N_2O flux measurements at the St. Denis transect for the 15 sampling dates in 2003 and 2004. Black cell indicate distributions that were not significantly different from each other at a 0.05 probability level. Data is in order of decreasing mean N_2O flux.

3.4.5 Spatial Dependence of N_2O Flux

Table 3.2 shows the results of the nested model fit to the indicator semivariogram for the 25, 50, and 75% quartiles of the cumulative probability distribution for N_2O flux. The data is in ranked order according to mean N_2O flux. For each sampling date and each quartile, the contribution of semivariance to the total semivariance or sill is shown for the nugget model and the 15-, 50- and 125-m range of spatial dependence. On four dates in 2003, the number of zero values in the data set was such that the threshold level was zero at both the 1st and 2nd quartiles, and hence the results of the model fit are given only for the 2nd quartile. On 19 June 2003 and three dates in 2004 the threshold values were zero for all three quartiles, indicating that at least 75% of the values on those days were zero. A complete cross date comparison of parameters of spatial dependence is really only possible for the 3rd quartile. However, it is clear that as mean flux decreases the number of zero values in the data increases.

In the 3rd quartile the nugget semivariance as a fraction of the total variance was > 0.7 on seven dates, and between 0.3 and 0.7 (inclusive) on the eight remaining sampling dates. The 15-m range of spatial dependence contributes to the total semivariance on nine dates, whereas the 50-m range of spatial dependence only contributes to the total semivariance on three dates. The 125-m range of spatial dependence contributes on 10 dates; however on 29 Apr. 2004 there is a strong trend in the data (not shown) and the estimate of the contribution of that range to the total semivariance is not reliable. This was the only date for which the indicator semivariogram could not overcome a trend in the data. Contribution to total semivariance by the 125-m range on the other nine dates is smaller than that contributed by the 15-m range.

Table 3.2: Semivariance expressed as a fraction of total semivariance for a nugget model and spherical models for three ranges of spatial dependence (15, 50 and 125 m) nested in indicator semivariogram for the N_2O data from 15 sampling times at the St. Denis transect in 2003 and 2004. Threshold values for indicator semivariogram represent the 25, 50 or 75% quartiles of the distribution of N_2O flux measurements. Data is in order of decreasing mean N_2O flux.

Sampling Date	1st Quartile					2nd Quartile					3rd Quartile				
	Z_k†	Nug‡	15§ (m)	50 (m)	125 (m)	Z_k	Nug	15 (m)	50 (m)	125 (m)	Z_k	Nug	15 (m)	50 (m)	125 (m)
4 Apr. 2004	8.3	0.2	0.4	0.4	0	16.5	0.3	0.3	0.3	0.1	26.8	0.3	0.7	0	0
7 July 2003	5.7	1.0	0	0	0	11.7	0.7	0.2	0.1	0	21.7	0.6	0.2	0.1	0.1
29 Apr. 2004	0	0.7	0	0.1	0.2	0.7	0.6	0	0.1	0.3	5.7	0.6	0	0	0.4
16 July 2003	¶					0	0.8	0	0	0.2	10.8	0.8	0	0	0.2
10 Sep. 2003	¶					0	0.9	0	0	0.1	12.0	0.7	0.2	0	0.1
25 June 2003	¶					0	0.4	0.4	0	0.2	6.4	0.4	0.4	0.2	0
7 Aug. 2003	¶					0	0.9	0	0	0.1	10.3	0.9	0.1	0	0
3 June 2004	0	0.8	0	0	0.2	2.4	0.8	0	0.1	0.1	7.9	0.5	0.1	0.2	0.2
15 July 2004	1.7	1.0	0	0	0	3.1	0.8	0.1	0	0.1	4.8	0.8	0.1	0	0.1
30 Mar. 2004	0	0.8	0	0.2	0	0.8	0.8	0	0.2	0	3.7	0.5	0.3	0	0.2
15 Oct. 2004	¶					¶					0	0.9	0	0	0.1
19 June 2003	¶					¶					0	1.0	0	0	0
7 Oct. 2004	-0.7	0.6	0	0	0.4	0	0.5	0	0	0.5	1.7	0.4	0.4	0	0.2
18 Aug. 2004	¶					¶					0	1.0	0	0	0
23 June 2004	¶					¶					0	0.8	0	0	0.2

† Threshold value of nitrous oxide flux (ng N m^{-2} s^{-1})

‡ Nugget semi-variance expressed as a fraction of the total semivariance.

§ Semivariance attributed to spherical model using 15, 50 and 125 m range of spatial dependence expressed as a fraction of total semivariance.

¶ Threshold value is same as next highest quartile due to proportion of zero values in data set resulting in same modeled results.

3.5 Discussion

Soil N_2O flux measurements from hummocky, agricultural landscapes in the Canadian Prairie region are not common. However, Corre et al. (1996) reported a median value of 1050 μg N_2O-N m^{-2} d^{-1} (12.2 ng N_2O-N m^{-2} s^{-1}) for spring N_2O flux measurements from unfertilized, fallow, agricultural land in the Black soil zone of Saskatchewan. Lemke et al. (1998) recorded mean N_2O flux values as high as 350 μg N_2O-N m^{-2} h^{-1} (97.2 ng N_2O-N m^{-2} s^{-1}) from the Parkland region of Alberta. Hence, the highest mean value of N_2O flux obtained from the St. Denis site (25.3 ng N_2O-N m^{-2} s^{-1}) is within the range of previously published data.

Skewed probability distributions for N_2O flux data are very common (Parkin, 1987; Ambus and Christensen, 1994; Corre et al., 1996). Parkin (1987) described a probability distribution for a denitrification rate measured from intact soil cores as approximately log normal. However, this distribution may be more appropriately described as a reverse J-shaped; i.e., strongly skewed with the peak at the left end, at or near zero (Williams, 1984). Many of the probability distributions for the data from the St. Denis NWA are reverse J-shaped or semi-reverse J-shaped. In general, however, the probability distributions for the St. Denis data represent a range of distribution shapes (Fig. 3.5). The symmetrical distributions represent shapes transitional between normal and log normal distributions. The semi-reverse J-shape represents a transition between log normal and the reverse J-shape distributions.

The data presented in Table 3.1 show a clear relationship between the magnitude of the mean N_2O flux and the distribution shape. The reverse J-shape distributions are generally associated with a range in values that is an order of magnitude greater than that associated with the other distributions—the only exception occurring on 25 June 2003. As the mean flux declines, the distribution decreases in skewness and evolves into shapes that are log normal and, finally, symmetrical. This relationship is also evident in the results of the Chi square tests (Fig. 3.6), where the dates with the highest mean fluxes and reverse J-shape distributions are statistically similar to each other.

The relationship between mean N_2O flux and the distribution shape can be explained by grouping the 15 sets of flux measurements into event-based and background emission patterns as proposed by Brumme et al. (1999) or as transitional

between the two patterns. Brumme et al. (1999) proposed that N_2O emissions rise and fall seasonally over and above a low level (background) emission pattern that is occasionally interrupted by extreme peak emissions due to a climatic event (event-based). Such events may be re-wetting of the soil following a dry period or frost/thaw events which could be considered analogous to high precipitation events and spring snow melt that occur at the St. Denis site.

The July 2003 and Apr. 2004 flux measurements each represent event-based emission patterns. The triggering event in each case is an increase in WFPS (Fig. 3.4) to a value approaching or exceeding the 60% threshold needed to restrict oxygen diffusion to microsites of activity and trigger denitrification. In Apr. 2004, the event is spring snow melt and in July 2003, an intense precipitation event that occurred just prior to the 7 July sampling date (Fig. 3.3). Although soil temperature was low in Apr. 2004, it did not prevent peak emissions from occurring. It can be assumed that available N was not limiting in Apr. 2004 as it has been found that in the spring, labile N from the previous growing seasons is available for mineralization (Boone, 1994). This would be in addition to N made available due to the flush of mineralization upon re-wetting of the soil (Cabrera, 1993) during snow melt, and freeze/thaw effects (van Bochove et al., 2000). The July precipitation event followed a long dry period, (Fig. 3.3) and a flush of mineralization upon re-wetting of the soil may have provided the N necessary for the N_2O emission event.

The event-based emission patterns in July 2003 and Apr. 2004 have similar reverse J-shape distributions and high mean N_2O fluxes that reflect the inclusion of a small number of extreme flux values. As the effects of the event diminish (i.e., as WFPS and probably available N decline) the frequency of extreme flux values decreases. This is first observed in the measurements made immediately after the peak emissions (16 July 2003 and 29 Apr. 2004). On these two days, the frequency of values in the zero bin increased (Table 3.1) at the expense of high and extreme values (Fig. 3.5) even though the mean N_2O flux is still relatively high (Table 3.1). This occurs because of a decline in denitrification as hot spots of activity shut down. As this trend continues the flux distribution transitions towards a background emission pattern, represented by small mean N_2O flux, which is probably a reflection of continued nitrification. In 2003,

this background pattern had become established by 7 Aug. but was interrupted by a precipitation event on 9 Sep. (Fig. 3.3) that saw an increase in mean N_2O flux and a movement of the distribution pattern back to the reverse J-shape on 10 Sep. (Table 3.1). Following the Sep. event, the pattern again became symmetrical during the early fall (i.e., by 15 Oct.).

In 2004, the transition from a spring event-based emission pattern to the background emission pattern (i.e., the transition from a reverse J-shape distribution to a symmetrical distribution) included a period when the distributions were log normal. This may reflect the more even distribution of precipitation that occurred during 2004 (Fig. 3.3) which, in turn, may have slowed the transition. As well, precipitation events did not have the dramatic effect they had in 2003 perhaps because the soil did not go through extended dry periods as it did during 2003 (Fig. 3.3) and because establishment of the grass cover may have reduced the amount of N available for denitrification. Certainly the precipitation event prior to 23 June failed to produce any large emission of N_2O (Table 1).

The transition towards the background emission pattern and the background emission pattern itself were related to specific distribution shapes, but there was little statistical similarity in these shapes (Fig. 3.6). Exceptions to this occurred on 19 June 2003 and 10 Sep. 2003, and again on 30 Mar. 2004 and 3 June 2004 (Figs. 3.4 and 3.5). In both sets of comparisons, the probability distributions were similar despite differing soil conditions (Fig. 3.6). It should be noted, however, that the mean N_2O flux was similar on both 30 Mar. 2004 and 3 June 2004, suggesting that different limiting factors may result in the same pattern of emission. The low soil temperature on 30 Mar. (Fig. 3.4) may have restricted microbial activity, thus reducing oxygen demand and preventing anaerobic microsites from fully developing even during a period when the soil was wet and N availability should be non-limiting. On 3 June, the WFPS was greater than 60%, but by this time much of the labile N from spring thaw may have been used up during the burst of activity that occurred in Apr. It appears that multiple controls on N_2O production during the year can result in combinations of flux values that produce a distinctive distribution shape. Thus, enhanced knowledge of how process-

level factors change across a season will be needed to predict distribution shapes and the magnitude of mean N_2O fluxes.

Cambardella et al. (1994) suggested that strong spatial dependency existed if the nugget semivariance of a variable expressed as a fraction of the total semivariance was <25%, moderately spatially dependent if it was 25 to 75%, and weakly spatially dependent if the ratio was >75%. The spatial dependency for the soil N_2O emissions could be clearly described as moderate to weak based on the nugget variance in Table 3.2. However, there is a trend for the nugget model fraction of the total semivariance to increase with decreasing mean N_2O flux. Overall, the ratio is lowest on the first five dates shown which are associated with the event- based emission pattern. The highest overall ratios are associated with the last five dates when fluxes were lowest and activity exhibited the background emission pattern. Lowering of the mean N_2O flux probably magnifies measurement error, reducing our ability to estimate the spatial dependency.

Although it is difficult to make an across-date comparison for each quartile of the indicator semivariogram, we can observe that the range of spatial dependency, as determined using the nested model approach, is not stable over time. As a fraction of the total semivariance, each chosen range varies in its importance to the spatial dependency from date to date. For the 3rd quartile, where a complete across date comparison can be made, the 15-m range appears to account for the most semi-variance. This is likely a reflection of the range of the slope class or sub units of the catenas along the transect. Overall, the catena sequences (upper to lower slope) (Figure 3.1) were represented by the 50-m range and did not have much influence on the spatial dependency of N_2O emission. The 125-m range contributed to the total semivariance on several days and probably reflects the broad geomorphologic structure of the site which appears to host a broad ring of vegetated depressions in the center of the site that is crossed by the transect.

Corre et al. (1996) observed a topographic control to the distribution of hot spots, finding that hot spots of denitrification were concentrated in positions of low relief. The extreme values in the St. Denis data tended to be associated with foot-slope and certain depressional positions in the cultivated area of the transect (data not shown). In contrast, vegetated depressions produced either low, undetectable, or negative fluxes and as a

consequence, had little impact on the distribution of the data. This suggests that extreme values are an important characteristic of this landscape (i.e., combined agricultural and non-agricultural land use in a hummocky terrain) that cannot be rejected, but may be location specific. The indicator semivariogram and the nested model approach provided insight into the spatial scales of the N_2O emissions at the site. There was only one date, 29 Apr., 2004 that the indicator semivariogram was unable to remove the strong trend in the data. As well, an across-date comparison was not possible with the indicator semivariogram due to the large number of zero flux values in several of the data sets. It might be useful to apply methods of analysis that do not require the assumption of stationarity and can provide local (point by point) information on scale and variance as opposed to globally, over the entire transect. In this way we can examine extreme values and their temporal variation directly so we may better understand the implications for modeling and prediction of soil N_2O emissions. Models must be validated through their ability to reproduce the range of distributions associated with the pattern of emissions that occur in these landscapes.

3.6 Conclusions

The objectives of this study were to describe the shape and temporal stability of the probability distribution for soil N_2O emission data and to estimate and assess the temporal stability of the spatial dependence of this data. The shape of the probability distributions for soil N_2O emission data at the St. Denis site had poor temporal stability. The shape of the distribution ranged from symmetrical through log normal to a reverse J-shape. The reverse J-shaped probability distribution was associated with the highest mean N_2O flux and short-term temporal stability in distribution shape at times when controlling factors to N_2O production were non-limiting.

The pattern of emission can be grouped into event-based, transitional, and background emission patterns. The event-based pattern is a result of a triggering event, such as high water-filled pore space that coincides with non-limiting conditions of soil temperature and available N. As soil moisture declines or available N is used up these microsites shut down, mean flux decreases, and the probability distributions change towards symmetrical as the emission pattern changes to a background level.

Spatial dependency was characterized by high nugget:sill ratio on most sampling days. The nugget:sill ratio decreased on days when soil conditions were most conducive to denitrification and hot spot activity was highest. The indicator semivariogram was able to overcome the influence of extreme values on most days, however a strong trend was present on at least one day and proper spatial analysis for data of that nature will require alternative methods not sensitive to stationarity. Due to the high number of zero fluxes in several data sets, an across date comparison over all threshold values was not possible. Extreme values are important to these data sets and an understanding of their influence on variability and scale is necessary for improvement and validation of models designed to predict N_2O emission in these landscapes.

4.0 WAVELET SPECTRA OF NITROUS OXIDE EMISSION FROM HUMMOCKY TERRAIN DURING SPRING SNOWMELT.

4.1 Preface

The previous chapter identified the importance of extreme fluxes to the mean value and distribution shape of the data. The spatial dependency of soil N_2O flux appeared to change over time, but high variability and non-stationarity in the data makes interpretations difficult. As well, extreme fluxes in terrains with variable topography may be location specific. Wavelets can reveal the distribution of variance by location and scale and is not affected by stationarity. Thus, we can get a clearer picture on how the scales of soil N_2O flux change over time and location.

4.2 Introduction

Nitrous oxide (N_2O), a greenhouse gas, has a 100-year global warming potential approximately 296 times that of carbon dioxide (CO_2) (IPCC, 2001) and it is estimated that up to 70% of anthropogenic N_2O emissions are due to agriculture (Agriculture and Agri-food Canada, 1998a) with the soil identified as the chief source (FAO and IFA, 2001). The majority of soil N_2O is believed to be produced by respiratory denitrification (Tiedje, 1988). The synthesis and activity of the nitrate reductase enzyme is controlled by the availability of oxygen (Tiedje, 1988) and denitrification occurs in anaerobic soil microsites or hotspots (Parkin, 1987). Anaerobic conditions depend on the rate of oxygen diffusion versus consumption (Tiedje, 1988). The diffusion of O_2 is slowed by water in soil pores (Renault and Stengel, 1994). Denitrification becomes the dominant process producing N_2O when water-filled pore space (WFPS) exceeds approximately 60% (Lemke et al., 1998; Davidson and Verchot, 2000). Above a WFPS of 80%, production of N_2O declines as denitrification consumes N_2O and produces dinitrogen (N_2) (Veldkamp et al., 1998). Below a WFPS of 60%, increased diffusion of O_2 is limiting to denitrification and N_2O produced is attributed to nitrification (Robertson and Tiedje, 1987). However, Müller et al. (2004) concluded that reduction of NO_3^- and

subsequent production of N_2O was occurring under aerobic conditions underscoring their observation that soil N_2O flux is a combination of N_2O produced under a variety of microbial processes.

Nitrous oxide emission data is commonly observed to be highly skewed (Parkin, 1987; Corre et al., 1996). The high degree of skewness in soil N_2O emission data is thought to be the result of the patchy distribution of denitrification in anaerobic microsites (Parkin, 1987). Corre et al. (1996) observed that the occurrence of anaerobic microsites or hotspots was landscape controlled and that this knowledge may be useful in the development of spatial models designed to estimate N_2O emissions at a landscape level. In Yates et al. (2006a) (Chapter 3) it was demonstrated that the extreme flux values are part of an event-based / background emission pattern model as proposed by Brumme et al. (1999) and the high fluxes that occurred during an emission event may be associated with specific locations in hummocky, agricultural landscape. However, during the transition from an event-based pattern to a background pattern, the magnitude and number of extreme values changed and these changes altered the probability distribution of soil N_2O emission data. The shape of the probability distribution, over multiple flux measurements, ranged from a highly skewed, reverse J-shaped through log-normal to a symmetrical or nearly normal shape. In Yates et al. (2006a) (Chapter 3) it was also observed that extreme values can be highly localized in space. This may represent disproportionate distribution of variance across the area making it difficult to use spatial analytical tools that rely on the assumption of stationarity to estimate the scale of the processes controlling soil N_2O emission. Stationarity assumes that all values of a soil property within an area are drawn from the same population such that the value of that soil property at each location is an estimate of the same mean and variance of a normally distributed field of values (Trangmar et al., 1985). To improve our understanding of the spatial scales of soil N_2O emission and their change during and following an N_2O emission event, it is necessary to use statistical tools that do not rely on the assumption of stationarity.

Wavelet analysis is a statistical technique that meets this requirement (Si, 2003). Wavelets provide location-specific information on scales and variance allowing a detailed study of non-stationary processes (Si and Farrell, 2004). Wavelets have been

used to analyze spatial scales of soil properties (Si and Farrell, 2004) and specifically N_2O emission from soil cores (Lark et al., 2004). However, the use of wavelets for scale analysis of soil N_2O flux data that has been collected from undisturbed field locations on multiple occasions has, to the best of our knowledge, not been reported.

The first objective of this chapter was to use wavelet analysis to describe the spatial distribution of the variance associated with soil N_2O flux data measured on successive dates from a hummocky, agricultural landscape. The second objective was to identify the important scales of variability of the processes controlling soil N_2O emission and assess the change in these scales over the snowmelt period.

4.3 Method and Materials

4.3.1 Field Site and Sampling Design

The research site is located approximately 40 km east of Saskatoon, Saskatchewan, Canada in the St. Denis National Wildlife Area, 52° 12' N latitude, 106° 5'W longitude. The terrain is hummocky with slopes of 10 to 15%. The parent material is a combination of unsorted calcareous till and glacio-lacustrine sediments. The glacio-lacustrine sediments blanket the till in a thin mantle and the till is very close to surface or exposed on topographically high positions and some convergent areas that lead into low slope positions. In June of 2003 a 128-point, linear transect was installed at the site on fallow, cultivated land. Locations were evenly spaced (4.5 m) and represented numerous landform cycles including three vegetated depressions. A detailed topographic survey of the site was completed using a Sokkisha Set 5 Electronic Total Station, (Sokkisha Co. Ltd. Tokyo, Japan) and a Trimble^{TR} Pro XRS, Global Positioning System (Trimble Navigation, Sunnyvale, CA). A digital elevation model was produced with a 5 X 5 m grid cell extent. Elevation and visual inspection of the site was used to segment the transect locations into a set of landscape elements defined by profile curvature and land use (cultivated versus uncultivated).

Locations in the cultivated area of the transect were classified as either convex (CX), concave (CV), or cultivated wetland (CW). Convex elements were topographically high positions with a positive profile curvature. Concave elements were positions with negative profile curvature. Cultivated wetlands were depressional positions, roughly circular in shape,

which temporally collect rain or snowmelt water. The mean bulk density of the soils at CX positions was 1.292 ± 0.104 g cm^{-3} the mean bulk density at CV and CW positions was slightly lower (1.236 ± 0.136 g cm^{-3}). Non-agricultural portions of the transect included vegetated depressions and were classified as uncultivated wetlands (UW). Mean bulk density in the UW elements was lower than that of the surrounding cultivated units (0.845 ± 0.289).

Soil types ranged from thin Chernozemic Rego Dark Brown (Typic Calciborolls) on the top of CX elements through thicker Chernozemic Orthic Dark Brown (Typic Haploborolls) down-slope from CX to CV elements. Chenozemic Eluviated Dark Brown (Albic Argiborolls) and Gleysolic Humic Luvic (Argic Cryaquolls) were found in CW and UW elements. Chernozemic Calcareous Dark Brown (Haplic Calciborolls) were found in CX elements as well as some CV elements. Soil profiles were described in the field, classified and converted to the U.S. taxonomic system using the Canadian System of Soil Classification (Agriculture and Agri-Food Canada, 1998b). Overall, soil textures ranged from loam at CX elements to silt loam in CV and CW elements. The hydrological pattern of the site was such that precipitation and snowmelt generated runoff concentrated in the numerous depressions where the bulk of water infiltrated laterally through the wetland margins and was subsequently lost to evaporation and transpiration (Hayashi et al., 1998a).

In May of 2004 the east side of the site, including the area of the transect, was seeded to grass by Ducks Unlimited Canada. The mix consisted of *Agropyron elongatum* (Host) Beauvois, *Agropyron intermedium* (Host) Beauvois, *Bromus biebersteinii* Roem. and Schult., *Elymus dauricus Turcz. exgriseb.*, *Festuca rubra* L., *Onobrychis viciifolia* Scop., *Elymus Canadensis* L., *Agropyron trachycaulum* (Link) Malte and *Medicago sativa* L. Establishment of the grass cover was gradual and the change in management was not expected to have a significant impact on the N_2O flux, as it would have been measured from the field in a cultivated state, until after the period of data collection reported here. However, to distinguish this transect from other site activities, this transect is referred to as the Seeded-Grass transect.

In total, N_2O fluxes were measured on all transect points 18 times between June 2003 and 2005. It is not possible to address all 18 data sets due to space limitations and instead five, consecutive transect samplings have been selected as a representative

subset to illustrate the main relationships. The first of the five samplings occurred on 30 Mar. 2004. At this time the transect had a snow cover of approximately 80%. A snow survey conducted on 24 Feb. found a mean snow depth of 18.4 cm and a mean snow water equivalent of 45.6 mm for the transect area. By the next sampling date, 4 Apr., the snow cover was reduced to 5% and the transect was snow free by 29 Apr., the third date. The transect was sampled again in the summer, 3 June and 23 June.

4.3.2 Soil N_2O Flux Measurements

Soil N_2O flux was measured at each location along the seeded-grass transect using a two-piece, closed, vented chamber (International Atomic Energy Agency, 1992) consisting of a polyvinyl chloride (PVC) ring base and vented cap with sampling port. Vent tube design was similar to that proposed by Hutchinson and Mosier (1981). Prior to the start of data collection, the bases were pressed into the soil and secured using 20 cm spikes where they remained for the duration of the field season. At each sampling event, the chamber was placed onto the base and sealed by a rubber ring within the cap. When attached to the base, the head space of each chamber was 2.25 L and covered a soil surface area of 0.02 m^2. Samples of the headspace gas were drawn from the chamber at time zero (t_0) and at 8, 16 and 24 minutes, with a 20-mL syringe and injected into 12-mL Labco Exetainer® (Labco Limited, UK) evacuated tubes for transport back to the laboratory. Gas sampling for each time interval was completed by a single individual moving from location to location every 45 s. This allowed for a complete transect sampling in less than 2 h. Gas sampling was timed to begin at midday. Samples were returned to the lab, placed in cold storage and analyzed in 1 to 2 wks.

Nitrous oxide concentrations were determined using a Varian CP3800 GC (Varian Canada Inc., Mississauga, ON) equipped with dual electron capture detectors (ECD). The injector temperature = 100°C, column temperature = 35°C, detector temperature = 370°C; separations were carried out using Poraplot Q columns (12.5-m × 0.32-mm i.d. fused silica capillary column, DF (film thickness) = 8 μm; includes a 2.5-m particle trap) with ultra high purity He (14.4 mL min^{-1}) as the carrier gas and P5 (95:5 v/v Ar:CH_4 mix) as the make-up gas (12.0 mL min^{-1}). The system was calibrated using standard gases (N_2O in N_2) obtained from PraxAir (Mississauga, ON). Internal

calibration curves were obtained by applying linear, least squares regression to the gas concentration (ppbV N_2O) *versus* peak area data; N_2O concentrations in the headspace samples were then calculated automatically from the regression equations.

Samples of ambient air were included in each analytical run as reference samples to check the 'within run' precision, calculate the minimum detectable concentration difference (MDCD), and correct for detector drift. The MDCD was calculated by (i) analyzing matched pairs of the reference gas samples at regular intervals during each analytical run; (ii) calculating the average difference between sample pairs (μ_p) as well as the standard deviation (σ_p); and (iii) calculating the MDCD using Eq. [4.1].

$$\text{MDCD} = \mu_p + (2\sigma_p) \qquad [4.1]$$

The MDCD was used to filter the raw data when calculating the actual N_2O flux; i.e., concentration differences between t_0 and each subsequent time step that were less than the MDCD were not considered to be significantly different from the t_0 concentration. The use of the MDCD is based on Anthony et al. (1995) where they used twice the mean absolute difference between pairs of ambient air samples. The MDCD used in this study provides a value that is within the upper bound of the 95% confidence interval for the mean paired difference and hence, provides a statistical basis.

The vertical flux of N_2O at the soil–atmosphere interface (ng N_2O-N m^{-2} s^{-1}) was calculated as the slope of the tangent to the concentration (ng L^{-1}) *vs*. time (min) curve at t_0. That is, the flux at t_0 was calculated as the 1st derivative of the 2nd-order polynomial equation ($y = at^2 + bt + c$) used to describe the concentration *vs*. time relationship. The flux (ng N L^{-1} min^{-1}) was then converted to an area basis by multiplying by the chamber volume / (surface area × 60 s min^{-1}). In cases where 'rogue' data points prevented the use of the 2nd-order polynomial model, the flux was calculated as the slope of the linear, least-squares regression equation that best described the concentration *vs*. time relationship (Hutchinson and Mosier, 1981). Our preference to use a polynomial equation to describe the concentration *vs*. time relationship was based on Anthony et al. (1995) who concluded that the linear model may represent a serious source of measurement bias. Our experience with flux measurements in the Canadian Prairie

region indicated that concentration vs. time relationship for soil N_2O flux is usually non-linear.

4.3.3 Wavelet Analysis

The use of wavelets in this study was as a tool of analysis and is not meant to be an exercise in wavelet analysis *per se*. This intention is reflected in the following basic explanation of the wavelet approach used in this study. For a comprehensive and mathematical understanding of wavelets see Kumar and Foufoula-Georgiou (1997). Si (2003) and Si and Farrell (2004) give an explanation of wavelets as applied to scale analysis of soil properties.

A wavelet is a mathematical function representing a small wave form. It is considered small because it is contained within a finite domain (Graps, 1995) in contrast to the sine and cosine functions used in Fourier analysis which stretch out to infinity (i.e., have infinite span and are globally uniform in time (Lau and Weng, 1995)). Thus, where Fourier analysis does a poor job in approximating sharp spikes in data – like that typical of soil N_2O emissions – wavelet analysis is well suited.

A wavelet transform takes a data series that represents a physical process and, like the Fourier transform, decomposes the variance of this process into series of coefficients representing the distribution of the variance across different frequencies (scales) and space (location) or time (Percival, 1995; Lindsay et al., 1996). Unlike the Fourier transform, the spatial context of the data is retained.

Scale analysis using wavelets is performed by contraction and dilation of the wavelet function. Contraction and dilation changes the size of the interval in time or space (window) that the wavelet function is applied to in the data series. Increasing window size increases the scale at which the coefficient for a particular location is calculated. In this manner a wavelet coefficient is obtained for each location in a data series over a range of scales and thus, the scale of analysis is matched to the size of the feature(s) in the data series.

There are various types of wavelet transforms and generally are grouped as continuous or discrete (Si and Zeleke, 2005). Several types of discrete wavelets are orthogonal so there is no redundant information between wavelet coefficients and scales

are discrete. This makes discrete wavelets very useful for data compression. Continuous wavelets are not orthogonal and therefore there is overlap between wavelet coefficients resulting in redundant information between scales and locations and making the continuous wavelet very useful for scale analysis (Si, 2003). The mother wavelet is rescaled by powers of two; hence, a data series that contains a binary number of points is optimal for computation speed (Si, 2003).

There are several types of wavelets (see Kumar and Foufoula-Georgiou, 1997) and it is important that one chooses a wavelet that is appropriate for the objectives of the proposed analysis. The wavelet chosen for this study was the Mexican Hat which is continuous wavelet that is sensitive to peaks in data (Si, 2003), such as one would expect in soil N_2O emission. The Mexican Hat (Eq. [4.2]), a 2nd derivative of a Gaussian function,

$$\psi(x) = \frac{-1}{\sqrt{\Gamma(2.5)}} \frac{\mathrm{d}^2}{\mathrm{d}x^2}\left[\exp(-0.5x^2)\right] \qquad [4.2]$$

as described by Si and Farrell (2004) where $\Gamma(\ )$ is the Gamma function.

In the continuous wavelet transform, after Si and Farrell (2004), y(x) is a spatial series with y representing the measurement and x representing the location (Eq. [4.3]).

$$W(\eta,\tau) = \int_{-\infty}^{\infty} y(x)\psi^*_{\eta,\tau}(x)\mathrm{d}x$$

$W(\eta,\tau)$ is the wavelet coefficient that is the integral of the product of $y(x)$ and $\psi_{\eta,\tau}(x)$ as of function of the scaling parameter (η) where

$$\psi_{\eta,\tau}(x) = \frac{1}{\sqrt{\eta}}\psi_{\eta,\tau}\frac{(x-\tau)}{\eta} \qquad [4.4]$$

This allows the wavelet function to calculate a wavelet coefficient for each scale over a range of scales (expands or contracts the scale over which a coefficient is calculated) and the spatial translation (τ). The spatial translation (τ) is the factor that shifts the function ($\psi_{\eta,\tau}(x)$) from one location (x) to another along the spatial series to obtain a wavelet coefficient for each location. Thus, a wavelet coefficient is calculated for each location at each scale.

The continuous wavelet transform is implemented using fast Fourier transform. The local wavelet spectrum is obtained by squaring the wavelet coefficient for each scale at each location and is plotted as a 2 dimensional field of values of wavelet variance. Edge effects were controlled by zero padding of the data set to 256 from 128 points. Edge effects are the result of the start and end of the data set acting similar to an abrupt change in value which can influence the coefficients determined for points away from the ends. This effect also tends to increase with increase in scale. The Mexican hat wavelet is also a good choice in this regard because it is less susceptible to edge effects because it is narrow and has less oscillations than other wavelets (Si and Farrell, 2004).

To test the significance of the local wavelet spectrum we used a permutation test (Pardo-Iqúzquiza and Rodríquez-Tovar, 2000) that compared the global wavelet spectrum for each original data series against the global wavelet spectrum for multiple reordering of the data series. The premise of a permutation test is that if a spatial pattern exists in a data series then a random reordering of the series will destroy this pattern. If the reordering of the series is performed multiple times then the chance of recreating the data series with the original spatial pattern can be determined. In this case, the null hypothesis is that all scales in the power spectrum of the original series will not be significantly different from the power spectra, below a predetermined significance level, of the multiple random realizations of the series. A significance level (5%) can be applied by sorting the power spectra of the multiple random realizations into increasing order and using the highest power spectrum for the first 95% of these spectra as the level of power that is required to be surpassed in order to reject the null hypothesis.

The global wavelet spectrum is the average of local wavelet spectra ($W_{(\eta,\tau)}$) over all locations of a spatial series and can be written as:

$$\overline{W}^2(\eta) = \frac{1}{N}\sum_{i=0}^{N-1}\left|W(\eta,\tau_i)\right|^2 \qquad [4.5]$$

with N as the number of data points in the spatial series. The global wavelet power spectrum provides an estimation of the contribution of variance at any particular scale. For the permutation test, 1000 random realizations of the data series were generated from consecutive data pairs (Pardo-Iqúzquiza and Rodríquez-Tovar, 2005). The power

spectrum of each realization was determined and sorted in increasing order. If the wavelet power of the original spectrum, at a specific scale, fell with the wavelet power of the 950 out of 1000 realizations, then the null hypothesis was not rejected for that particular scale.

The use of consecutive pairs instead of individual data points incorporates the concept of red noise into the permutation test. Red noise is a measure of the background variability that is inherent to soil landscapes because of the short range dependency between adjacent locations (autoregressive process of 1 lag) that occurs simply because of their close proximity (Torrence and Compo, 1998) and resulting sedimentary, hydrological and biological communication. As the distance between locations increases (increasing scale), the variance of the soil property increases, like that of red noise (Si and Farrell, 2004). The question is whether an increase the variance is due to the imposition of order on the distribution of soil properties by processes such as, for example, topographic variation, or is it due simply to an increase in the red noise with an increase in scale? Alternatively, the use of individual data pairs would assume that the background variation is completely random (white noise) and that there is no autocorrelation between soil properties. Other significance tests of the local wavelet power spectrum require comparison of Gaussian white or red noise with the wavelet spectrum (Si and Zeleke, 2005; Si and Farrell, 2004). This assumes normally distributed data, which is an invalid assumption in our case. The permutations test is non parametric (Pardo-Iqúzquiza and Rodríquez-Tovar, 2005).

The local wavelet spectrum is presented as a contour map of wavelet coefficients that represent highs and lows in variance and which are plotted according to the distance (m) along the transect and the scale (m) of the variation. Darker shades are associated with higher wavelet variance. Each spectrum has been contoured with the same intervals and shades. The interpretation of the wavelet spectrum is visual. Peaks in wavelet variance are represented by contours that form concentric patterns, like a bull's eye or target. Features of interest are areas of high variance that appear as repetitive peaks in the contours such that they form a series along the x axis of the figure within a narrow scale range (a global event) or as a single, non-repetitive high in variance at a discrete location on the x axis (localized event) (Si and Farrell, 2004). A series of

repeated features is an indication of cyclic behavior and the period of that cycle is the scale of the underlying process. Localized features do not cycle and therefore cannot be assigned to a particular scale. The scale range assigned to a series of repetitive features is that along which the centers of these features have a tendency to line up. Thus, a global feature consisting of a series of repetitive highs in wavelet variance may have peaks that occur at various scales (44, 53, 59 m, for example) however they will be described as a global feature that is controlled by an underlying process that cycles over a 40 to 60 m range in scale.

The global wavelet spectrum for each sampling date to be discussed was determined and compared to the 95% significance level that was also determined for the same date (data not shown). The result was that on some days not all the scales presented in the local spectra were significant. On those spectra for which all the scales were not significant, the non-significant scales, and the anomalies included in those scales, were indicated in the figure caption. The scales (m) that are indicated as non-significant in the local spectrum were scales at which the global wavelet variance was equal to or less than the 95% significance level (i.e., the null hypothesis could not be rejected). The purpose of this was to be clear on the significance of the scales compared to the 95% significance level, but allow the reader to view all the anomalies because, although non-significant, they may still be of interest.

4.3.4 Measurement of Soil Moisture and Soil Temperature

Time domain reflectometry (TDR), after Topp and Ferre (2002), was used at each location on each sampling date (except 30 Mar.) to measure soil moisture content over the 0 to 15 cm depth. On 30 Mar. frozen ground prevented use of the TDR. Readings were taken manually using a Tektronix 1502 B cable tester (Tektronix, Wilsonville, OR). The soil temperature was measured at the 5- and 20-cm depths using buried T type thermocouples made with twisted wire pairs of copper and constantan (45% Ni and 55% Cu) and read with a Barnant DuaLogR™ thermocouple reader (Barnant Company, Barrington, IL).

4.4 Results

4.4.1 Soil N_2O Flux Measurements

Yates et al. (2006a) (Chapter 3) provides summary statistics of soil N_2O flux for the 15 transect samplings. A subset of that data for the five successive transect samplings in spring of 2004 is shown in Table 4.1. All means were characterized by a high standard deviation. The highest mean flux was on 4 Apr. and highest range in values was 29 Apr. The high flux measurements in Apr. had reverse J-shaped distributions. The mean fluxes of 30 Mar. and 3 June were one order of magnitude lower than that of Apr., and this data was log-normally distributed. The mean flux on 23 June was negative and the data was symmetrical (nearly normal) in distribution.

Table 4.1: Mean N_2O flux (ng N_2O-N m^{-2} s^{-1}), standard deviation, range, and distribution shape for the first five sampling dates at the seed grass transect at St. Denis transect in 2004.

Sampling Date	Mean	Standard Deviation	Range	Distribution Shape
30 Mar.	2.3	4.8	30.0	Log Normal
4 Apr.	25.3	50.5	510.9	Reverse J-shaped
29 Apr.	17.3	92.7	884.3	Reverse J-shaped
3 June	4.3	5.8	37.4	Log Normal
23 June	-0.2	1.9	15.4	Symmetrical

4.4.2 Local Wavelet Spectrum and Scales of Variation

Local wavelet spectra for the five sampling dates are shown in Figures 4.1 through 4.5. Included with each spectrum is relative elevation and individual flux measurements. Two CW and three UW were identified. The relative elevation also shows a depression-like feature at the north end of the transect, but an east-trending slope prevents it from holding water like a true CW (data not shown).

The individual flux measurements for 30 Mar. ranged between -7.8 and 22.3 ng N_2O-N m^{-2} s^{-1} (Fig. 4.1). High fluxes were associated with CX elements. Negative fluxes were more prevalent at the north end of the transect. The local wavelet spectrum shows three scales of variation. There was a band of repeated, narrow features at scales between 5 and 25 m. Between approximately 40 and 60 m in scale there was a set of wider, higher variance anomalies and from approximately 80 to 100 m scale there was a set of three broad anomalies. According to the permutation test (data not shown) only scales greater than 55 m were significant ($p < 0.05$).

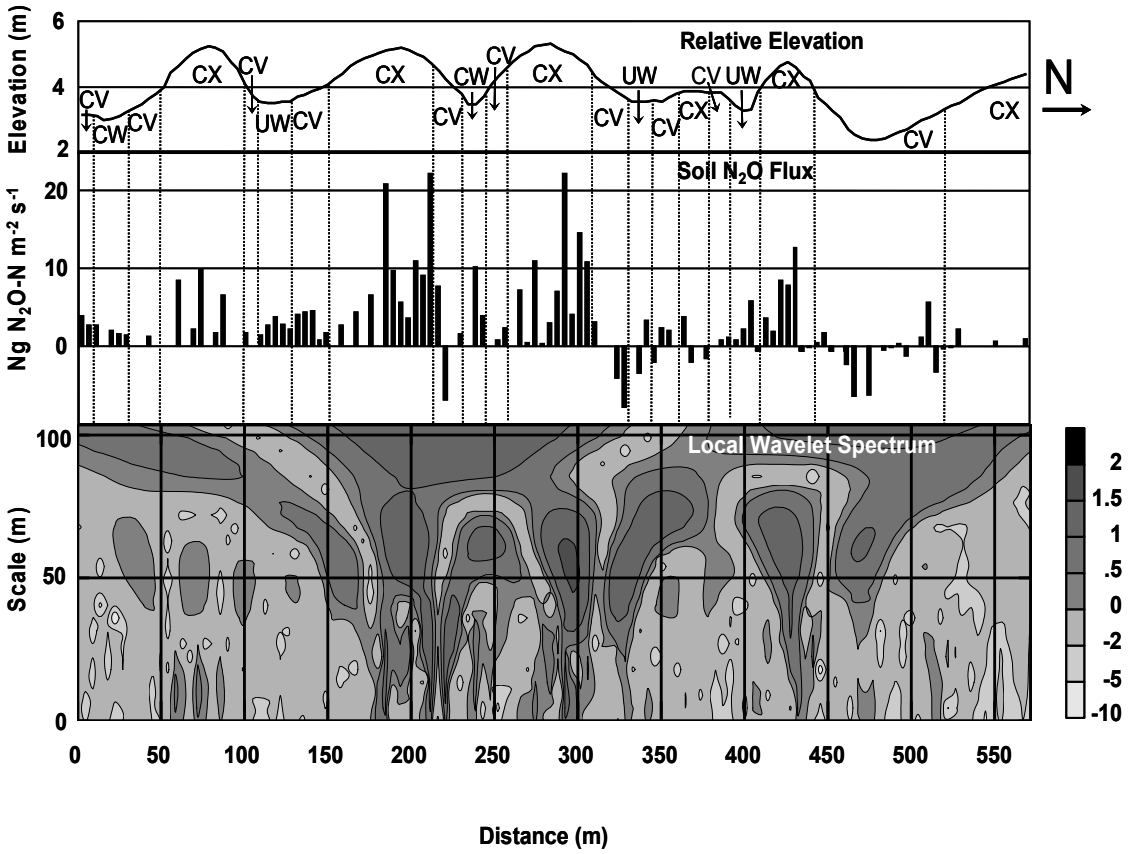

Figure 4.1: Relative elevation, soil N_2O flux, and local wavelet spectrum for Seeded-Grass Transect, 30 Mar. 2004. Landscape elements are convex (CX), concave (CV), cultivated wetland (CW) and uncultivated wetland (UW). Shaded bar is log of wavelet variance. Scales < 55 m are not-significant according to a permutation test ($P < 0.05$).

On 4 Apr. individual fluxes increased by an order of magnitude or more at several locations (Fig. 4.2). Fluxes ranged from 0.0 to 510.9 ng N_2O-N m^{-2} s^{-1}. Fluxes were low in all CW and UW elements. High and extreme flux values were associated with CV elements. At approximately 145 and 320 m, the flux was highest. The local wavelet spectrum showed a broad, discontinuous band of features that peaked within a scale range of 30 to 50 m. At 320 m there was an intense anomaly in wavelet variance that cuts across nearly the full scale range. This was a local feature that was associated with the high flux value at that location. The permutation test (data not shown) indicated that scales < 30 m and > 65 m were not significant (Fig. 4.2).

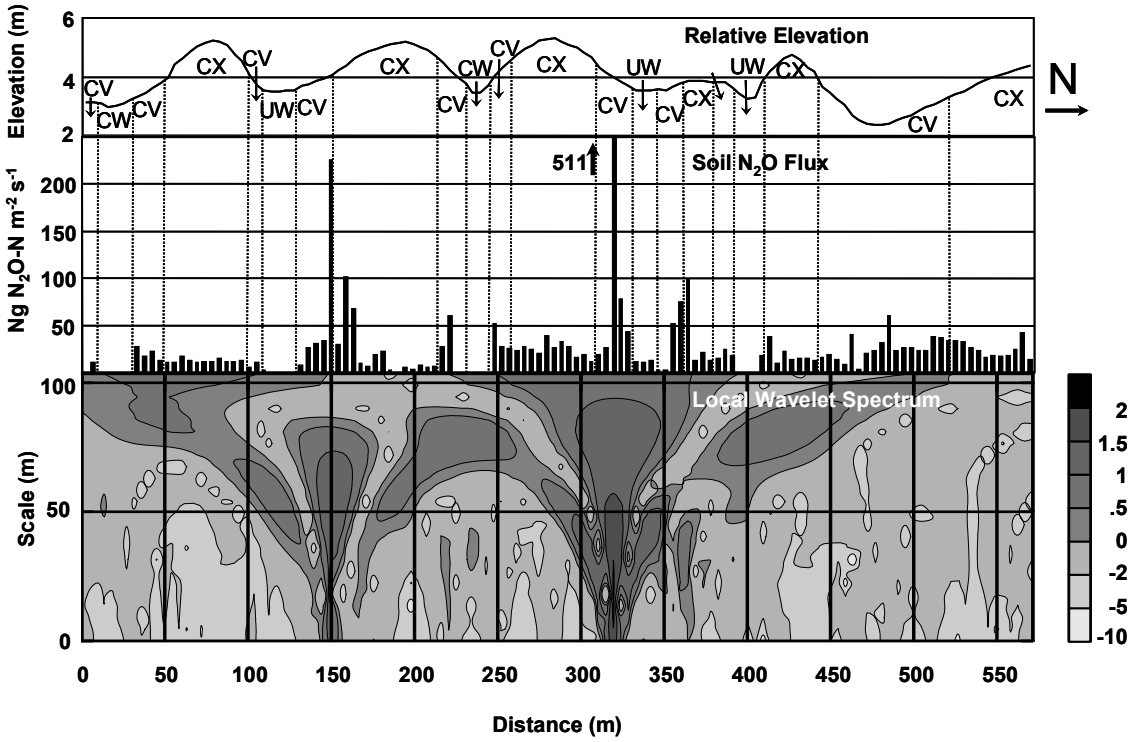

Figure 4.2: Relative elevation, soil N_2O flux, and local wavelet spectrum for Seeded Grass Transect, 4 Apr. 2004. Landscape elements are convex (CX), concave (CV), cultivated wetland (CW) and uncultivated wetland (UW). Shaded bar is log of wavelet variance. Scales < 30 m and > 65 m are not-significant according to a permutation test ($P < 0.05$).

The distribution of fluxes along the transect on 29 Apr. was different from the preceding date (Fig. 4.3). The fluxes ranged from -8.2 to 876 ng N_2O-N m^{-2} s^{-1}; however most, excepting the extreme values between 225 and 245 m, were < 21 ng N_2O-N m^{-2} s^{-1}. The cluster of extreme values was associated with the larger CW element. Fluxes were generally higher on the south and included negative values. The local wavelet spectrum was dominated by a local feature at 235 m , across all scales, which corresponded to the cluster of extreme values at the CW element. The local spectrum south of this local feature indicated some weak, cyclic behavior in the flux pattern at a 20 to 40 m scale. The cyclic pattern is not developed in the north. According to the permutation test (data not shown) scales > 30 m were significant ($p < 0.05$).

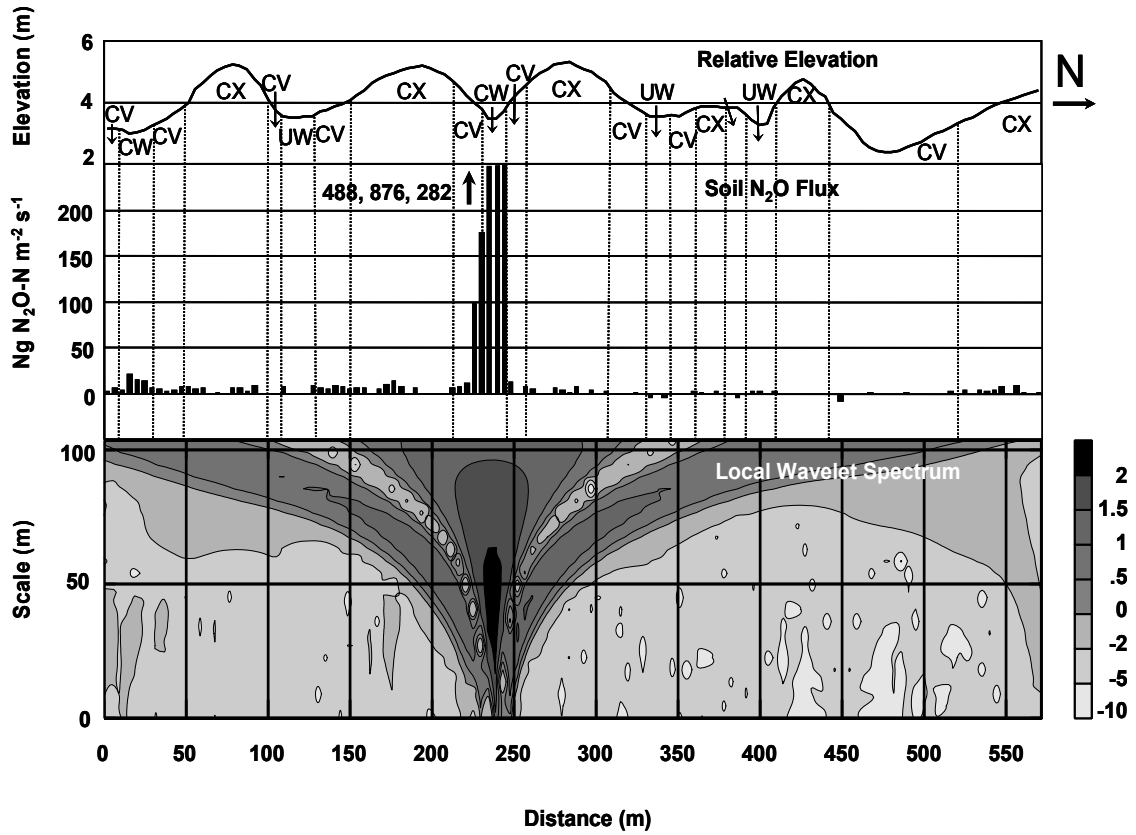

Figure 4.3: Relative elevation, soil N_2O flux, and local wavelet spectrum for Seeded-Grass Transect, 29 Apr. 2004. Landscape elements are convex (CX), concave (CV), cultivated wetland (CW) and uncultivated wetland (UW). Shaded bar is log of wavelet variance. Scales < 30 m are not-significant according to a permutation test ($P < 0.05$).

The flux pattern for 3 June was similar in magnitude and distribution to that observed on 30 Mar. (Fig. 4.4). The fluxes ranged from -7.9 to 29.5 ng N_2O-N m^{-2} s^{-1}. Unlike 30 Mar., higher fluxes were associated with CV and CW elements. The local wavelet spectrum showed three cyclic patterns: a small-scale band at <25 m, a mid-scale band between approximately 40 and 60 m, and a large-scale band >75 m. Similar to 30 Mar. only scales greater than 65 m were significant ($p < 0.05$).

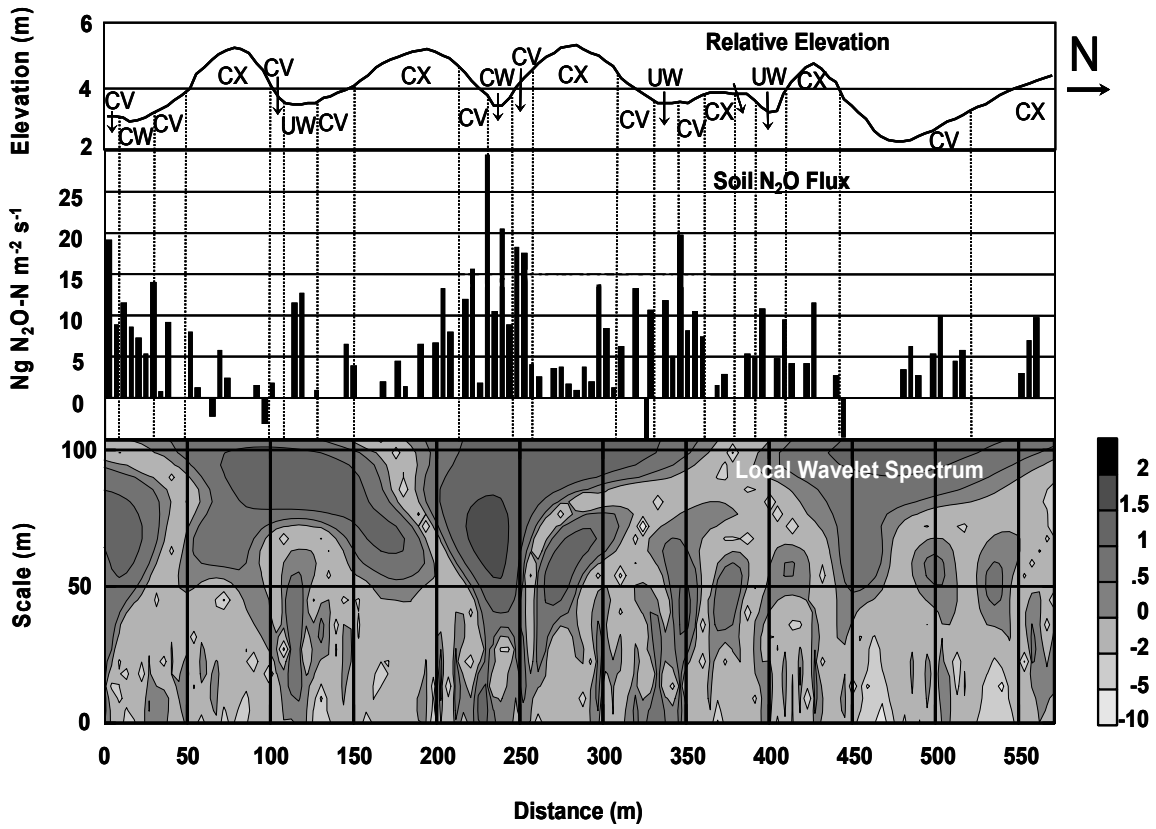

Figure 4.4: Relative elevation, soil N_2O flux, and local wavelet spectrum for Seeded-Grass Transect, 3 June 2004. Convex (CX), concave (CV), cultivated wetland (CW) and uncultivated wetland (UW) landscape elements are indicated. Color bar is log of wavelet variance. Scales < 65 m are not-significant according to a permutation test ($p < 0.05$).

Activity was greatly reduced by 23 June. Fluxes ranged from -10.2 to 5.2 ng N_2O-N m^{-2} s^{-1}, although at most locations the flux was 0 (Fig. 4.5). There did not appear to be any association between fluxes and landscape elements. The local wavelet spectrum indicated a weak cyclic band within a scale range <25 m and a weak cyclic band at approximately 35 to 55 m. Neither pattern was strongly developed and the spectrum at all scales was not significant.

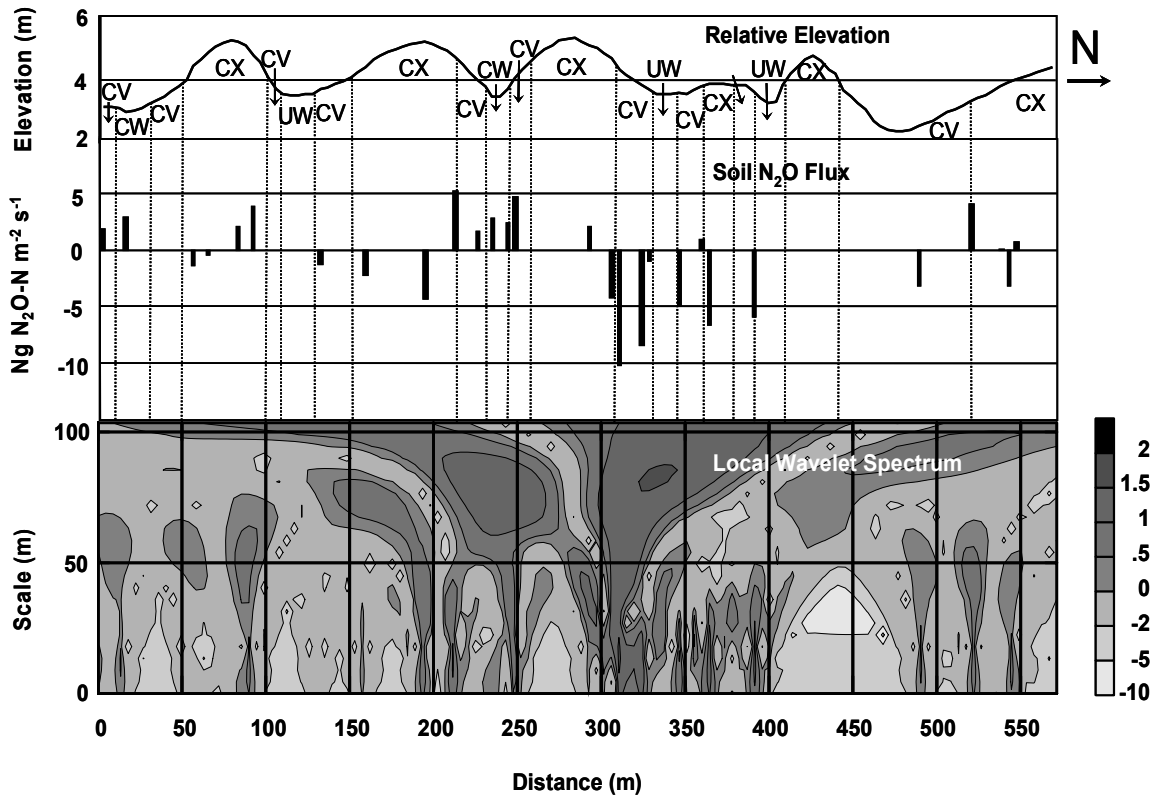

Figure 4.5: Relative elevation, soil N_2O flux, and local wavelet spectrum for Seeded-Grass Transect, 23 June 2004. Convex (CX), concave (CV), cultivated wetland (CW) and uncultivated wetland (UW) landscape elements are indicated. Color bar is log of wavelet variance. All scales are not-significant according to a permutation test ($p < 0.05$).

4.4.3 Soil Moisture and Soil Temperature

The soil moisture and temperature data is presented in Table 4.2 as mean values per landscape element on each sampling date. The soil moisture data is shown as WFPS (%). In place of WFPS for 30 Mar. is given the number of locations that were free of snow for each landscape element. On 30 Mar. the majority of exposed locations were on CX elements. Mean WFPS was highest (> 80%) for all elements on 4 Apr. after which it declined except for CX and CV elements where it increased between 29 Apr. and 3 June. By 23 June mean WFPS was almost 60% for CW elements and < 60% for CX, CV and UW elements. The highest variation in mean WFPS was in UW elements.

The soil temperature at both depths for all elements on 30 Mar. was < 0.0°C. By 4 Apr. soils remained frozen at the 20-cm depth, but by 29 Apr. the soil at all elements had thawed. Overall the CX elements had the highest mean soil temperatures and the

UW elements had the lowest; however the range in values on any particular date between elements at the same depth is less than 10 ºC.

Table 4.2: Number of bare soil locations on 30 Mar. and mean water-filled pore space (%) and mean soil temperature at the 5- and 20-cm depths with standard deviation (in brackets) for convex (CX), concave (CV), cultivated wetland (CW) and uncultivated wetland (UW) landscape elements at the seeded grass transect, St. Denis, SK in 2004.

		30 Mar.†	4 Apr.	29 Apr.	3 June	23 June
CX	WFPS	25	83 (14)	58 (7)	72 (13)	58 (9)
	5 cm	-0.9 (0.6)	3.9 (1.3)	2.6 (0.6)	20.2 (3.0)	21.2 (1.5)
	20 cm	-1.0 (0.4)	-0.6 (0.3)	1.5 (0.4)	14.0 (0.9)	14.3 (0.7)
CV	WFPS	3	87 (13)	57 (6)	71 (13)	56 (8)
	5 cm	-0.9 (0.6)	3.1 (1.8)	2.3 (0.7)	19.7 (1.9)	19.5 (2.0)
	20 cm	-1.0 (0.4)	-0.8 (0.4)	1.4 (0.5)	13.4 (2.0)	13.7 (0.9)
CW	WFPS	0	100 (0)	80 (14)	79 (8)	63 (4)
	5 cm	-1.0 (0.4)	‡	2.2 (0.3)	18.8 (0.7)	18.3 (1.3)
	20 cm	-1.1 (0.2)		1.8 (0.3)	12.7 (0.3)	12.8 (0.5)
UW	WFPS	0	90 (15)	67 (24)	60 (21)	55 (19)
	5 cm	-1.0 (0.5)	0.7 (1.6)	2.0 (0.6)	14.0 (2.6)	12.9 (1.8)
	20 cm	-0.4 (0.3)	-0.3 (0.3)	2.2 (1.1)	11.2 (0.6)	10.7 (0.7)

† Water-filled pore space absent for 30 Mar. due to frozen soil. Number of bare soil locations given to provide some indication of soil conditions on this date.
‡ Soil temperature absent for CW elements on 4 Apr. due to flooding.

4.5 Discussion

Nitrous oxide flux measurements from soils in the Canadian Prairie region on hummocky, agricultural landscapes are not common. However, on an undulating, agricultural landscape Pennock et al. (2005) reported means from several crop types ranging from 11.7 to 32.2 ng N_2O-N m^{-2} s^{-1} for non-manured soil. Corre et al. (1996) reported a median value of 1050 µg N_2O-N m^{-2} d^{-1} (12.2 ng N_2O-N m^{-2} s^{-1}) for measurements from unfertilized, fallow, agricultural land. Both studies report spring measurements made in the Black soil zone of Saskatchewan. Hence, the highest mean value of N_2O flux obtained from the St. Denis site (25.3 ng N_2O-N m^{-2} s^{-1}) is within the range of values available.

The probability distribution of the N_2O flux data and the mean N_2O flux are both a product of the control that landform position and land use have on the distribution of

fluxes measured along the transect. This can be clearly observed in the local wavelet spectrum. On 30 Mar. fluxes are measured from the snow surface and the small areas of exposed soil at CX elements where snow cover was thinnest and first to melt away. High variance features in the spectrum were associated with peaks in N_2O flux at the exposed CX elements and the low or negative N_2O fluxes in-between. This repetition of N_2O flux pattern, due to the CX elements resulted in the cyclic pattern observed in the wavelet spectrum. The exposed areas on the CX elements were more numerous in the middle portion of the transect (175 to 300 m), thus there were higher fluxes in this portion of the transect resulting in the large variation observed in the local wavelet spectrum at scales of 80 to 100 m. Compared to later dates, the flux values for 30 Mar. were low (mean value 2.3 ± 4.8 ng N_2O-N m^{-2} s^{-1}) but there was a high number of locations at which a flux was measurable (Table 4.1).

By 4 Apr. the majority of the transect was snow free and snow melt water had concentrated in the CW and UW elements resulting in mean WFPS as high as 100% (Table 4.2). Mean N_2O fluxes increased by an order of magnitude (Table 4.1) and a shift in the position of the peak fluxes from the CX elements down-slope to the CV elements occurred (Fig. 4.2). Extreme values in the data set also increased in magnitude resulting in a greater range in measured N_2O flux values, severely skewing the data and changing the probability distribution shape from a log-normal to a reverse J-shaped (Table 4.1). The distribution of variance (according to the local wavelet spectrum) showed periodicity at a scale of 30 to 50 m associated with both the low fluxes from the flooded CW and UW elements and the high to extreme flux values from the CV elements (Fig. 4.2). The spectrum also showed the influence of the extreme value at 320 m which appears as a non-repetitive variance anomaly (i.e., localized feature).

The effect of a localization of variance is taken to the extreme on 29 Apr. Overall fluxes decreased with the exception of the large CW element near the middle of the transect (Fig. 4.3). Here the soil was wettest (Table 4.2), probably because snowmelt runoff was retained here the longest, while at other locations the soil had dried. The result was a concentration of locations emitting a flux at the same order of magnitude as the previous date, although the activity along the rest of the transect was much lower.

The concentration of variance in this one location overshadowed the cyclic pattern of low level of activity present along the majority of the transect.

The wavelet spectrum for 3 June was similar to that of 30 Mar. On the 3rd of June wavelet spectrum of soil N_2O flux on the transect indicated three scales of spatial variation, as they were on 30 Mar. (Fig. 4.4). As well, there are no strong localized features present. The highs in variance on 3 June were at a scale of 40 to 60 m and were associated with peaks in flux that occurred primarily in CW and UW elements, although mean flux had dropped by one order of magnitude since the last sampling date (Table 4.1) and these highs in variance were non significant. The lack of local features indicates that the extreme values needed to skew the distribution to a reverse J-shape were absent. Hence, the distribution had returned to log-normal, as was the data for 30 Mar. The large-scale, significant variation evident in the spectrum appears to be related to the high overall fluxes in the middle portion of the transect; however on this date the highest fluxes were from the CW and not the CX elements as it was on 30 Mar.

Between 3 June and 23 June soil N_2O flux continued to decrease. The weak cyclic pattern in the < 25 m scale range reflected the alternation between positive and negative fluxes and had no direct connection to the landscape elements, hence its non significance. The low variance, random spatial pattern on this day is confirmed by a symmetrical distribution of flux values about zero and a net negative mean flux.

The local wavelet spectra demonstrated that landscape position can be an important control on the spatial variation in soil N_2O emission. Landform imposed a periodicity to the distribution of the fluxes and controlled the occurrence of the non-stationary, localized features that were strong contributors to the mean N_2O flux magnitude and variance. The local wavelet spectra also demonstrated that a certain type of landscape position determines the spatial variation of N_2O flux on a specific date, but the type of position important to the spatial variation will change between dates. For example, through the first four sampling dates, the landscape positions of importance changed in the order: CX, CV, CW, and UW/CW.

There is a definite down-slope trend in the above order that indicated the importance of the redistribution of water in the landscape during spring snowmelt. Wind scouring during winter removes snow from high areas between depressions

(catchment boundaries) where CX elements are found (Hayashi et al., 1998a). Thin snow cover on CX elements lead to first exposure of soil at these positions. The air temperature at the Saskatoon Airport for 30 Mar. ranged from -1.4 to 16.8 ºC (Environment Canada, 2005c). Thus, snow melt was proceeding, limited by cool temperatures, and the soil was still frozen at the 5-cm depth. Under these conditions a thin, wet, active layer formed on the soil surface because the snow melt water was prevented from infiltrating, and created and the conditions for denitrification. As snowmelt accelerated and completed, water flowed into CW and UW elements resulting in flooded soils with a high WFPS, but the water surface prevented major fluxes from occurring at these positions; however, exposed, soils with a WFPS high enough to promote denitrification were possible at the CV elements on the margins of the pooled water. As the water receded at CW positions, the exposed soils were temporarily at a WFPS conducive to denitrification while soils at the topographically higher CV and CX positions had already dried and flux had diminished.

It is clear that the topography did control the timing and distribution of the major fluxes during the spring period at the St. Denis site; however, this trend does not explain the relatively low fluxes from CX elements on 4 Apr. or 3 June when the mean WFPS for that element was high (Table 4.2). Although there is no data to support this, our assumption is that the available N at CX elements was limiting. Hydrolysable N (Gianello and Bremner, 1986) is considered to be a measure the labile N pool and has been found to be lowest in soils on topographically high positions in hummocky terrains (Walley et al., 2002).

In addition to the control that the redistribution of water had on the spatial pattern of the N_2O flux was the control that soil temperature and land use had on the spatial pattern. Frozen soil can act as a barrier to the infiltration of water if soil pores are blocked with ice, as observed in agricultural soils by Granger et al. (1984). In our study, the reduced drainage maintained a high WFPS and allowed formation of the thin, active layer at CX positions that lead to the 30 Mar. spatial pattern of fluxes. The absence of major fluxes in the UW elements suggests that soils under long-term vegetated growth may not experience extreme flux events, perhaps due to high porosity and better soil aeration. As described above, soils in UW have much lower bulk densities. It is also

possible that available N may have limited N_2O emissions from UW elements as it may have at CX elements. Perhaps the perennial growth of vegetation in the UW elements results in differences in N cycling between cultivated and non-cultivated elements.

If higher soil porosity and better soil aeration as well as reduced available N is indeed responsible for the absence of major fluxes in the UW elements, then this has implications in regards to best management practices (BMPs) that might be employed to reduce soil N_2O emissions produced from agricultural activities in these types of terrains. These results suggest that removing CW elements from cultivation and allowing some form of restoration to a land use represented by the UW element is a logical management practice that would reduce yearly emissions. The assumption is that such a change in land use would promote an increase in soil porosity at locations within former CW elements improving soil aeration and minimizing the peak in N_2O flux that occurs at these locations in the spring. However, the degree of restoration required, a range from establishment of a permanent grass cover with periodic forage removal to no equipment activity with an introduction of tree species, is unknown. Also unknown is the time required under such a new management practice to see significant reductions in emissions. These unknowns open the door to new and valuable field research.

The role of landform was critical to the event-based emission pattern present in this terrain. The "event" was the spring snow melt that began just prior to 30 Mar. Landform controlled the pattern of emissions from the outset. As melt water began to concentrate in the landscape the high N_2O fluxes that created the event-based pattern developed quickly and were markedly displayed in the wavelet spectra for 4 Apr. and 29 Apr. As melt water evaporated from- and infiltrated into the soil, moisture conditions necessary for the extreme fluxes produced by the event diminished. The spatial effects of the event decayed towards a background emission pattern. Thus the event-based pattern itself evolved, and the course of this evolution was dependent on factors such as distribution of the snow pack (i.e., which locations are exposed first), redistribution of snowmelt and resulting soil moisture conditions, land use and bulk density.

Although this pattern evolves, there is some continuity from date to date in the scales of variation associated with soil N_2O emission. Although not always significant, the scale of variation that is related to the landscape ranged between 20 and 60 m across

the five data sets depending on the landscape element controlling the highest fluxes. This is interesting because Velthof et al. (2000) found temporal stability in the spatial pattern of soil N_2O flux in the short term (4 d), but observed that the range of spatial dependence increased over the duration of their study.

The short- and long- range variations were not always evident or significant in the wavelet spectrum due to the influence of localized features on the distribution of variance. The localized features were associated with different landscape elements on different dates, but their occurrence was of shorter duration than the cyclic pattern of emissions. The localized features essentially represented a pattern of emission that was super-imposed on the background emission pattern because of the snow melt event.

The local wavelet spectra demonstrate that in a hummocky topography, such as at the St. Denis site, we may add spatial context to the event-based, background emission model proposed by Brumme et al. (1999) and this has implication for measurement of fluxes in these terrains for inventory and up-scaling purposes. The temporally stable, landscape controlled cyclic pattern of emissions could be monitored using a sampling design with a minimum number of locations based on the spatial scale. The temporary, localized pattern of emissions could be monitored by stratifying the landscape into elements that capture a range of CV and CW units and sampling a randomly chosen subset to monitor with particular attention to the critical spring snowmelt period. This may work because the spring flux event was not random, but occurred at specific elements in the landscape during a specific period of time. Certainly this research would need to be confirmed by repeat findings in other sites with hummocky topography.

The control of landscape position on the spatial variation of soil N_2O emission and the change in spatial variation over time was tied to the control that landform had on the redistribution of water. Wavelet analysis provided us with spatial information on the cyclic and non-stationary processes controlling soil N_2O over a period of active water redistribution and demonstrated that this technique can be applied to the relationship between landscape position, soil moisture and soil N_2O emission. As well, the location and impact of peak fluxes on the variability in N_2O emissions is clearly illustrated

allowing for the development of management strategies that may reduce the emissions at peak times.

4.6 Conclusions

The two objectives of this chapter were to use wavelet analysis to examine the distribution of localized variance of soil N_2O flux, and to identify the important scales of variability and their temporal stability for these fluxes for a hummocky agricultural landscape. The local wavelet spectra showed that the distribution of variance was associated with landscape over a 20- to 60-m scale range. Date-to-date variation within this range of scales was due to the changing spatial pattern of N_2O flux; however, this scale was generally temporally stable. The spatial pattern changed as specific landscape elements became sources of peak N_2O flux and then declined as peak emissions moved to positions down-slope. The order of landscape elements with peak fluxes over the first four sampling dates was CX, CV, CW, and UW/CW. The shift in peak flux between landscape elements was driven primarily by the pattern of snowmelt and the redistribution of water in the landscape. Extreme fluxes from specific landscape elements, represented by localized features in the wavelet spectrum are part of the fluid spatial pattern, but are of shorter duration and can be thought of as an event-based emission pattern superimposed on the background emission pattern. The wavelet analysis clearly identifies these localized features as non-cyclic and, therefore, not associated with a specific spatial scale.

The results suggest that the distribution of fluxes in, general, have implications regarding best management practices designed to reduce soil N_2O emissions, and that the cyclic and non-cyclic pattern of emissions has implications for measurement of soil N_2O in these landscapes. These are directions that should be taken in their own right with the data from St. Denis and future research projects

5.0 TIME, LOCATION AND SCALE DEPENDENCE OF SOIL NITROUS OXIDE EMISSION, WATER AND TEMPERATURE USING WAVELETS, CROSS WAVELETS, AND WAVELET COHERENCY ANALYSIS

5.1 Preface

The wavelet analysis in chapter 4 showed that the event-based / background emission pattern introduced in chapter 3 could be described as a combination of global and local features representing the distribution of variance in soil N_2O flux along the transect. The local features stand apart from the global distribution in variance in that they do not represent cyclic behavior and cannot be associated with a particular scale of variation. This immediately indicates that measuring or modeling soil N_2O flux in this landscape may have to involve more than one approach. It must then be known if the relationship between soil N_2O flux and controlling factors such as soil water and soil temperature also fits into the two patterns. Wavelet coherency analysis uses local wavelet coefficients to describe the distribution of the dependency of one variable on another and can show how the correlation is likely to change spatially. Examining more than one sampling date will demonstrate if there are temporal changes.

5.2 Introduction

Nitrous oxide (N_2O) is a reactive greenhouse gas whose atmospheric abundance appears to be increasing at a rate of 0.8 ppb yr^{-1} and has a 100 yr global warming potential 296 times that of carbon dioxide (CO_2) (IPCC, 2001). The primary sink for N_2O is photo-oxidation in the stratosphere to nitric oxide (NO) leading to consumption of ozone in a catalytic reaction (Cicerone, 1987).

Flux estimates and information on the important variables controlling sources of N_2O at specific scales are needed to use and validate atmospheric models (Asman et al., 1999). Although N_2O has a variety of sources, including industrial activities and the

burning of fossil fuels, agriculture and the use of mineral fertilizers is considered the most important (FAO and IFA, 2001). It was estimated that in 1996 soils were responsible for 50% of the N_2O emissions due to agriculture in Canada (Agriculture and Agrifood Canada, 1998a). It is well known that measurements of soil N_2O emission are plagued by wide spatial and temporal variability (Parton et al., 1988; Parkin, 1987; Folorunso and Rolston, 1984). This variability in N_2O measurements at the surface-atmosphere interface leads to uncertainty in flux estimates in addition to the uncertainty that exists in model assumptions, parameters and representations of controlling processes that are required to extrapolate flux estimates from small to regional or global scales (Lapitan et al., 1999).

The bulk of soil N_2O is produced by respiratory denitrification (Tiedje, 1988), although it is also produced as a by-product of nitrification (Skiba et al., 1993). Emissions resulting from either process are dependent on the level of available oxygen (O_2), carbon (C) and nitrogen (N) (Robertson, 1989). Denitrification occurs in anaerobic soil microsites (Parkin, 1987) created when rate of O_2 diffusion cannot meet the demands of consumption (Tiedje, 1988). The presence of water in soil pores and as films on soil aggregates slows the diffusion of O_2 (Renault and Stengel, 1994). Soil water content is in turn controlled by a variety of factors operating at a range of spatial and temporal scales. Seasonal changes in precipitation and temperature control long- and short-term changes in soil moisture status in addition to availability of C and N (Groffman et al., 2000). As well, topography controls the redistribution of water inputs to a landscape controlling the spatial distribution of denitrification (Pennock et al., 1992).

Using wavelet analysis to show the distribution of variance in soil N_2O emission in a hummocky topography, Yates et al. (2006b) (Chapter 4) demonstrated that there were two patterns to emissions in this landscape. The first was a landscape controlled cyclic pattern that operated over a narrow scale range. The second was characterized by non-cyclic (non-scalable) highly localized features. Both patterns were the result of climatic conditions and the redistribution of moisture inputs in the landscape. This knowledge may benefit model development; however greater improvements may be made by an understanding of the relationship between soil N_2O emission, water content

and soil temperature. The cyclic and non-cyclic patterns in N_2O emission described by Yates et al. (2006b) suggest the relationship between these three variables may be scale- and / or location-dependent. This may explain why field-scale correlations between these three variables tend to be poor. For example, a low field-scale correlation between N_2O flux and % water-filled pore space (WFPS) may be the result of several, stronger negative and positive correlations related to sub-units or specific locations with the field.

A number of statistical methods exist that examine the scale-dependent relationship between two soil properties such as the co-dispersion coefficient of multivariate geostatistics (Goovaerts and Chiang, 1993) and spectral coherency (Kachanoski and de Jong, 1988). The use of either method is dependent on the assumption of stationarity in the data. Data sets of N_2O emissions have been observed to be highly skewed and characterized by extreme values which may lead to unevenly distributed variance and non-stationarity (Yates et al., 2006a).

Statistical methods used to study the scale-dependent relationships between two soil properties and that do not rely on stationarity include joint multifractal analysis (Kravchenko et al., 2000; Si and Zeleke, 2005) and the cross wavelet spectrum (Si and Farrell, 2004). Multifractal analysis cannot provide location specific information. The cross-wavelet spectrum can provide location specific information; however it is dependent upon the individual variance between the variables under study. A strong variance with one variable combined with a low variance with the other variable can result in a strong co-variance suggesting a strong correlation where a correlation does not exist (Si and Zeleke, 2005). A statistical method that does not rely on stationarity, provides location specific information and is not subject to the co-variance artifacts possible in the cross wavelet spectrum is wavelet coherency analysis. This technique has been used recently by Si and Zeleke (2005) on saturated hydraulic conductivity, sand and organic carbon content of soil. The first objective of this chapter was to use wavelet coherency to describe the scale- and location-dependent relationship between N_2O emission and soil water content, and between N_2O emission and soil temperature for data collected from a hummocky terrain in the Dark Brown soil zone of Saskatchewan, Canada. The second objective was to compare the local wavelet, cross

wavelet and wavelet coherency spectra of N_2O emissions, soil moisture and soil temperature data to understand the distribution of local variance for the individual soil properties relates to the local co-variance and coherency for compared soil properties, and how the three methods of analysis influence interpretation of the relationship between variables.

5.3 Method and Materials

5.3.1 Field Site and Sampling Design

The field site is in Saskatchewan, Canada at the St. Denis National Wildlife Area, 52° 12' N latitude, 106° 5'W longitude, approximately 40 km east of the city of Saskatoon. The area is characterized by glacial geomorphology and the site is on a hummocky terrain with a parent material of unsorted calcareous till and glacio-lacustrine sediments. Soil types were based on profiles described in the field using the Canadian System of Soil Classification (Agriculture and Agri-Food Canada, 1998b) and converted to the U.S. taxonomic system. Soil types included thin Chernozemic Rego Dark Brown (Typic Calciborolls) found on the shoulders of knolls, thicker Chernozemic Orthic Dark Brown (Typic Haploborolls) in mid-slope and toe-slope positions, and Chernozemic Eluviated Dark Brown (Albic Argiborolls) and Gleysolic Humic Luvic (Argic Cryaquolls) in adjacent depressions. Chernozemic Calcareous Dark Brown (Haplic Calciborolls) were found at shoulder and mid-slope positions as well as some toe-slope positions. Soil textures were found to have a limited range from loam at shoulder positions to silt loam in the depressions. Water inputs are redistributed to depressions where the bulk of infiltrating waters move laterally through the depression margins and are lost through evapotranspiration (Hayashi et al., 1998a).

On an agricultural portion of the wildlife area a 128-point linear transect was established in June of 2003 on cultivated land that had been fallow since 2002. The sample locations were spaced 4.5 m apart and represented a series of knolls and depressions. Three of the depressions had not been cultivated since 1968 and had been allowed to re-vegetate. In May of 2004 an area of the site that included the transect was seeded to a dense nesting cover grass by Ducks Unlimited Canada. The grass mix consisted of a selection of cultivar and common varieties (Yates et al., 2006a) (Chapter

3). Data collection ended in May of 2005. In total, the transect was sampled 18 times. For the purposes of this paper, three data sets, 30 Mar., 29 Apr. and 23 June of 2004 have been selected.

5.3.2 Definition of Landscape Units

The site was topographically surveyed using a Sokkisha Set 5 Electronic Total Station, (Sokkisha Co. Ltd. Tokyo, Japan) and a Trimble^{TR} Pro XRS, Global Positioning System (Trimble Navigation, Sunnyvale, CA). From this information a digital elevation model was produced with a 5-m X 5-m grid cell extent. Elevation and visual inspection of the site was used to segment the transect locations into a set of landscape elements defined by profile curvature and land use (cultivated versus uncultivated) and previously described in Yates et al. (2006b) (Chapter 4). Locations within the cultivated area of the transect were classified as either convex (CX), concave (CV), or cultivated wetland (CW). The CX elements were topographically high positions with an overall positive profile curvature. Concave elements were positions with an overall negative profile curvature, adjacent to wetlands. Depressional positions, roughly circular in shape and which would temporally collect rain or snow melt water, were classified as CW elements. The re-vegetated depressions were considered non-agricultural portions of the transect were classified as uncultivated wetlands (UW).

5.3.3 Nitrous Oxide Flux Measurements

Flux measurements were made at each location using a two-piece, closed, vented chamber (International Atomic Energy Agency, 1992) consisting of a polyvinyl chloride (PVC) ring base and vented cap with sampling port. Vent tube design was similar to that proposed by Hutchinson and Mosier (1981). Prior to the start of data collection, the bases were pressed into the soil and secured using 20-cm spikes where they remained for the duration of the field season. At each sampling event, the chamber was placed onto the base and sealed by a rubber ring attached to the cap. When in use the head space of each chamber was 2.25 L and covered a soil surface area of 0.02 m^2. Samples of the headspace gas were drawn from the chamber with a 20-mL syringe and injected into 12-mL evacuated tubes for transport back to the laboratory. This was done

at three equally spaced time intervals of 8 min with separate time zero samples collected from each chamber. Gas sampling for each time interval was completed by a single individual moving from location to location every 45 s. This allowed for a complete transect sampling in less than 2 h. Gas sampling was timed to begin at midday. Samples were returned to the lab, placed in a freezer and analyzed as soon as possible (within one to three weeks depending on equipment availability).

Nitrous oxide concentrations were determined using a Varian CP3800 GC (Varian Canada Inc., Mississauga, ON) equipped with dual electron capture detectors (ECD). The temperatures of the injector, column, and detector were 100, 35 and 370 ºC, respectively. Separations were carried out using Poraplot Q columns (12.5-m × 0.32-mm i.d. fused silica capillary column, DF = 8 μm; includes a 2.5-m particle trap) with UHP He (14.4 mL min^{-1}) as the carrier gas and P5 (95:5 v/v Ar:CH_4 mix) as the make-up gas (12.0 mL min^{-1}). Samples (300 μL) were introduced using a CombiPAL™ auto-sampler (CTC Analytics AG, Switzerland) with on-column injection and a split ratio of 10:1. The system was calibrated using standard gases (N_2O in N_2) obtained from PraxAir (Mississauga, ON). Data processing was performed using the Varian *Star Chromatography Workstation* (ver. 6.2) software. Internal calibration curves were obtained by applying linear, least squares regression to the gas concentration (ppbV N_2O) *versus* peak area data; N_2O concentrations in the headspace samples were then calculated automatically from the regression equations.

Samples of ambient air were included in each analytical run as reference samples to check the 'within run' precision, calculate a minimum detectable concentration difference (MDCD), and correct for detector drift. The MDCD was calculated by (i) analyzing matched pairs of the reference gas samples at regular intervals during each analytical run; (ii) calculating the average difference between sample pairs (μ_p) as well as the standard deviation (σ_p); and (iii) calculating the MDCD using Eq. [5.1].

$$MDCD = \mu_p + (2\sigma_p) \qquad [5.1]$$

The MDCD was used to filter the raw data when calculating the actual N_2O flux; i.e., concentration differences between t_0 and each subsequent time step that were <MDCD were not considered to be significantly different from the t_0 concentration. Anthony et al. (1995) arbitrarily chose to use twice the mean absolute difference between pairs of ambient air samples. Using the form presented in this study brings a statistical basis to the MDCD by calculating a value that is within the upper bound of the 95% confidence interval for the mean paired difference. The variability in our data is such that the method employed here to calculate the MDCD is slightly more rigorous than that used by Anthony et al. (1995).

The vertical flux of N_2O at the soil–atmosphere interface (ng N_2O-N m^{-2} s^{-1}) was calculated as the slope of the tangent to the concentration (ng L^{-1}) *vs*. time (min) curve at t_0. That is, the flux at t_0 was calculated as the 1st derivative of the 2nd-order polynomial equation ($y = ax^2 + bx + c$) used to describe the concentration *vs*. time relationship. The flux (ng N L^{-1} min^{-1}) was then converted to an area basis by multiplying by 1.867 L min m^{-2} s^{-1} [i.e., the chamber volume ÷ (surface area × 60 s min^{-1})]. In cases where 'rogue' data points prevented the use of the 2nd-order polynomial model, the flux was calculated as the slope of the linear, least-squares regression equation that best described the concentration *vs*. time relationship (Hutchinson and Mosier, 1981) (Eq. [5.2]).

$$F_{N_2O} = \frac{V}{k_t A} m \qquad [5.2]$$

Where F_{N_2O} is the flux at t_0, V = chamber volume (L), A = cross-sectional area of soil covered by the chamber (m^2), k_t = time constant (60 s min^{-1}), and m = slope of the linear, least-squares regression equation (ng L^{-1} min^{-1}).

5.3.4 Measurement of Soil Moisture, Soil Temperature and Climate Data

At each location, volumetric soil moisture over a 15-cm depth was measured at the time of gas sampling using time domain reflectometry (TDR) after Topp and Ferre (2002). Readings were obtained manually from a Tektronix 1502 B cable tester (Tektronix, Wilsonville, OR). Also at each location, soil temperature was measured at the 5- cm depth using a buried type T thermocouple constructed of twisted copper and

constantan (45% Ni and 55% Cu) wire pairs and read using a Barnant DuaLogR™ thermocouple reader (Barnant Company, Barrington, IL). A meteorological station on site recorded hourly averages of precipitation, air temperature and wind speed.

5.3.5 Wavelet analysis, cross wavelet spectrum and wavelet squared coherency

A wavelet is a mathematical function representing a small wave form. It is considered small because it is contained within a finite domain (Graps, 1995) in contrast to the sine and cosine functions used in Fourier analysis which stretch out to infinity [i.e., have infinite span and are globally uniform in time (Lau and Weng, 1995)]. Thus, where Fourier analysis does a poor job in approximating sharp spikes in data – like that typical of soil N_2O emissions – wavelet analysis is well suited. This feature of wavelets allows the function to have a rapid decrease to zero about a finite point or interval in space or time (Si, 2003) yielding a coefficient associated with a specific location. A wavelet transform takes a data series and, like the Fourier transform, treats it as a signal and decomposes this signal into series of coefficients representing variance (Lindsay et al., 1996). Unlike the Fourier transform, the spatial context of the data is retained.

Scale analysis using wavelets is performed by contraction and dilation of the wavelet function. Contraction and dilation changes the size of the interval in time or space (window) that the wavelet function is applied to in the data series. Increasing window size increases the scale at which the coefficient for a particular location is calculated. In this manner a wavelet coefficient is obtained for each location in a data series over a range of scales and the scale of analysis is matched to the size of the feature(s) in the data series.

The various types of wavelet transforms are generally grouped as continuous or discrete (Si and Zeleke, 2005). Discrete wavelets can be orthogonal so there is no redundant information between wavelet coefficients and scales are discrete. This makes discrete wavelets very useful for data compression. Continuous wavelets are not orthogonal therefore, there is overlap between wavelet coefficients resulting in redundant information between scales and locations and making the continuous wavelet very useful for scale analysis (Si, 2003). The mother wavelet is rescaled by powers of

two; hence, a data series that contains a binary number of points is optimal for computation speed (Si, 2003).

There are several types of wavelets (see Kumar and Foufoula-Georgiou, 1997) and it is important that one chooses a wavelet that is appropriate to the objectives of their analysis. The wavelet chosen for this study was the Morlet wavelet. The Morlet is a continuous wavelet that is good for extracting features (Si and Zeleke, 2005), such as one would expect in soil N_2O emission data. In Yates et al. (2006b) a Mexican Hat wavelet was used to look at the local wavelet spectrum for a series of transect measurement of soil N_2O flux. However, the Mexican Hat wavelet is a real function and provides a coefficient with a real component. The Morlet wavelet provides a coefficient with both a real and imaginary component, which is necessary for the wavelet coherency analysis. The Morlet wavelet is defined as

$$\psi(\eta) = \pi^{-1/4} e^{i\omega\eta - 0.5\eta^2} \qquad [5.3]$$

where ω is dimensionless frequency and η is dimensionless space (Torrence and Webster, 1999; Grinstead et al., 2004). For a comprehensive explanation of wavelet analysis see Kumar and Foufoula-Georgiou (1993, 1997). Si (2003) and Si and Farrell (2004) provide a good example of the application of wavelet analysis to soil properties.

The Morlet wavelet is good for extracting features, such as extreme values in an N_2O flux data series, and providing information on the spatial scales related to these features. For this application ω = 6 striking a balance between space and frequency localization. The scale (s) is varied to stretch the wavelet in space (x) such that $\eta = s \cdot x$. For the Morlet wavelet, the Fourier period is nearly equal to the scale ($\lambda = \frac{4 \cdot \pi \cdot s}{\omega + \sqrt{\omega^2 + 2}} \approx 1.03 \cdot s$; Meyers et al., 1993). The CWT for any given wavelet is defined as the convolution of Y_i with the scaled and normalized wavelet written as

$$W_i^Y(s) = \sqrt{\frac{\delta x}{s}} \sum_{j=1}^{N} Y_j \psi\left[(j-i)\frac{\delta x}{s}\right] \qquad [5.4]$$

for a spatial series of length N (Y_i, i=1…N) with distance δx that is equal and incremental. Thus, for each combination of scale and location a wavelet coefficient is calculated. The continuous wavelet transform is applied using a discrete fast Fourier

transform because the flux measurements are made at discrete locations (Si and Farrell, 2004).

The local wavelet spectrum is obtained by squaring the wavelet coefficient $W_i^Y(s)$ for each scale at each location and can be plotted as a 2 dimensional field of values of wavelet variance. These coefficients are generally complex with real and imaginary components a and b, respectfully, and are expressed as $a + ib$. The polar form of the complex numbers is $W_i^Y(s) = \left|W_i^Y(s)\right| \cdot (\cos\theta + i\sin\theta)$, where $\theta + arc\ \tan\frac{b}{a}$ and this is called the local phase or the complex argument of $W_i^Y(s)$. The wavelet power spectrum is defined as $\left|W_i^Y(s)\right|^2$.

The cross wavelet spectrum of two spatial series whose wavelet transforms are W_i^X, and W_i^Y can be defined as $\left|W_i^{XY}\right| = \left|W_i^Y(s) \cdot \overline{W_i^X(s)}\right|$, where $\overline{W_i^X}$ is the complex conjugate of W_i^X. Thus, the complex argument W_i^{XY} can be defined as the local relative phase between X_i and Y_i in the spatial frequency domain.

The wavelet square coherency of two spatial series is defined as

$$R_i^2(s) = \frac{\left|S\left(s^{-1}W_i^{XY}(s)\right)^2\right|}{S\left(s^{-1}\left|W_i^X(s)\right|^2\right) \cdot S\left(s^{-1}\left|W_i^Y\right|^2\right)} \qquad [5.5]$$

after Torrence and Webster (1999), and Grinstead et al. (2004) where W^{XY} is the cross wavelet spectrum, and W^X and W^Y are the continuous wavelet spectrums for a spatial series. The structure of the equation is not unlike that for calculating a product moment correlation coefficient, which is defined by Ebdon (1985) as the ratio of joint variation to total variation of two variables. The smoothing operator (S) is defined as $S(W) = S_{scale}\left(S_{space}(W)\right)$ and is applied to both scale (S_{scale}) and distance (S_{space}) of the cross wavelet spectrum, before normalization, and the continuous wavelet spectrums, after normalizing (Torrence and Webster (1999). The smoothing operator has been designed to have a footprint similar to the Morlet wavelet:

$$S_{scale}(W, s) = \left(W_i(s) \cdot c_1^{\frac{-x^2}{2s^2}}\right)\Big|_s \qquad [5.6]$$

$$S_{space}(W,s) = \left(W_i(s) \cdot c_2 \cdot \prod(0.6s)\right)\Big|_i \qquad [5.7]$$

Where c1 and c2 are coefficients that represent numerically determined normalization constants after Grinstead et al. (2004), Π is the rectangle function, and 0.6 represents the empirically determined scale decorrelation length for the Morlet wavelet after Torrence and Campo (1998).

The significance of the local wavelet spectrum was tested by its comparison to a background red-noise after Si and Zeleke (2005). Red-noise represents a univariate lag-1 autoregressive process (AR(1)) that is the result of dependency in a spatial series with a short sampling interval. This is in contrast to white noise in which there is no spatial dependency with a zero mean and equal variance. Irrespective of the site, adjacent soil locations will naturally have some degree of similarity simply due to movement and mixing of soil components and microbial activity. If spatial dependency exists above this red-noise then the spatial pattern is being controlled by some processes. Therefore, the red noise can be used as if it were a null hypothesis for a statistical test of the local wavelet spectrum.

A Monte-Carlo simulation was used to generate 1000 realizations of a spatial series for an AR(1) process. The wavelet transform for each series was determined and for each the wavelet power was computed. The wavelet powers were sorted in ascending order and the first 95% of this wavelet power was considered background red noise. The 95% level is then the 95% confidence level or 5% significance level. If the wavelet power of a true spatial series did not exceed the wavelet power level at 95% for a certain scale, then that wavelet power was not significantly different from the background red noise at that particular scale.

The local wavelet, cross-wavelet and wavelet coherency spectra are presented as contour maps of the wavelet coefficients that represent highs and lows in variance and which are plotted according to the location along the transect and the scale (m) of the variation. Lighter shades are associated with higher wavelet coefficients. The interpretation of the spectra is visual. Significant areas in wavelet coefficients are represented by a heavy contour line that represents the 95% confidence interval. Features of interest are areas of high coefficients that appear as light bands across the x axis of the spectrum within a narrow scale range (a global event) or as a single, non-

repetitive high in variance at a discrete location on the x axis (localized event) (Si and Farrell, 2004). A distinct band or global feature is an indication of cyclic behavior and the period of that cycle is the scale of the underlying process. Localized features do not cycle and therefore cannot be assigned to a particular scale.

5.4 Results

Mean N_2O flux on 30 Mar. was 2.3 ng N_2O-N m^{-2} s^{-1} and ranged between -7.8 and 22.3. A cyclic pattern is visible in the distribution of the flux measurements along the transect (Figure 5.1). The majority of values were under 5 ng N_2O-N m^{-2} s^{-1} and most negative fluxes occurred in the second half of the transect. Higher flux values appear to occur in groups that are associated primarily with locations on CX landscape positions. There are no values of WFPS for 30 Mar. because the soil at the majority locations was frozen at time of sampling and TDR could not be used. Soil temperature varied 3 ºC between the highest and lowest values (Figure 5.1) and higher temperature values tend to be associated with the higher flux values.

The local wavelet spectra for soil N_2O emission and soil temperature on 30 Mar. is shown in Figure 5.2a and 5.2b. Most prominent in this scale range is an anomaly indicating high variance between the 72 and 144 m scales over locations 40 to 95. This anomaly is significantly different from that of the red noise and is greater than 5% of the area within the cone of influence. This anomaly corresponds to the portion of the transect where the fluxes had highest variability (Figure 5.1). The high flux was at CX elements, which had developed the thinnest snow cover over winter and were first to be exposed during the spring snowmelt. The exposed locations, the majority of which were still frozen at the 5-cm depth (Figure 5.1), were observed to have had thawed on surface and were areas of wet, actively denitrifying soil. The anomalies below the 36 m scale are significant by comparison to the red noise, but individually are less than 5% of the area within the cone of influence, and thus may be spurious.

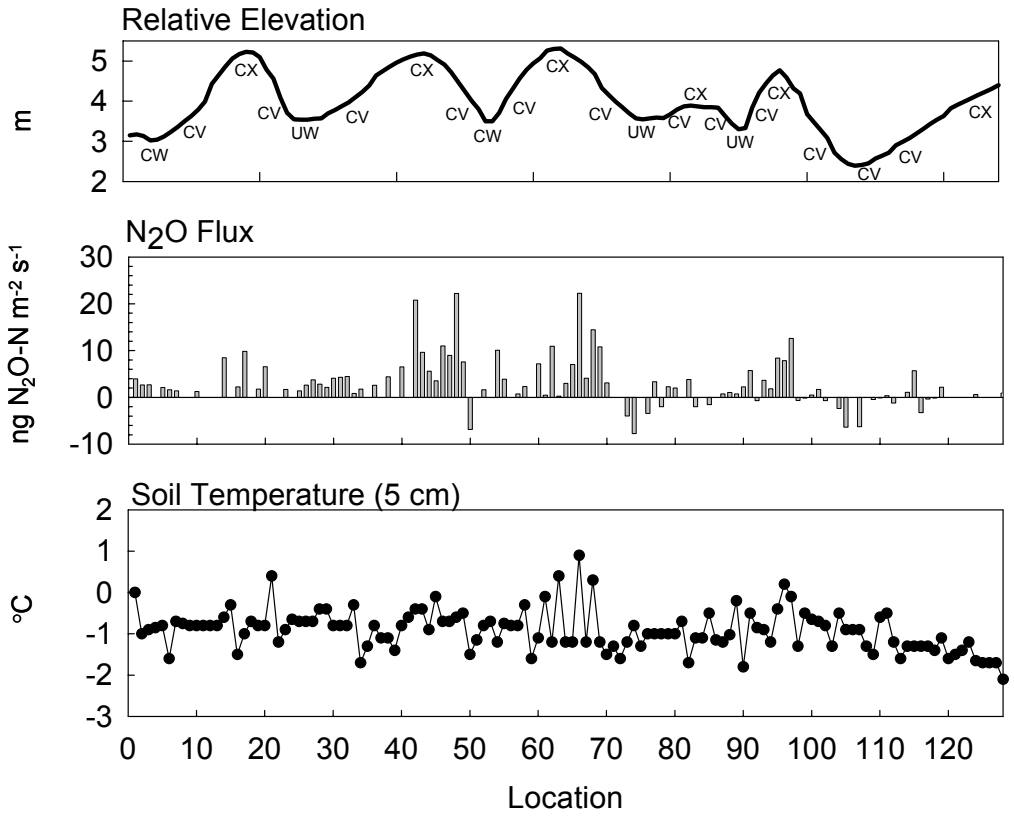

Figure 5.1: Profile of relative elevation (m), soil N_2O flux (ng N_2O-N m^{-2} s^{-1}) and soil temperature (ºC at the 5-cm depth) by location on 30 Mar. 2004 on the transect at St. Denis, SK. Convex (CX), concave (CV), cultivated wetland (CW) and uncultivated wetland (UW) landscape elements are shown.

The local wavelet spectrum for soil temperature at the 5-cm depth (Figure 5.2b) indicates that the variance is distributed more randomly with few distinct anomalies. At a scale > 144 m a significant anomaly occurs over locations 62 to 128, but this is primarily outside the cone of influence. Centered at location 50 is a small, possibly spurious anomaly that is part of a diffuse band indicating high variance approximately at the 72-m scale. Below the 72-m scale variance appears to be randomly distributed. At a scale < 18 m there is a local feature that is, although significant compared to the red noise, less than 5% of the area within the cone of influence.

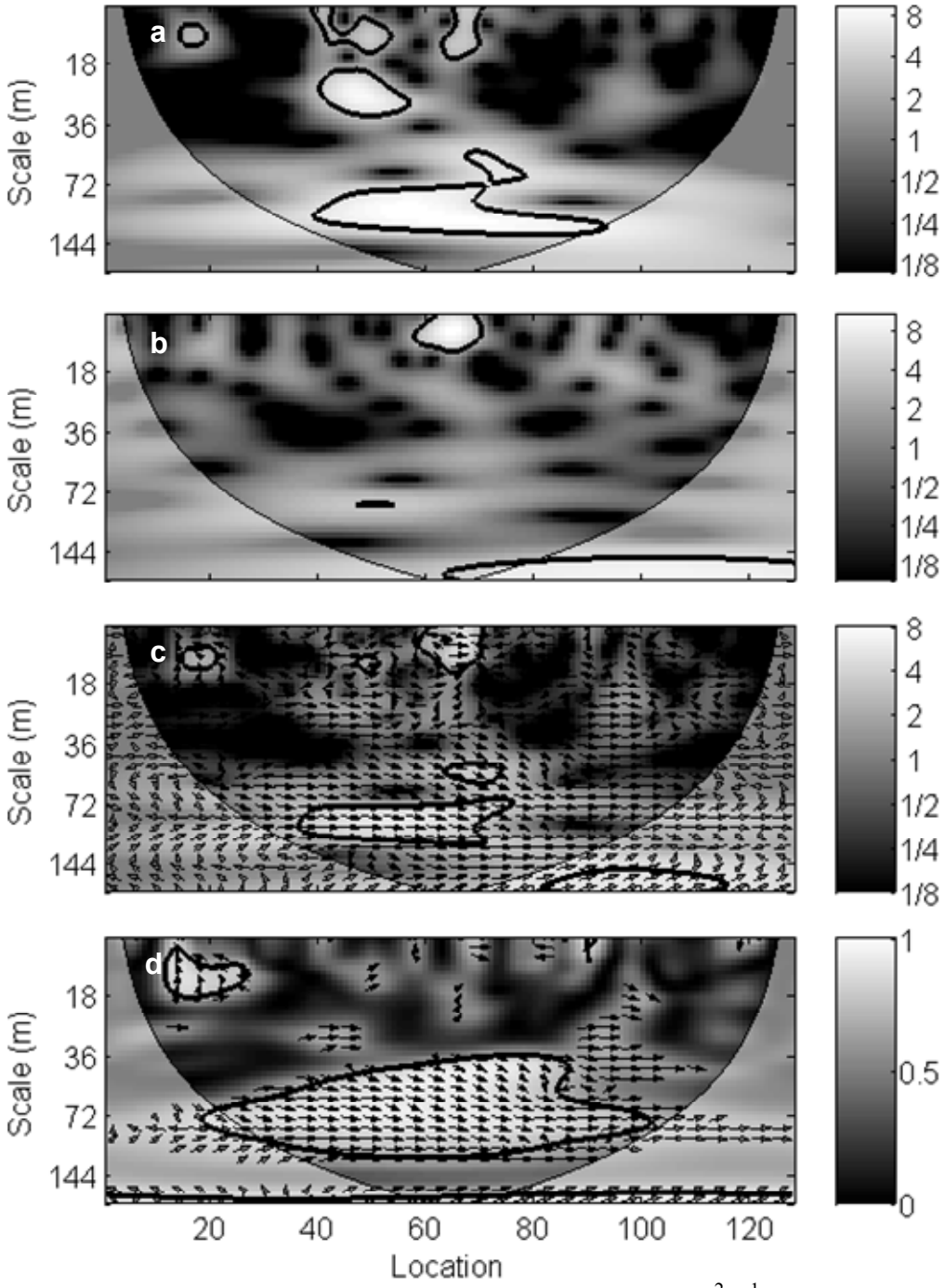

Figure 5.2: Local wavelet spectra for soil N_2O flux (ng N_2O-N m^{-2} s^{-1}) (a) and soil temperature (ºC at the 5-cm depth) (b), and their local cross wavelet spectrum (c) and local wavelet coherency spectrum (d) on 30 Mar. of 2004 on the transect at St. Denis, SK. Thin solid lines indicate the cone of influence and thick solid lines indicate the 95% confidence level. Phase angle of cross and coherency wavelet spectra are shown by arrows.

The cross wavelet spectrum for soil N_2O flux and soil temperature (Figure 5.2c) for 30 Mar. is similar to the wavelet spectrum for soil N_2O in that the higher co-variance appears to be distributed across the larger scales (> 36 m) and peaks in a broad, significant anomaly along locations 40 to 75 over a scale range of 72 to 110 m. The position of this high variance is similar to the significant anomaly also visible in the spectrum for soil N_2O (Figure 5.2a). Other anomalies visible have cross-spectra larger than the 95% confidence level, but have an area <5%, thus may be spurious.

The wavelet coherency confirms a strong relationship between soil N_2O and soil temperature at a scale of 72 to 100 m over locations 20 to 100 (Figure 5.2d). The cyclic pattern imposed by the distribution of exposed soil is visible in the wavelet spectrum for soil temperature at the 5-cm depth (Figure 5.2a); however the range in soil temperature over the length of the transect is such that the soil temperature at the exposed positions do not represent a change in variance sufficient to be significantly different from background. The coherency spectrum indicates a strong, in-phase (positive) relationship between soil N_2O flux and soil temperature. The high coherency is significant through the cone of influence. The coherency spectrum also indicates that high coherency exists across all locations at a scale >144 m, although most of the anomaly is outside the cone of influence and the phase angles suggest the relationship between soil N_2O flux and soil temperature, if it does exist at this scale, is complex.

On 29 Apr. mean N_2O flux was 17.3 ng N_2O-N m^{-2} s^{-1} (Figure 5.3), which is an order of magnitude higher that that observed on 30 Mar. The increase in mean flux is primarily due to a few extreme values, as high as 876 ng N_2O-N m^{-2} s^{-1}, that occur as a group across locations 50 to 56 associated with a CW landscape unit. The majority of the remaining values ranged between +/- 8.0 ng N_2O-N m^{-2} s^{-1} (Figure 5.3) except for locations 4 to 6 (12.7 to 20.5 ng N_2O-N m^{-2} s^{-1}) that are also associated with a CW position. Fluxes are notably low or absent from UW positions. Mean WFPS was 61.5% and its distribution along the transect was visibly cyclic in the first half, but weakened to the north (Figure 5.3). High values (>60%) are associated primarily with UW and CW landscape units with the exception of the UW unit represented by locations 74 to 77 where values are as low as 34%. Soil temperature at the 5-cm depth ranged from 1.3 to

3.8 ºC. The temperature measurements (Figure 5.3) follow a cyclic pattern with high values on CX positions.

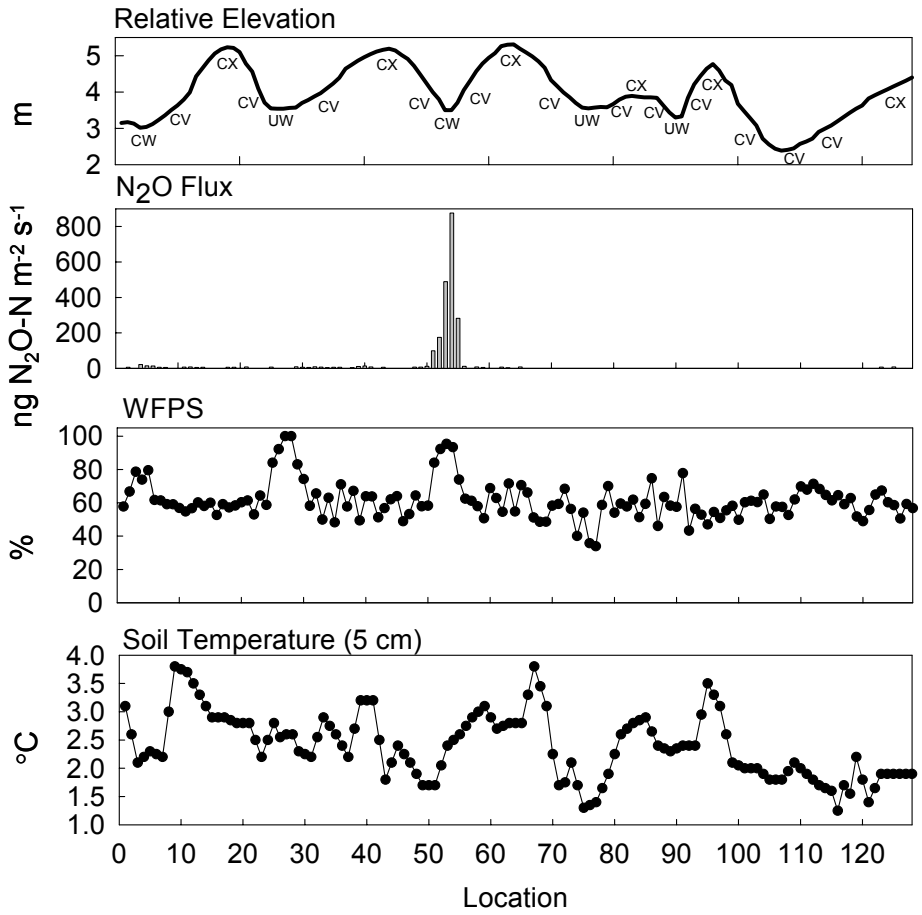

Figure 5.3: Profile of relative elevation (m), soil N_2O flux (ng N_2O-N m^{-2} s^{-1}), water-filled pore space (% WFPS) and soil temperature (ºC at the 5-cm depth) by location on 29 Apr. 2004 on the transect at St. Denis, SK. Convex (CX), concave (CV), cultivated wetland (CW) and uncultivated wetland (UW) landscape elements are shown.

On 29 Apr. the local wavelet spectrum for soil N_2O emission is characterized by a single, intense, anomaly centered on location 55 (Figure 5.4a). This coincides with the extreme values of soil N_2O flux visible in the profile of flux measurements on the transect (Figure 5.3). These extreme values are concentrated in five consecutive locations within a CW landscape element. The wavelet spectrum for WFPS on this date (Figure 5.4b) indicates that variance is higher at the larger scales (>36 m). There are two larger variance anomalies at approximately at 36 to 72 m and 72 to 144 m scales. There are no significant peaks at scales <18 m. The anomaly at the 72 to 144 m scale is a

significant portion of a more diffuse band of high variance that appears to extend across the spectrum. The wavelet spectrum for soil temperature shows a similar feature (Figure 5.4c) and these features are probably global representing a periodicity in the soil temperature and WFPS related to the topography of the site as was the distribution of variance for soil N_2O on 30 Mar.

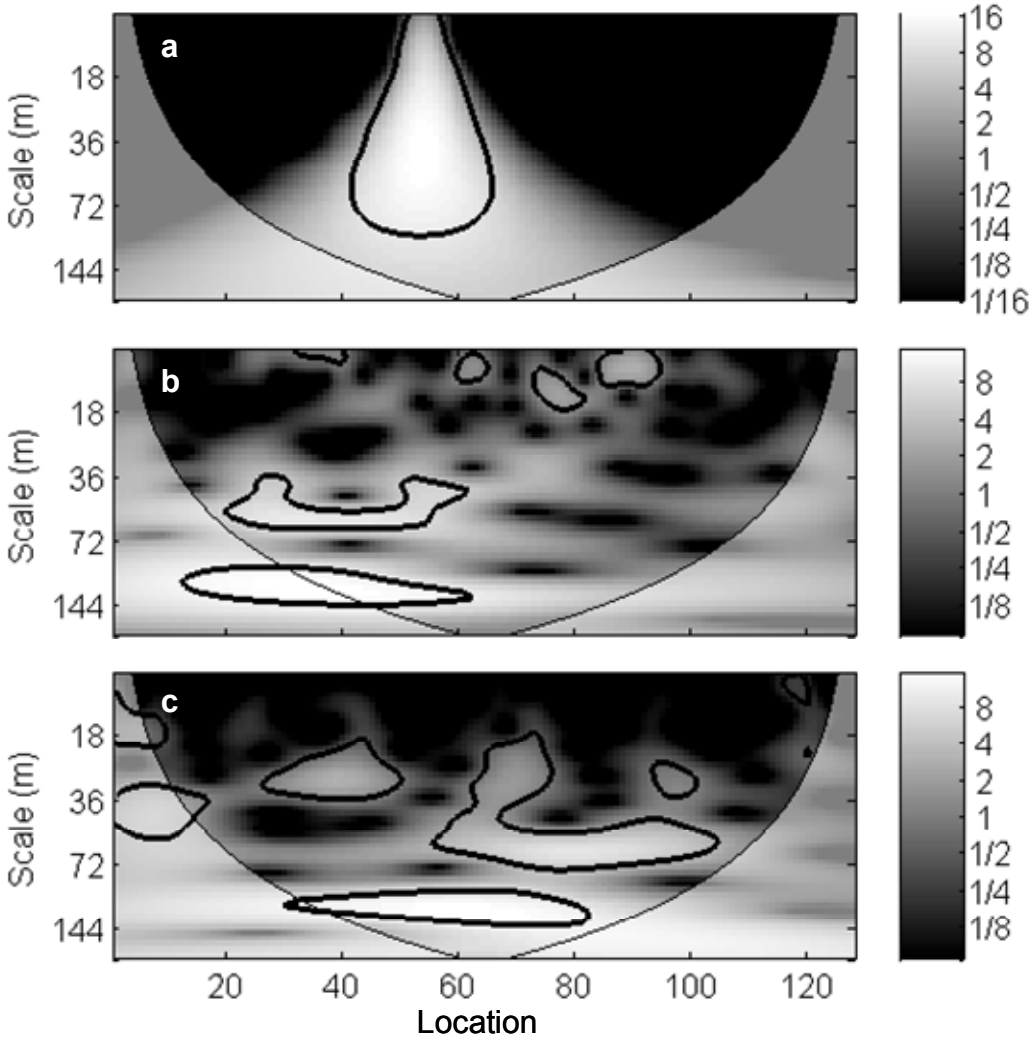

Figure 5.4: Local wavelet spectra for soil N_2O flux (ng N_2O-N m^{-2} s^{-1}) (a), soil temperature (ºC at the 5-cm depth) (b), and water-filled pore space (% WFPS) (c) on 29 Apr. of 2004 on the transect at St. Denis, SK. Thin solid lines indicate the cone of influence and thick solid lines indicate the 95% confidence level.

As expected, the concentration of variance represented by the local feature in the wavelet spectrum for soil N_2O on 29 Apr. produces a concentration of co-variance in

both cross wavelet spectra for soil N_2O and WFPS, and soil N_2O and soil temperature (Figures 5.5a and 5.5b). In both spectra the co-variance is distributed between two anomalies, a significant irregular feature that appears to be influential over a large scale range and a smaller non-significant feature that appears confined to a scale range of 72 to 144 m. The larger irregular anomalys, although significant, represents a localized feature and is highly influenced by the wavelet spectrum for soil N_2O; thus it may be misleading to think that a strong co-variance actually exists between soil N_2O and WFPS or soil temperature. Certainly the complex phase relationships shown in Figure 5.5b indicate that may be the case for soil N_2O and soil temperature. The smaller, non-significant anomalies are probably the result of the spike in soil N_2O flux near the center of the transect (Figure 5.3). The position of these high emissions breaks the transect into three nearly equal portions: a high flux central portion flanked on either side by a low flux portion. This creates a very broad cycle in the emission pattern that also dominates the distribution of co-variance; hence the indication of a global relationship between N_2O and WFPS or soil temperature is spurious.

The wavelet coherency spectrum for soil N_2O and WFPS on 29 Apr. (Figure 5.5c) indicates that the co-variance between soil N_2O and WFPS was real. The irregular, significant anomaly in coherency centered on location 55 indicates strong, positive relationship between soil N_2O and WFPS occurred locally at the CW landscape element shown in Figure 5.3. Unlike the wavelet coherency spectrum for soil N_2O and soil temperature on 30 Mar., the underlying process is not cyclic and does not relate to a particular spatial scale. This feature is not present in the coherency spectrum for soil N_2O and soil temperature (Figure 5.5d) confirming that the co-variance suggested in Figure 5.5b was spurious. However, the large scale, non-significant co-variance suggested by Figure 5.5a and 5.5b comes through in the coherency spectra as global features suggesting that at scales greater than 100 m, there is some degree of dependency between soil N_2O and WFPS or soil temperature.

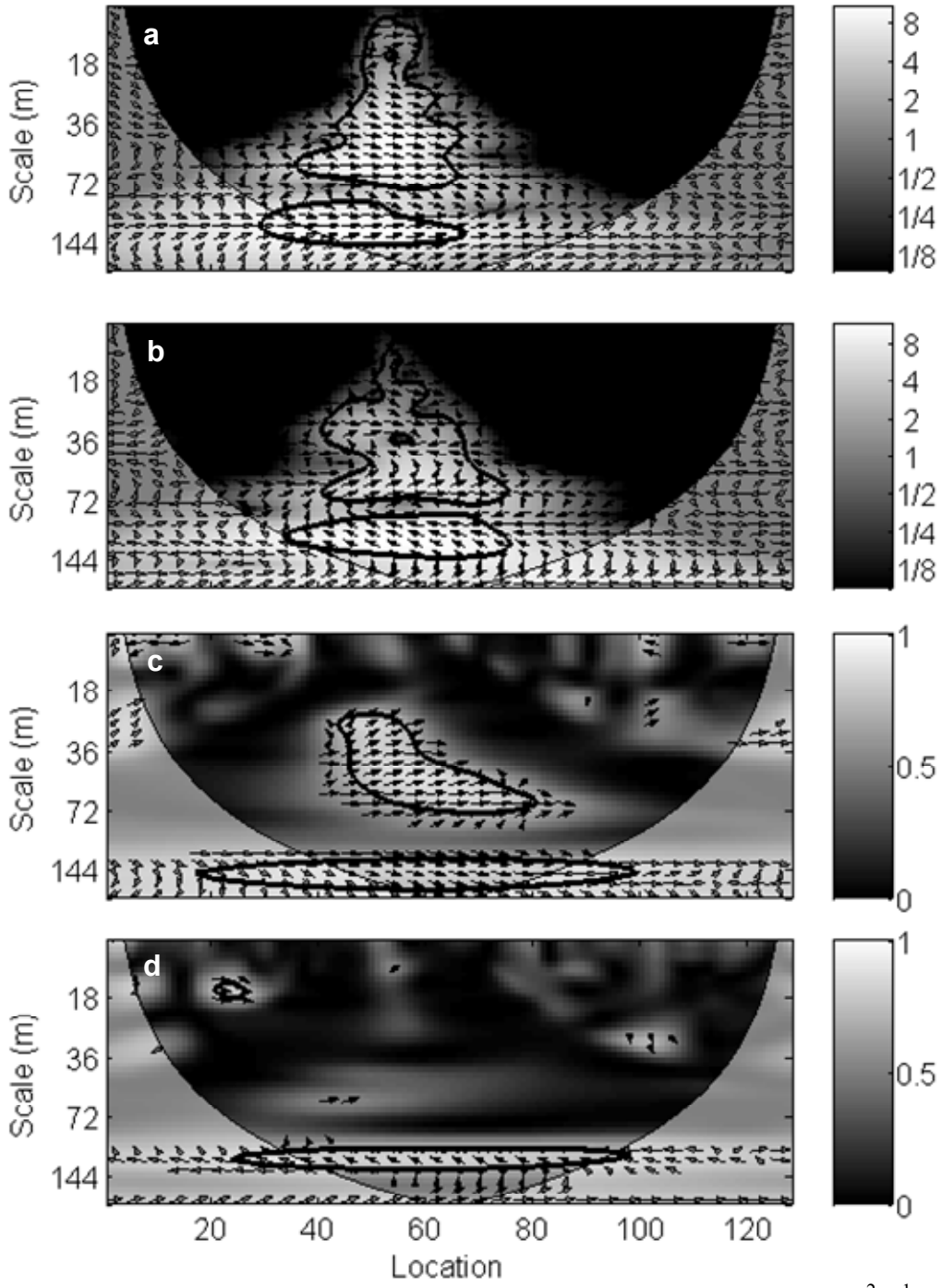

Figure 5.5: Local cross wavelet spectrum between soil N_2O flux (ng N_2O-N m^{-2} s^{-1}) and water-filled pore space (% WFPS) (a), and between soil N_2O flux and soil temperature (ºC at the 5-cm depth) (b). Local wavelet coherency spectrum soil N_2O flux and water-filled pore space (c), and between soil N_2O flux and soil temperature (ºC at the 5-cm depth) (d) on 29 Apr. 2004. Thin solid lines indicate the cone of influence and thick solid lines indicate the 95% confidence level. Phase angle of wavelet spectra are shown by arrows.

The transect on 23 June was a net sink for N_2O as the mean flux was -0.2 ng N_2O-N m^{-2} s^{-1}, one order of magnitude lower than 30 Mar. (Figure 5.6). Values ranged between -10.2 and 5.2 ng N_2O-N m^{-2} s^{-1}. The strongest negative fluxes occur between locations 70 and 88, inclusive, an area that includes an UW landscape unit. A set of positive fluxes occur over locations that straddle the larger CW landscape unit (48 to 50, inclusive).

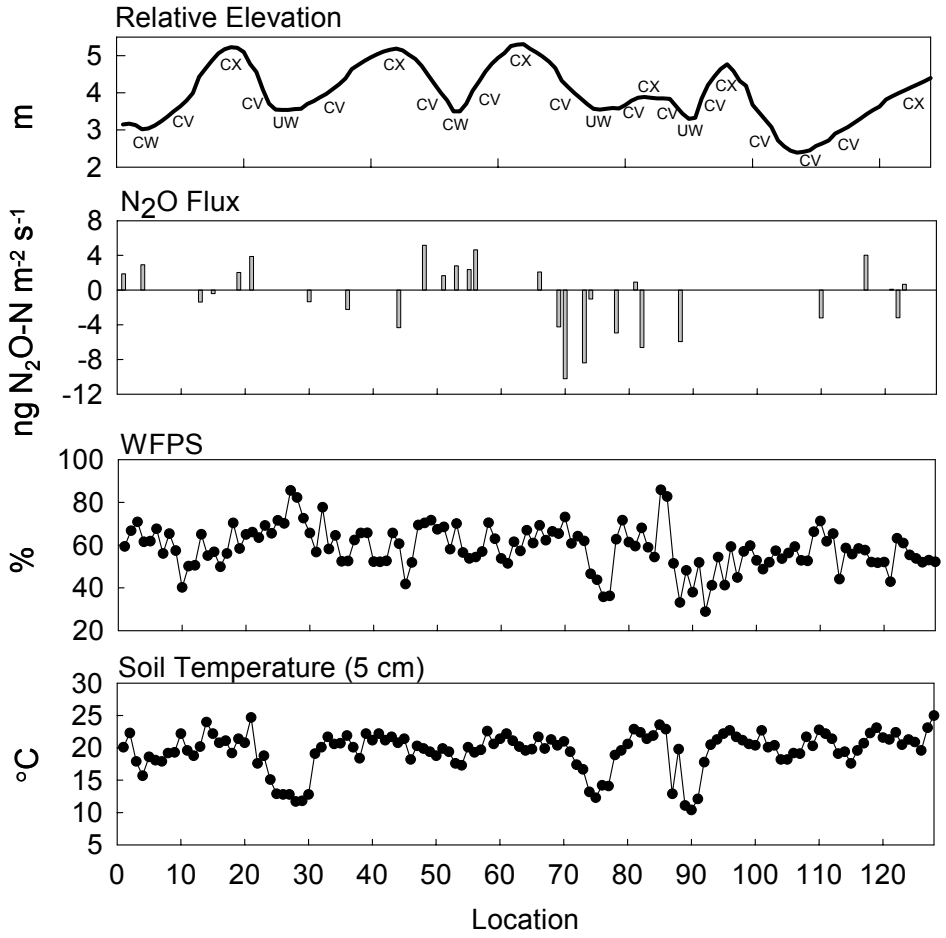

Figure 5.6: Profile of relative elevation (m), soil N_2O flux (ng N_2O-N m^{-2} s^{-1}), water-filled pore space (% WFPS) and soil temperature (ºC at the 5-cm depth) by location on 23 June 2004 on the transect at St. Denis, SK. Convex (CX), concave (CV), cultivated wetland (CW) and uncultivated wetland (UW) landscape elements are shown.

Overall there is little relationship between the occurrence of a flux, negative or positive, and landscape. Mean WFPS (58.5%) is similar to 29 Apr., but more randomly distributed with high and low values measured at all landscape positions (Figure 5.6). In

general, low values of WFPS appear associated with CX positions; however UW positions have both relatively high values (locations 27 and 28) and low values (locations 89 and 90) resulting in a weak cyclic pattern with more point to point variability. Although soil temperature at the 5-cm depth ranged from 10.4 to 25.0 ºC, the values across CX, CV and CW elements were at the higher end of this range and the values at the UW positions were notably lower (Figure 5.6).

The wavelet spectrum for soil N_2O on 23 June does not indicate any features that are both significant at the 95% confidence level and >5% of the area of the spectrum (Figure 5.7a). This reflects the random distribution of fluxes along the transect (Figure 5.6). The same can be said for the spectrum of WFPS (Figure 5.7b) including the anomaly at the 72 m scale over locations 65 and 95. At approximately this same scale and locations a similar feature is visible in the spectrum for soil temperature (Figure 5.7c). This anomaly is significant and was likely the result of the variation in soil temperature across the series of CX, CV and UW units across those same locations. The same variation is present across locations 15 to 35, but the wavelet feature associated with this variation is not >5% of the area of the spectrum (Figure 5.7c).

The distribution of co-variance between soil N_2O and both WFPS and soil temperature is similar in that there is a trend for higher co-variance at larger scales (Figure 5.8a and 5.8b). Co-variance appears to peak in both spectra between locations 60 to 85; however these anomalies are not significant, nor are they clearly associated with any global feature, although they both occur at a scale of 72 m. The wavelet coherency spectra are similar (Figure 5.8c and 5.8d) with no significant regions of high coherency although anomalies occur at about the same scale and locations as the co-variance suggesting that a dependency between soil N_2O and WFPS or soil temperature probably exists, but is very weak. The orientation of phase arrows in both spectra suggest that the relationship between soil N_2O and WFPS or soil temperature, along the transect, is location-dependent and may be either positive or negative depending on the scale and location.

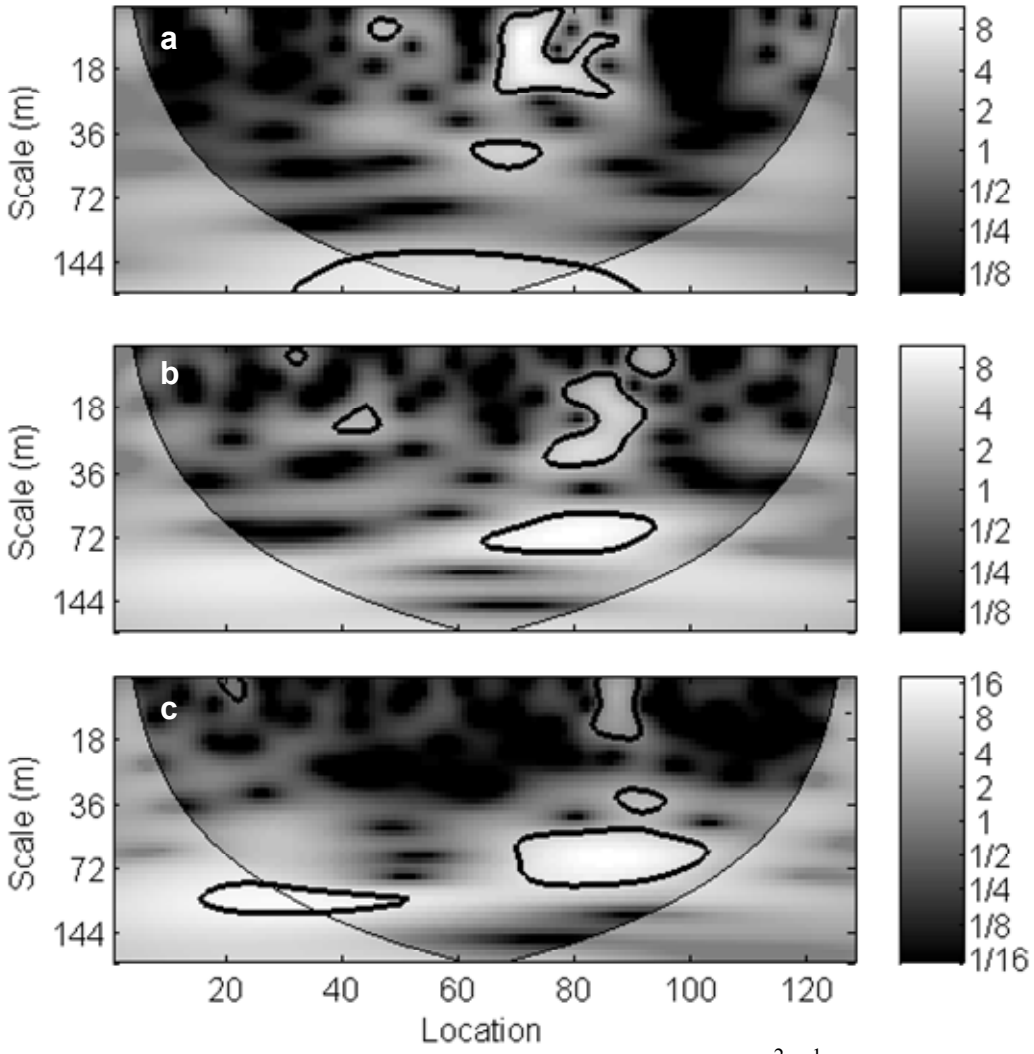

Figure 5.7: Local wavelet spectra for soil N_2O flux (ng N_2O-N m^{-2} s^{-1}) (a), soil temperature (ºC at the 5-cm depth) (b), and water-filled pore space (% WFPS) (c) on 23 June of 2004 on the transect at St. Denis, SK. Thin solid lines indicate the cone of influence and thick solid lines indicate the 95% confidence level.

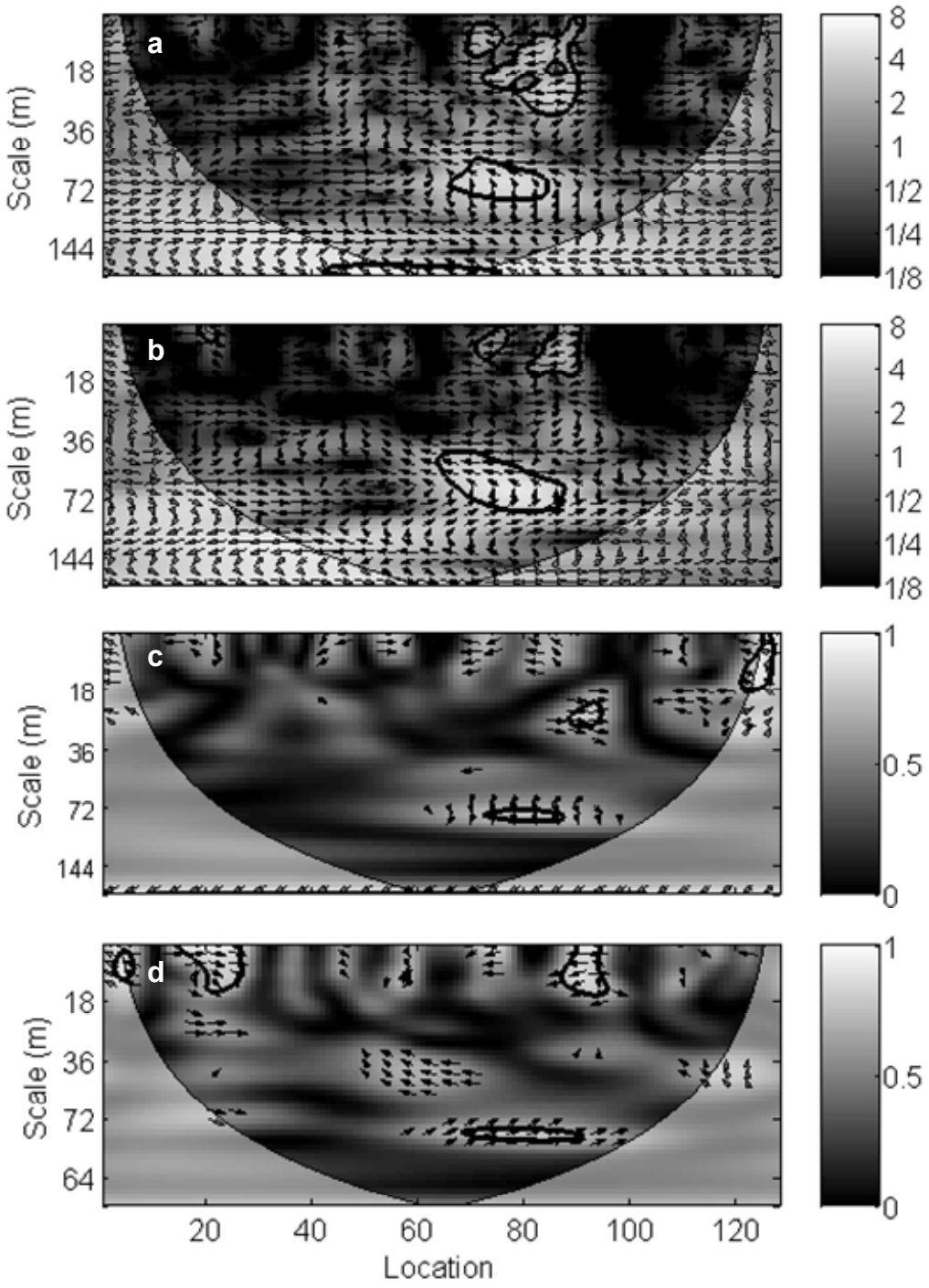

Figure 5.8: Local cross wavelet spectrum between soil N_2O flux (ng N_2O-N m^{-2} s^{-1}) and water-filled pore space (%WFPS) (a), and between soil N_2O flux and soil temperature (ºC at the 5-cm depth) (b). Local wavelet coherency spectrum soil N_2O flux and water-filled pore space (c), and between soil N_2O flux and soil temperature (ºC at the 5-cm depth) (d) on 23 June 2004. Thin solid lines indicate the cone of influence and thick solid lines indicate the 95% confidence level. Phase angle of wavelet spectra are shown by arrows.

5.5 Discussion

The significant anomalies and global features displayed in the wavelet, cross-wavelet and wavelet coherency spectra indicate that the distribution of variance, co-variance and coherency is controlled by large-scale processes related to the topography of the site. The distance between points of high elevation ranged from approximately 90 to 150 m for an average of approximately 125 m. The local spectra showed spatial scales of significance that were primarily between 72 and 144 m. Soil N_2O flux peaked at specific landscape elements such as CX elements on 30 Mar. and the CW element on 29 Apr.; however, the spectra suggest that the scale of soil N_2O flux and its relationship to WFPS and soil temperature was controlled by the combination of elements that make up a landform cycle (CX – CV – CW or UW – CV – CX). Thus, the difference in flux between the elements of a landform gives the range in values needed to form a cycle in the data and the distance between any two of the same elements is an average of 125 m.

The spike in soil N_2O flux at the CW element on 29 Apr. further refines this concept as it demonstrates the importance of the land-use component of the landscape element to the pattern of fluxes in a hummocky terrain. High values were not associated with UW elements even though they are a depressional feature, like that of the CW element. The distinct difference in land-use between the two elements is a major factor in the difference in the emissions measured at points within them which determines the distribution of variance, co-variance and the localized coherency on that day. However, overall it is the combination of elements that determines the spatial scale of the process when a cyclic process is detectable.

Perhaps of more interest is that the expression of the landscape control on the spatial and scalar distribution of variance, co-variance and coherency changed over time as a result of change in soil conditions. On 30 Mar. the variance is globally distributed on the transect as a result of the control that the topography had on the distribution of soil temperature. Exposed areas of soil where snow cover had been thinnest and first to melt away were warmer allowing an active soil layer to form on the surface. This global distribution of variance changes to a local concentration of variance, on 29 Apr., at a specific CW element, where limitations to the processes producing N_2O were much less than other depressional elements (UW and the smaller CW element). These limitations

may have been related to N availability as the WFPS was high at two other depressional elements where little or no N_2O was produced. As soil moisture decreased after 29 Apr. a primarily random pattern developed and was apparent by 23 June.

As discussed in Yates et al (2006b) (Chapter 4), the driving force for the changing pattern is the spring snow melt and the redistribution of water in the landscape. The pattern of flux follows an event- and background-based emission pattern as described by Brumme et al. (1999). It appears that the spatial dependency of soil N_2O on WFPS and soil temperature also changes during evolution from the event-based emission pattern to the background emission pattern. Early in the event, N_2O flux was dependent on soil temperature and this dependency was global. Near the end of the event N_2O flux was dependent upon WFPS and the pattern was highly localized. After the event, the dependency of soil N_2O flux is obscured by background variability.

The results suggest important implications for the modeling of soil N_2O emissions in terrains similar to the St. Denis site. The strong predictive relationship between soil N_2O flux and soil temperature indicated by the wavelet coherency on 30 Mar. should lend itself to the accurate modeling of soil N_2O emissions along a large portion of the transect based on soil temperature. As the spatial scale of this relationship was a result of the pattern of soil exposure during early stages of snowmelt, probably where snow was thinnest due to scouring and redistribution by prevailing winds, it may be assumed that this spatial pattern will be similar each year for the same management conditions and therefore, at the same spatial scale. The question that remains is the period of time that the 30 Mar. sampling represents, something that would likely change from year to year as overall yearly snowfall changes.

On 29 Apr. the local feature in the wavelet coherency between WFPS and soil N_2O emission for this date represents a small area of the transect where soil N_2O emissions may be predicted with some accuracy based on measurements of WFPS. This occurs at a single CW position as opposed to any of the UW positions and the CW position at the south end of the transect, implying that not only land-use was an important factor, but also the size or shape of landform units within a category. Modeling of emissions in such a terrain for these conditions would require identification of these active units within which accurate prediction may be possible. Outside of these

units, and under these conditions, no predictive relationships exist and estimation of N_2O flux would require direct measurement.

The lack of predictive relationships between soil N_2O flux and both WFPS and soil temperature on 23 June indicate that modeling under the conditions represented by this date would be futile. Direct measurement would be necessary for the entire area represented by the transect. However; as direct measurement appears necessary in situations when a spatial pattern is not discernable (i.e., random) the number of locations needed to accurately predict the mean may be low, depending on the expected variability.

The results for 30 Mar. demonstrates the differences in visual interpretation between the local wavelet, cross-wavelet and wavelet coherency spectra. The wavelet spectrum for soil N_2O indicated significant variance at the 72 to 144 m scale where as the spectrum for soil temperature did not. This would suggest that the significant co-variance indicated between the two soil properties in the cross-wavelet spectrum may be spurious, but this was not the case as the wavelet coherency clearly indicated that a strong, positive relationship existed between them. Conversely, the strong co-variance indicated between soil N_2O and soil temperature on 29 Apr. does not translate into any indication of a strong local feature in the wavelet coherency spectrum, as it did for WFPS. Clearly wavelet and cross-wavelet spectra need to be interpreted with care when discussing the relationship between soil properties, and wavelet coherency is critical to establishing the existence of relationships using these statistical techniques.

5.6 Conclusions

The processes behind the spatial pattern of soil N_2O flux were controlled by topography. This was expressed at a scale that coincided with the spacing of gross landscape units such as knolls and depressions (72 to 144 m) when high values in actual flux along the transect were associated with a repetitive landscape element. A strong cyclic pattern in N_2O emission occurred only on 30 Mar. due to a flux pattern controlled by exposed soil positions early in the spring snowmelt period. This resulted in a strong predictive relationship, as indicated by wavelet coherency, between soil N_2O and soil temperature. It is probable that accurate field-scale modeling of N_2O emissions is

possible for these conditions. However, by 29 Apr. the cyclic, landscape-scale pattern of emissions is lost and local wavelet variance is dominated by a singular feature within which a predictive relationship exists between soil N_2O flux and WFPS, but outside of that there is little or no predictive relationship. Modeling may only be possible within certain landscape units under these conditions and estimation of flux at these time would probably rely on direct measurement for most areas of the transect. On 23 June there is no landscape pattern to soil N_2O emissions and although there is some landscape control of soil temperature and WFPS, predictive relationships are not possible and modeling of N_2O emission on those dates would not be possible. Direct measurement would be necessary. Wavelet coherency analysis was shown to be a valuable tool in interpreting dependency between soil properties and should be used in conjunction with the analysis of the local wavelet and cross-wavelet spectra of soil properties.

6.0 CONTRIBUTION OF EPHEMERAL WETLANDS TO ANNUAL NITROUS OXIDE FLUX FROM AN AGRICULTURAL LANDSCAPE

6.1 Preface

The 128-point transect allowed the use of powerful statistical tools to describe the spatial pattern of soil N_2O flux showing the distribution of local variance and how this pattern changed over time. This method identified landscape elements key to the changing flux pattern, the scales of variation and localized features, and how this pattern relates to where and when predictive relationships can be used. However, even though the transect represented landscape elements proportionally, a direct comparison of the mean flux between elements is better served by equal representation. In this regard, the uncultivated wetland elements are under-represented by the transect. Resources only allow occasional sampling of the transect and estimates of yearly mean emissions across the site require more frequent sampling. To address these issues, in addition to the transect, a 50-point stratified sampling design was employed. This design allowed better representation of uncultivated wetland elements and more frequent sampling. In this way the concept of the event-based / background emission pattern, demonstrated by the transect data, can be applied across the research site and cumulative emission estimates can be up-scaled from the point to the field.

6.2 Introduction

Understanding the spatial and temporal variation in soil nitrous oxide (N_2O) emissions is important to compiling an accurate inventory of emissions as well as the scaling and modeling of emissions. To date there has been little research published on emission measurements from hummocky agricultural landscapes, common to the Prairie region that can contain considerable within-field variation in landform and land use.

Differences in N_2O flux measurements or denitrification between landform elements and between land use types have been observed and generally attributed to the

control these factors have on water redistribution, water-filled pore space and N availability. Pennock et al. (1992) attributed the spatial distribution of denitrification to the concentration of water in low areas of the landscape. Corre et al. (1996) found foot-slope elements to have a higher number of N_2O producing micro-sites compared to shoulder elements and low emissions in pasture and forest sites compared to cropped sites. Izaurralde et al. (2004) found summer fluxes to be controlled by topography and N rate.

It then follows that although spatial variability in N_2O emissions for an area with variation in both landform and land use may be high, a large portion of this variability may be accounted for by employing sampling strategies that account for the range of landforms and land use. A commonly used design for describing spatial variability is the linear transect. This is a flexible design that allows for a range of statistical and geostatistical analysis to be used and has been employed in these landscapes (Yates et al., 2006a). However, a stratified sampling design that employs an equal number of locations per element is more appropriate for comparisons between landscape elements and for calculating cumulative emissions.

Most agricultural landscapes in the Prairie region, especially those with variable topography such as a hummocky terrain, contain numerous wetlands. A large number of these wetlands are semi-permanent or seasonally hold water. Water is gained through snow melt and summer precipitation and lost through evapotranspiration and vertical drainage (van der Kamp et al., 1999). Typically the center of this type of wetland is surrounded by a complete ring of trees or shrubs or a combination of a partial tree ring and grass fringe. The outer boundary of both the tree ring and grass fringe is controlled by cultivation of the surrounding agricultural area of the field.

The magnitude of N_2O emissions from wetlands in the Canadian Prairie region is virtually unknown. The semi-permanent wetlands represent a hydrology and suite of soil types, soil physical properties and nutrient cycling distinct from the surrounding cultivated area of the landscape. Within the wetlands the basin center, tree ring and grass fringe also differ in vegetation type, hydrology, and nutrient cycling. Such differences may result in distinct differences between cultivated upland and wetland and

between wetland units in terms of net N_2O flux. It is necessary to know what these differences are so that accurate inventory estimates for these landscapes can be made.

The objective of this chapter was a) to quantify annual N_2O flux from convex, concave, riparian grass, riparian tree and basin center landscape elements representing both variation in topography and agricultural and non-agricultural land uses on hummocky topography at a site in the Dark Brown soil zone of Saskatchewan, b) to assess if it is necessary to subdivide uncultivated wetlands for the purpose of sampling soil N_2O flux and identify differences between the landscape elements in terms of the timing of N_2O flux and c) to show the relationship between N_2O flux and water-filled pore space, pond water level, and soil temperature.

6.3 Methods and Materials

6.3.1 Field site and sampling design

The research site was located in the St. Denis National Wildlife Area, 52° 12' N latitude, 106° 5'W longitude, approximately 40 km east of Saskatoon, Saskatchewan, Canada. The site was on a hummocky, till terrain (Figure 6.1). Slopes were 10-15% and the parent material was a combination of unsorted calcareous till and glacio-lacustrine sediments. The glacio-lacustrine sediments blanket the till in a thin mantle, leaving the till very close to the surface or exposed on topographically high positions and some convergent areas that lead into lower slope positions.

A detailed topographic survey of the site was completed using a Sokkisha Set 5 Electronic Total Station, (Sokkisha Co. Ltd. Tokyo, Japan) and a Trimble^{TR} Pro XRS, Global Positioning System (Trimble Navigation, Sunnyvale, CA). A digital elevation model was produced with a 5-m X 5-m grid cell extent.

Locations in the cultivated area of the site were classified as either convex (CX) or concave (CV). These topographic units were previously described in Yates et al. (2006b) (Chapter 4); however, for the sampling design used in this study, CV elements included any adjacent cultivated wetland locations (CW) referred to in the earlier study. Convex elements are topographically high positions with an overall positive profile curvature such as top and mid-slope of a knoll. The CX elements equate to the convergent and divergent forms of shoulder and divergent back-slope elements as

presented by Bedard-Haughn et al. (2006) who reported an aerial extent of 14.4 ha within the site. Concave elements are positions with an overall negative profile curvature such as foot-slopes and depressions. These equate to convergent back-slopes, and convergent and divergent forms of foot-slope elements and depressions as per Bedard-Haughn et al. (2006) and have an aerial extent of 11.8 ha. Mean bulk density of the soils at CX and CV positions were similar (1.29 ± 0.10 and 1.24 ± 0.14 g cm^{-3}, respectively).

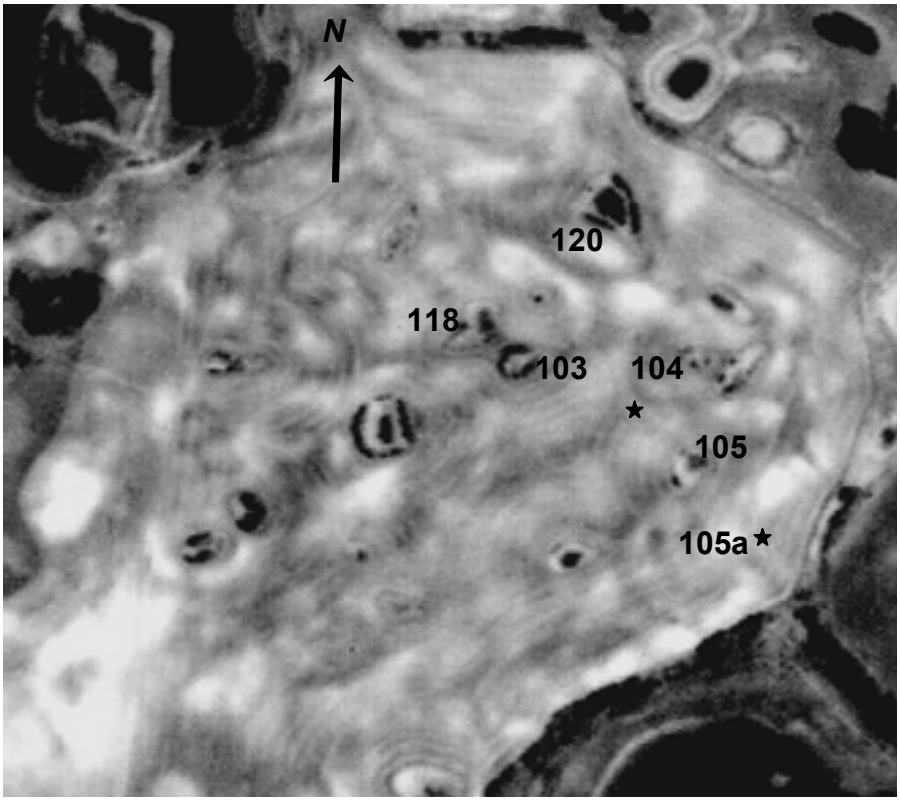

Figure 6.1: Air photograph of research site at St. Denis Wildlife Area prior to seeding of grass. Dark circular features are uncultivated ponds with tree rings. Sampled ponds have been marked with pond number as per Hogan and Conly (2002). Grey shaded areas are low relative elevation. White shaded areas are high relative elevation.

The semi-permanent wetlands represent uncultivated areas of the site, although all had been cultivated prior to 1968 when they were taken out of production by the Canadian Wildlife Service (Bedard-Haughn et al., 2006). The wetlands were further sub-divided into three landscape elements after preliminary surveys of soils and vegetation (Figure 6.2). The basin center (BC) is a level area covered by a variety of

non grasses such as *Mentha arvensis* L., *Cirsium arvense* (L) Scop., and *Urtica gracilis* Ait. The riparian grass (RG) is a non-level fringe area covered with grasses such as *Bromus inermis* Leyss. The riparian trees (RT) are a partial fringe of mixed trees and shrubs such as *Salix spp., Populus balsamifera* L., *and Populus tremuloides* Michx.

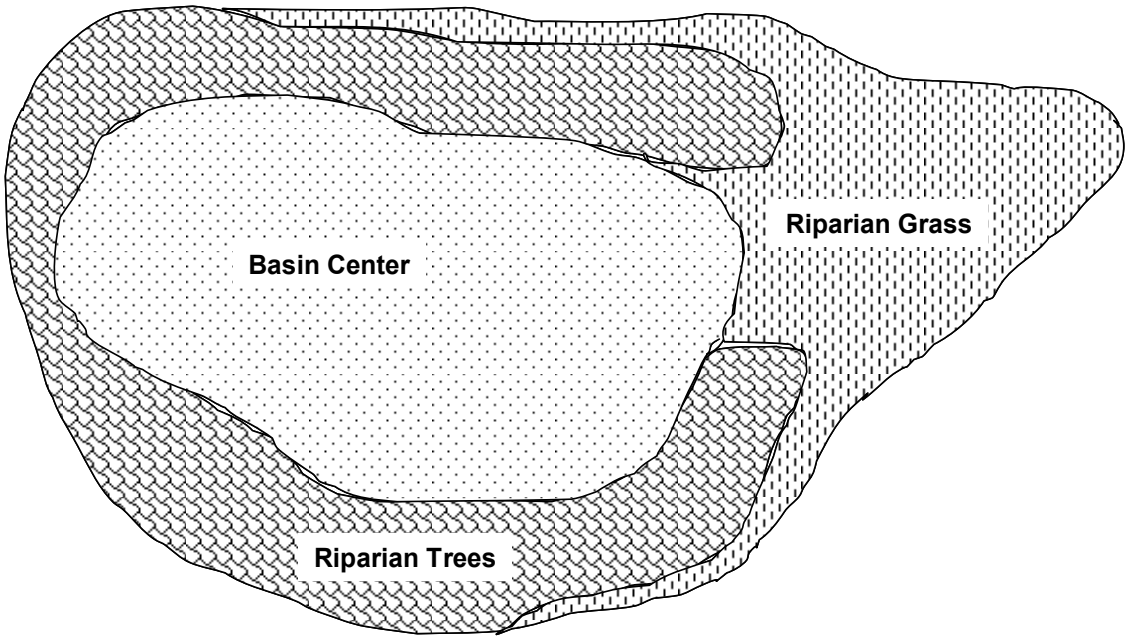

Figure 6.2: Drawing of typical uncultivated wetland at St. Denis Wildlife Area showing the landscape element riparian grass, riparian trees and basin center.

Originally, the stratification included a sediment fan unit that represented a grass area on the fringe whose underlying sediment had washed into the wetland from the adjacent cultivated area along a convergent landform (Bedard-Haughn et al., 2006). Sediment fans were found to have high SOC density and singled out for potentially high soil N_2O flux; however, this unit was dropped after the spring of 2004 when it was apparent that N_2O emissions from this element were not different from that of the RG element.

Bedard-Haughn et al. (2006) reports an aerial extent of 0.6 ha for BC, 1.0 ha for RG and 1.5 ha for RT elements. Mean bulk density in the wetlands was lower than that of the surrounding cultivated units at 0.83 ± 0.27, 0.93 ± 0.32, and 0.78 ± 0.29 g cm^{-3} for the BC, RG and RT landscape elements. Mean soil bulk densities are taken from

unpublished data based on 2 to 42 samples per position in the wetlands and 84 to 140 samples in the cultivated area of the site.

Soil types across the site ranged from thin Chernozemic Rego Dark (Typic Calciborolls) Brown at the CX positions through the thicker Chernozemic Orthic Dark Brown (Typic Haploborolls) in the CV positions, to Chernozemic Eluviated Dark Brown (Albic Agriborolls) and Gleysolic Humic Luvic (Argic Cryaquolls) in depressional positions. Chernozemic Calcareous Dark Brown (Haplic Calciborolls) soils were found in shoulder and back-slope positions as well as some foot-slope positions. Overall, soil textures range from loam at topographically high positions to silt loam in depressions.

The hydrological pattern on the site is controlled primarily by the depressions, which act as focal points for inputs and redistribution of precipitation and snowmelt water. The bulk of the water infiltrates laterally through the depression margins where it is recycled through evaporative and transpiration processes (Hayashi et al., 1998a). The primary source of water for the wetlands is spring snowmelt runoff. Summer precipitation extends the life of the ephemeral ponds; however, water loss from these closed basins is almost entirely by evapotranspiration (i.e., evaporation from the open water of the pond and transpiration from the vegetation in and around the pond). Some water infiltrates beneath the pond as vertical recharge to groundwater and aquifers at depth (Hayashi et al., 1998b).

In July of 2003 a 66-point stratified sampling design was established at the site in the wetlands and on the adjacent cultivated land, which had been fallow since 2002. The previous crop had been *Hordeum vulgare* L. This provided at least 10 locations per landscape element (including the sediment tongue). In May of 2004 the number of locations was reduced to 50 (10 locations per element) when the sediment tongue element was eliminated. The 50 locations were distributed in short transects over four uncultivated wetlands and two landform cycles (knoll-depression) within the cultivated uplands.

In May of 2004 the east side of the research site, including the transect area, was seeded to grass by Ducks Unlimited Canada. The mix consisted of *Agropyron elongatum* (Host) Beauvois, *Agropyron intermedium* (Host) Beauvois, *Bromus biebersteinii* Roem. and Schult., *Elymus dauricus* Turcz. exgriseb., *Festuca rubra* L.,

Onobrychis viciifolia Scop., *Elymus Canadensis* L., *Agropyron trachycaulum* (Link) Malte and *Medicago sativa* L.

6.3.2 Soil N_2O Flux Measurements

At each location soil N_2O flux was measured using a two-piece, closed, vented chamber (International Atomic Energy Agency, 1992) consisting of a polyvinyl chloride (PVC) ring base and vented cap with sampling port similar to Hutchinson and Mosier (1981). The chamber, when placed for sample collection, had a head space of 2.25 L and covered a soil surface area of 0.02 m^2. Prior to the start of data collection, the bases were pressed into the soil and secured using 20-cm spikes where they remained for the duration of the field season. At each sampling event, the chamber was placed onto the base and sealed by a rubber ring within the cap.

During early spring some measurements were made directly from the snow surface by inserting the ring base directly into the snow pack. This was done until all snow had melted at that location and the ring base was then inserted into the soil. Run off from snow melt that collected in the wetlands and CV areas of the landscape made some locations temporarily inaccessible. At these times measurements were taken from the surface of the water using an acrylic, non-vented chamber accessed from a wooden walkway and held in place by a metal rod imbedded into the ground below. The acrylic chambers had a headspace of 10.76 L and covered a water surface area of 0.06 m^2. Walkways and rods were installed the previous fall. Flux measurements from these chambers were calculated in the same manner as the PVC chamber and used to calculate and average water surface flux measurement per wetland or depression that was applied equally to all inundated locations in that wetland or depression.

Samples of the headspace gas were drawn from the chamber with a 20-mL syringe and injected into 12-mL evacuated tubes for transport back to the laboratory. Samples of the headspace gas were drawn at three equally spaced time intervals of 8 min. In 2003 the N_2O concentration in ambient air was used as the initial (time zero; t_0) concentration after Anthony et al. (1995). In 2004, individual time zero samples were collected from each chamber. Four people were involved in each sampling and this

allowed for a complete sampling in less than 1 h. Gas sampling was timed to begin at midday.

Nitrous oxide concentrations were determined using a Varian CP3800 GC (Varian Canada Inc., Mississauga, ON) equipped with dual electron capture detectors (ECD). The injector temperature = 100°C, column temperature = 35°C, detector temperature = 370ºC; separations were carried out using Poraplot Q columns (12.5-m × 0.32-mm i.d. fused silica capillary column, Df (film thickness) = 8 μm; includes a 2.5-m particle trap) with ultra high purity He (14.4 mL min^{-1}) as the carrier gas and P5 (95:5 v/v Ar:CH_4 mix) as the make-up gas (12.0 mL min^{-1}). Samples (300 μL) were introduced using a CombiPAL™ auto-sampler (CTC Analytics AG, Switzerland) with on-column injection and a split ratio of 10:1. The system was calibrated using standard gases (N_2O in N_2) obtained from PraxAir (Mississauga, ON). Data processing was performed using the Varian *Star Chromatography Workstation* (ver. 6.2) software. Internal calibration curves were obtained by applying linear least squares regression to the gas concentration (ppbV N_2O) *versus* peak area data; N_2O concentrations in the headspace samples were than calculated automatically from the regression equations.

Ambient air samples were included as reference samples in each analytical run to check the 'within run' precision, calculate the minimum detectable concentration difference (MDCD), and correct for detector drift. The MDCD was calculated by (i) analyzing matched pairs of the reference gas samples at regular intervals during each analytical run; (ii) calculating the average difference between sample pairs (μ_p) as well as the standard deviation (σ_p); and (iii) calculating the MDCD using Eq. [6.1].

$$MDCD = \mu_p + (2\sigma_p) \qquad [6.1]$$

The MDCD was used to filter the raw data when calculating the actual N_2O flux; i.e., concentration differences between t_0 and each subsequent time step that were <MDCD were not considered to be significantly different from the t_0 concentration. Anthony et al. (1995) arbitrarily chose to use twice the mean absolute difference between pairs of ambient air samples. Using the form presented in this study brings a statistical basis to the MDCD by calculating a value that is within the upper bound of the 95% confidence interval for the mean paired difference. The variability in our data is such that the

method employed here to calculate the MDCD is slightly more rigorous than that used by Anthony et al. (1995).

Although some studies assumed that the change in N_2O concentration within the chamber over time is linear it has been demonstrated that concentration (ng L^{-1}) *vs.* time (min) relationship is not linear due to a decreasing concentration gradient (Hutchinson and Mosier, 1981). Measuring N_2O concentration at t_0 and for each of the three 8-min time intervals produces 4 points for the concentration *vs.* time curve. The vertical flux of N_2O at the soil–atmosphere interface (ng N_2O-N m^{-2} s^{-1}) was then calculated as the slope of the line tangent to the concentration *vs*. time curve at t_0. That is, the flux at t_0 was calculated as the 1st derivative of the 2nd-order polynomial equation ($y = ax^2 + bx + c$) used to describe the concentration *vs*. time relationship. The flux (ng N L^{-1} min^{-1}) was then converted to an area-second basis by multiplying by 1.87 L min m^{-2} s^{-1} [i.e., the chamber volume ÷ (surface area × 60 s min^{-1})]. In cases where 'rogue' data points prevented the use of the 2nd-order polynomial model (i.e., only 3 points available instead of 4) the flux was calculated as the slope of the linear model that best described the concentration *vs*. time relationship (Hutchinson and Mosier, 1981) (Eq. [6.2]).

$$F_{N_2O} = \frac{V}{k_t A} m \qquad [6.2]$$

Where F_{N_2O} is the flux at t_0, V = chamber volume (L), A = cross-sectional area of soil covered by the chamber (m^2), k_t = time constant (60 s min^{-1}), and m = slope of the linear, regression equation (ng L^{-1} min^{-1}).

A mean flux of 10 ng N_2O-N m^{-2} s^{-1} was used as a threshold value to separate flux events from background emissions, in keeping with the event-based / background emission pattern proposed in the previous chapters as a model for the temporal change in flux pattern across the site. The expectation of the timing and distribution of event and background flux, based on the previous results, suggested that across a season background flux tended to be close to zero, but rapidly increased during an emission event. Although it is likely that a different threshold value for each landscape unit could be chosen, it was important to use a consistent value. The threshold value of 10 ng N_2O-

N m^{-2} s^{-1} is represents a magnitude change in mean flux, which would be expected during such an event.

6.3.3 Measurement of Soil Moisture, Soil Temperature and Climate Data

At each location, volumetric soil moisture over a 15-cm depth was measured at the time of gas sampling using time domain reflectometry (TDR) after Topp and Ferre (2002). Readings were obtained manually from a Tektronix 1502 B cable tester (Tektronix, Wilsonville, OR). Also at each location, soil temperature was measured at 5- and 20-cm depths using buried type-T thermocouples constructed of twisted copper and constantan (45% Ni and 55% Cu) wire pairs and read using a Barnant DuaLogR™ thermocouple reader (Barnant Company, Barrington, IL). Beginning in June of 2003 a meteorological station on site recorded hourly averages of precipitation, air temperature and wind speed. Monthly precipitation and air temperature data required prior to June was obtained from Environment Canada (2005a).

6.3.4 Cumulative emission estimate

Interpolation of the flux between sample dates to estimate the total emissions produced over the period of data collection was done similar to Pennock et al. (2005). The mean flux for a specific date (ng N_2O-N m^{-2} s^{-1}) was converted to g N_2O-N ha^{-1} and multiplied by a time interval (days) represented by ½ of the period between the specific date and the previous date and ½ of the period between the specific date and the next date. The results for each interval were summed over the period of data collection for a cumulative estimate. For example, the mean flux for on 31 July 2003 was multiplied by a period of time from 1200 on July 24 to 1200 Aug. 04 or 11 days. The flux for each day in 2003 was treated in a similar manner and summed to represent the 2003 period of sample collection that started on July 03 and ended Oct. 10 for a period of 108.5 d.

6.3.4 Statistical Analysis

The measurements of N_2O flux and soil moisture (presented as WFPS) are presented as means, with standard deviation, for landscape element on each sampling date. Soil temperatures are presented as ranges of mean values in each season per

landscape element at both depths. Mean soil temperatures at both depths for each sampling date in a specific year were ranked and the mean rank is presented. Temporal continuity of the rank for each date across the year was assessed using Kendall's Coefficient of Concordance (W test) as per Downie and Heath (1974). This test looks at the relationship between sets of ranked data. In this case the sets of ranked data were mean values of soil temperature for each measurement date. The means for each element were ranked from smallest to largest and the coordination coefficient (W) reflects the degree to which the order of elements changes across the measurement dates as a function of their mean soil temperature. A value of W close to 1 indicates temporal stability in the order of the relative differences in soil temperature between the landscape element and a value of W close to 0 indicates a lack of temporal stability. In this manner one can present information on soil temperatures at the St. Denis site without resorting to several tables of mean values. Spring mean soil monthly temperatures for the 5-cm depth are also presented graphically as a box and whisker plot. Pearson product moment correlations and regressions were performed using MINITAB® Release 14 (Minitab Inc. 2003).

6.4 Results

6.4.1 Precipitation and Air Temperature

For the measurement period of 30 Mar. to Oct. 31 the cumulative precipitation for 2003, 2004 and 2005 was respectively, 238, 282, and 400 mm (Figure 6.3). Normal precipitation for the Saskatoon area over this period of time is 259 mm (Environment Canada, 2005b). Rainfall events in 2003 were less frequent than in 2004. In 2005 rainfall was both frequent and intense (for the region), reaching as high as 100 mm over 48 h (June 17 and 18). Mean daily air temperatures (data not shown) compared to the 30 year daily means for the Saskatoon, SK area (Environment Canada, 2005b) were below normal in Mar. and above normal for Apr., May, June, and Aug. of 2003 by up to 2.4 °C. For Mar. to Oct. of 2004 and 2005 mean daily air temperatures were primarily below normal by up to 3.5 and 2.5 °C, respectively.

6.4.2 Nitrous Oxide Flux, Water-filled Pore Space and Pond Water Levels

In 2003 the cultivated area of the landscape was most active. The mean flux for CV elements was > 10 ng N_2O-N m^{-2} s^{-1} from 8 July to 12 Sep., as was the mean flux for the CX elements for a period in mid July and again in Aug. (Table 6.1). Mean flux in the wetland elements was < 10 ng N_2O-N m^{-2} s^{-1} on all dates except on 29 Aug. for the RT elements. On several occasions a net negative flux was measured for wetland elements, especially the BC elements where flux was negative on four out of nine samplings. In contrast, negative mean flux was measured only once at both CX and CV elements (10 Oct.).

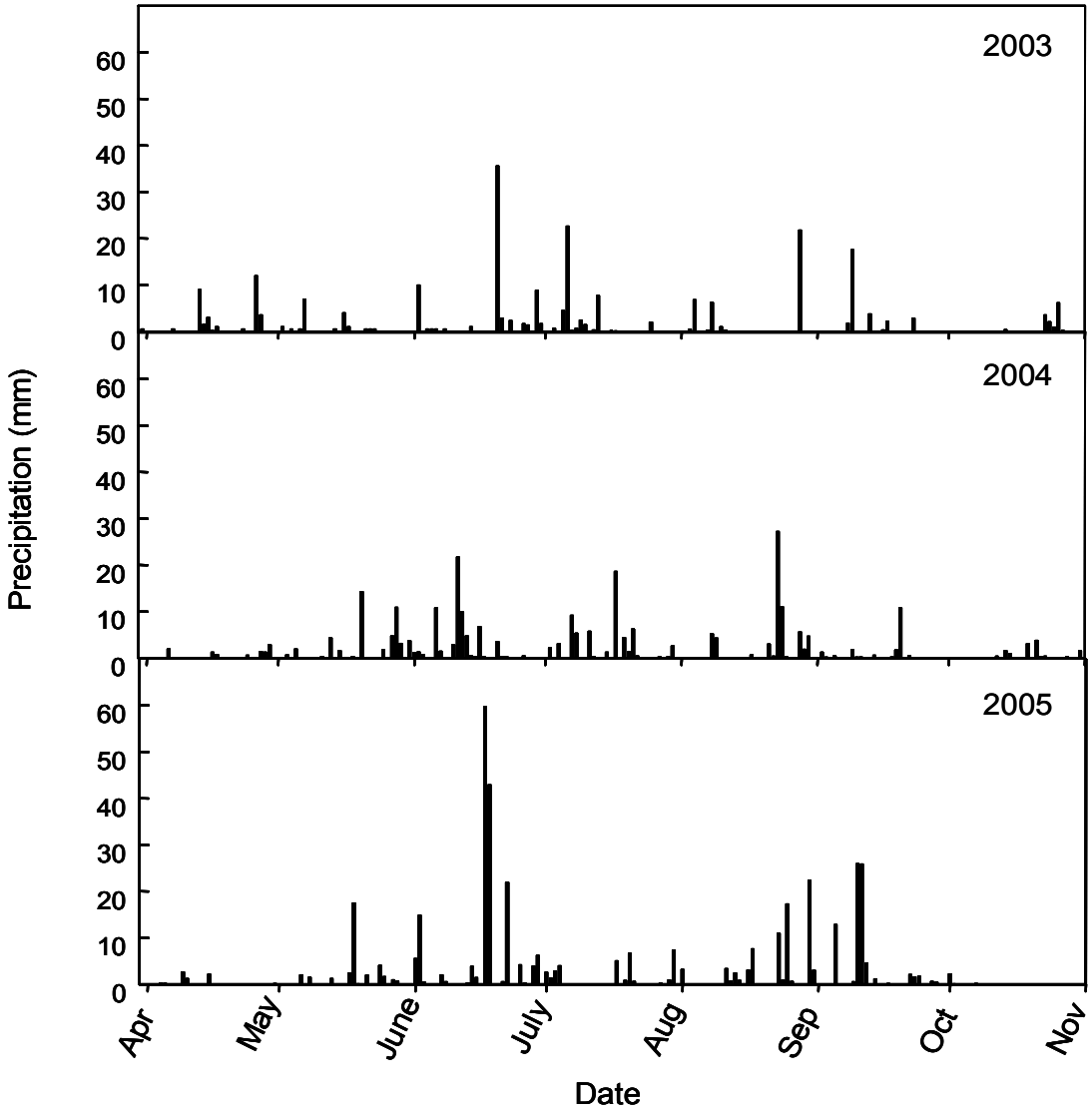

Figure 6.3: Daily rainfall (mm) at St. Denis Wildlife Area for 2003, 2004 and 2005.

Table 6.1: Mean N_2O flux and standard deviation (ng N_2O-N m^{-2} s^{-1}) from the landscape elements at St. Denis Wildlife Area in 2003. Fluxes > 10 ng N_2O-N m^{-2} s^{-1} are bolded.

Landscape Element		Date (month / day)								
		7/3	7/8	7/17	7/31	8/8	8/29	9/12	9/26	10/10
Cultivated										
Convex	mean	0.98	**13.21**	**17.73**	7.23	3.38	**16.90**	9.52	2.24	-1.44
	σ†	3.11	10.91	6.92	14.61	9.43	6.69	7.24	7.08	4.85
Concave	mean	4.82	**61.00**	**22.57**	**11.69**	**25.59**	**27.00**	**20.69**	1.80	-1.41
	σ	7.86	108.76	17.21	14.73	18.62	26.99	22.85	4.73	6.96
Uncultivated										
Riparian Grass	mean	4.14	0.83	-1.35	6.88	9.99	9.66	-2.37	2.36	0.37
	σ	10.13	3.12	13.81	11.32	9.40	11.30	5.02	12.15	6.03
Riparian Trees	mean	0.11	1.11	1.69	9.46	-3.22	**11.86**	-2.02	3.60	0.59
	σ	2.57	4.14	8.96	11.23	5.89	11.10	4.34	19.82	8.31
Basin Center	mean	1.02	-1.58	7.69	5.09	-4.41	9.19	-1.16	0.28	-1.73
	σ	3.52	6.49	9.52	8.25	5.24	11.56	2.96	3.31	10.57

† Standard deviation

Mean WFPS in 2003 exceeded 50% in CV elements on all sampling dates and exceeded 60% five times (Table 6.2). Convex elements were generally between 40 and 60% mean WFPS, exceeding 60% only on 12 Sep. following a rainfall that exceeded 20 mm (Figure 6.3) . At all wetland elements a lack of standing water in the ponds resulted in mean WFPS remaining less than 50% and ranging as low as 15% on all dates.

Flux measurement in 2003 did not begin until after spring snowmelt and the first flux measurement on 3 July showed emissions at all landscape elements were < 10 ng N_2O-N m^{-2} s^{-1} (Table 6.1). Following a three day rainfall event that peaked on 5 July (Figure 6.3) the mean emission measured 8 July had increased by an order of magnitude at CV and CX positions, whereas mean flux at other elements remained < 10 ng N_2O-N m^{-2} s^{-1}. A flux >10 ng N_2O-N m^{-2} s^{-1} was maintained until 12 Sep. at CV positions. This coincided with precipitation through the first part of July and intermittent rainfall in Aug. and Sep. that kept the WFPS at CV elements almost always above 60%, whereas it had been below 60% before and afterwards (Table 6.2). WFPS was lowest in wetland elements, including BC units, where mean fluxes virtually remained < 10 ng N_2O-N m^{-2} s^{-1}. The low bulk density in the upper 15 cm of soils at the uncultivated verses the cultivated areas of the site means more water is required in the uncultivated soils to achieve an increase in WFPS to the 60% threshold. It is likely that the summer precipitation events were not great enough to achieve the water contents needed.

The CV elements also showed the highest mean N_2O flux in 2004, with mean flux as high as 93.5 ng N_2O-N m^{-2} s^{-1} (Table 6.3). High flux occurred on four consecutive dates from 8 Apr. to 6 May after which the mean flux for CV elements remained below 10 ng N_2O-N m^{-2} s^{-1}. The BC elements also had mean flux > 10 ng N_2O-N m^{-2} s^{-1} on four dates; however, this activity occurred on non-consecutive days after 6 May and was only as high as 19.3 ng N_2O-N m^{-2} s^{-1}. Mean flux for the other landscape elements was < 10 ng N_2O-N m^{-2} s^{-1}. All elements had at least one negative mean flux in 2004, especially CX elements where mean flux was negative on nearly 50% of the dates.

Table 6.2: Mean water-filled pore space and standard deviation (%) from the landscape elements at St. Denis Wildlife Area in 2003 (0-15 cm). Values > 60% are bolded.

Landscape Element		Date (month / day)								
		7/3	7/8	7/17	7/31	8/8	8/29	9/12	9/26	10/10
Cultivated										
Convex	mean	47	59	54	46	54	56	**61**	47	41
	σ†	14	8	7	8	8	7	7	7	8
Concave	mean	52	**67**	**63**	55	**63**	**63**	**70**	56	50
	σ	8	6	9	8	09	8	9	4	6
Uncultivated										
Riparian Grass	mean	20	37	30	17	19	21	26	19	15
	σ	8	10	10	8	11	9	8	6	6
Riparian Trees	mean	21	37	32	19	24	23	28	21	17
	σ	5	6	7	5	5	8	6	4	4
Basin Center	mean	26	45	43	25	26	18	26	22	18
	σ	17	19	23	13	12	6	8	7	6

† Standard deviation

Table 6.3: Mean N_2O flux and standard deviation (ng N_2O-N m^{-2} s^{-1}) from the landscape elements at St. Denis Wildlife Area in 2004. Fluxes > 10 ng N_2O-N m^{-2} s^{-1} are bolded.

Landscape Element		Date (month / day)											
		3/5	3/12	3/23	4/8	4/15	4/21	5/6	5/14	5/28	6/8	6/16	7/8
Cultivated													
Convex	mean	-1.89	4.88	-3.05	0.41	-0.47	-1.32	0.55	1.30	-2.54	0.00	-1.76	0.35
	σ†	1.71	7.42	2.14	1.61	0.77	4.18	0.99	2.72	3.50	0.00	2.30	1.10
Concave	mean	-2.46	2.15	-3.04	**26.70**	**26.00**	**93.50**	**31.20**	9.43	8.18	2.54	1.75	1.61
	σ	2.57	3.61	2.47	73.14	35.61	184.55	70.09	15.20	20.20	4.83	2.67	2.37
Uncultivated													
Riparian Grass	mean	-0.02	-2.01	-1.53	2.04	-1.26	0.52	0.16	1.48	-3.64	0.00	1.90	3.59
	σ	3.00	3.98	1.82	3.88	4.03	3.59	1.16	2.66	2.99	0.00	12.41	6.03
Riparian Trees	mean	-0.35	-1.86	-1.39	0.17	0.23	-0.24	0.35	0.61	-1.35	0.00	-1.03	3.07
	σ	5.36	5.37	3.38	2.91	5.17	2.90	1.31	1.56	3.21	0.00	2.21	6.75
Basin Center	mean	-0.12	1.70	-0.90	5.46	-0.48	-0.38	0.58	**13.86**	5.97	1.60	-0.60	**19.30**
	σ	2.55	3.20	3.51	3.69	5.72	2.49	2.01	25.15	25.54	2.57	2.58	52.58

Landscape Element		Date (month / day)								
		7/22	8/11	8/25	9/1	9/8	9/15	9/22	9/29	10/13
Cultivated										
Convex	mean	-0.07	-0.93	2.76	-0.08	-2.34	0.83	2.46	0.92	0.40
	σ	0.21	1.22	2.71	0.51	2.49	1.75	3.55	1.01	1.87
Concave	mean	5.39	1.07	4.84	0.31	-0.02	0.38	2.59	0.54	1.27
	σ	5.77	3.40	4.26	0.86	1.47	0.93	4.25	0.94	2.21
Uncultivated										
Riparian Grass	mean	-0.06	-0.78	1.59	1.19	-0.09	0.79	3.11	1.01	0.80
	σ	1.71	1.55	2.25	1.86	1.70	1.56	3.74	1.85	1.16
Riparian Trees	mean	4.67	7.87	4.03	2.34	0.37	2.74	4.82	0.70	0.75
	σ	9.32	20.49	7.25	6.34	5.03	3.20	5.64	1.80	1.06
Basin Center	mean	4.29	8.15	**11.81**	2.05	2.44	2.73	**10.58**	1.50	0.86
	σ	5.22	11.34	17.75	4.34	2.20	2.48	12.90	2.28	1.39

† Standard deviation

After spring thaw in 2004 (Table 6.4) soil in BC elements were saturated through Apr. (100% WFPS) then gradually drained, maintaining a mean WFPS in excess of 60% until 22 July after which mean WFPS remained above 40%. The CV elements also maintained mean WFPS > 60% steadily until 16 June and intermittently until 1 Sep. Mean WFPS at CX positions exceeded 60% from 28 May until 16 June, and again on 25 Aug. At RG and RT elements mean WFPS exceeded 60% during Apr. then gradually declined and remained below 60% for the remainder of the sampling period.

Water levels in the wetlands were recorded in 2004 and 2005 (Table 6.5). In 2003 standing water in the wetlands had dropped to zero well before the start of gas sampling on 3 July. In 2004, water levels in most wetlands had dropped to zero by mid-May. Standing water was maintained in pond 120 until Aug. In 2005, standing water persisted in most of the ponds until Aug. and ponds 105 and 120 maintained standing water until the end of gas sampling in mid Oct.

The peak in emissions in the spring of 2004 coincided with the decline in pond water levels though Apr. and early May. This peak occurs first at CV elements where there was a high mean WFPS as a result of the redistribution of snowmelt runoff into the low areas of the landscape (Table 6.4). Few precipitation events occurred during this time to otherwise account for the moisture contents measured. Mean flux > 10 ng N_2O-N m^{-2} s^{-1} was primarily at ponds 104 and 105a and lasted after standing water had disappeared. Flux at BC elements peaked on 14 May (Table 6.3), which coincided with the loss of standing water in ponds 103, 105 and 118, although the high flux is predominantly from pond 103 (Table 6.5). For both CV and wetland elements, major emissions occur when all or part of the pond bottom is exposed. Similar mean flux was measured at pond 120 on 25 Aug. also when standing water had reached 0 cm (Table 6.5).

Table 6.4: Mean water-filled pore space and standard deviation (%) from the landscape elements at St. Denis Wildlife Area in 2004 (0-15 cm). Values > 60% are bolded.

Landscape Element		Date (month / day)										
		3/5	3/12	3/23	4/8	4/15	4/21	5/6	5/14	5/28	6/8	6/16
Cultivated												
Convex	mean				57	59	59	46	57	**60**	**64**	**65**
	σ†				9	7	07	6	6	5	05	9
Concave	mean				**81**	**76**	**71**	**60**	**68**	**67**	**77**	**72**
	σ				21	22	18	17	11	10	12	12
Uncultivated												
Riparian Grass	mean				**69**	**65**	**63**	48	46	52	47	47
	σ				18	17	15	13	9	10	9	10
Riparian Trees	mean				59	**65**	**65**	59	51	46	52	50
	σ				20	26	25	21	16	12	15	21
Basin Center	mean				**100**	**100**	**100**	**94**	**83**	**72**	**73**	**74**
	σ				0	0	0	13	20	25	26	28

Landscape Element		Date (month / day)									
		7/8	7/22	8/11	8/25	9/1	9/8	9/15	9/22	9/29	10/13
Cultivated											
Convex	mean	56	56	40	**63**	59	52	44	57	44	38
	σ	7	7	4	6	6	5	06	6	6	5
Concave	mean	57	60	43	**63**	**62**	58	47	58	43	39
	σ	10	11	6	8	7	7	6	7	5	7
Uncultivated											
Riparian Grass	mean	44	44	31	41	41	38	31	40	34	30
	σ	08	7	6	7	8	8	7	10	10	7
Riparian Trees	mean	45	46	37	44	42	40	34	40	32	31
	σ	13	11	9	6	9	8	8	8	9	6
Basin Center	mean	**67**	**63**	49	53	53	50	44	50	45	41
	σ	26	26	24	19	18	16	17	15	15	18

† Standard Deviation

Table 6.5: Level of standing water (cm) and mean N_2O flux (ng N_2O-N m^{-2} s^{-1}) from ponds at St. Denis Wildlife Area during 2004 and 2005. Flux > 10 ng N_2O-N m^{-2} s^{-1} are bolded. Mean flux occurred on date or within one day of date shown.

	Pond (landscape element)											
	103 (UW)		104 (CV)		105 (UW)		105a (CV)		118 (UW)		120 (UW)	
2004	N_2O	cm	N_2O	cm	N_2O	cm	N_2O	cm	N_2O	cm	N_2O	cm
4/4		44		41		39		25		51		56
4/5		49		39		45		20		62		59
4/8	5.08	52	1.46	31	2.33	42	**51.90**	14	0.62	57	2.20	58
4/10		51		25		39		9		55		56
4/14		48		19		32		1		51		51
4/16	-2.25	44	-0.69	14	9.78	27	**52.68**	0	-1.93	47	-2.28	47
4/20		39		10		21				35		47
4/21	-0.96	30	**76.51**	6	0.00	20	**110.48**		-0.47	34	1.17	44
4/27		18		0		17				26		39
5/6	0.42	8	**61.36**		0.00	9	1.08		0.76	13	0.00	35
5/14	**15.20**		**17.20**		0.86		1.66		1.70		1.47	27
5/19		0				0				0		
5/27	1.65		**17.67**		2.83		-1.29		4.07		-5.96	23
6/9	2.10		4.99		0.00		0.08		0.21		0.18	22
6/16	-2.69		2.38		0.00		1.13		2.41		-0.29	31
6/23												14
7/5												18
7/8	4.39		2.63		**32.88**		0.57		4.36		-0.34	10
7/22	2.07		7.95		4.24		2.84		4.21		1.47	8
8/11	4.28		2.15		3.09		0.00		-1.18		**13.20**	0
8/25	7.42		4.57		0.64		5.12		0.96		**13.00**	
2005	N_2O	cm	N_2O	cm	N_2O	cm	N_2O	cm	N_2O	cm	N_2O	cm
4/8	2.58	80	2.28	63	4.81	81	3.96		0.96	85	1.68	103
4/22	-1.13		-1.10		0.07		3.09		-0.30		1.06	
5/5	-0.44		3.28		0.00		3.05		1.09		0.00	
5/19	1.30		**88.62**		4.96		3.99		0.38		2.38	
5/24	0.00		**67.79**		0.12		1.30		0.00		3.85	
6/2	7.77		**21.17**		**19.87**		**13.15**		6.24		1.31	
6/9	6.76		**61.26**		3.90		-4.04		2.81		2.86	
6/22	1.15	54	4.07	35	0.89	66	0.86		2.46	56	-1.18	111
7/4	**10.23**	47	-2.22	27	2.88	60	7.77		0.93	45	6.55	110
7/11	-0.95		**24.61**		0.00		7.11		3.70		2.30	
7/13		36		16		55				39		101
7/25	1.68	17	**51.92**	0	0.76	40	-1.89		0.73	15	0.37	85
8/2	**11.43**		**42.29**		**21.46**		9.11		7.83		2.53	
8/8	**34.29**		**11.50**		5.81		0.16		**19.38**		4.37	
8/16	**83.04**	0	4.06		5.15	16	9.51		**40.96**	0	9.02	75
8/22	**72.52**		1.52		6.10	12	0.90		**15.92**		**11.78**	72
9/6	**26.30**		4.06		1.27		1.86		5.97		9.11	
9/20	**23.38**		1.29		0.50		-1.34		4.93		3.21	
10/19	1.80		1.20		1.96	2	1.70		0.22		0.26	70

Mean WFPS was > 60% at both CV and BC elements through Apr., May and June, and into July for BC elements (Table 6.4). The similarity in WFPS and the difference in N_2O flux between CV and BC elements suggests controlling factors beyond WFPS are also involved. The peak in mean flux at BC elements on 25 Aug. and 22 Sep. coincides with rain fall events that occurred the day prior in each case (Figure 6.3). The same rainfall events did not appear to trigger a similar response from CV elements as the mean flux remained < 5 ng N_2O-N m^{-2} s^{-1} on both dates even though mean WFPS was near or slightly above 60% for CV elements, and yet was < 60% for the BC elements. At RG and RT elements, WFPS exceeded 60% in Apr.; however, mean fluxes remained low or were negative at these elements. The situation was the same for CX elements when WFPS exceeded 60% in May, June, and later in Aug. Pore size may be a factor in that a WFPS of 60% in some vegetated wetland units is not sufficient to restrict oxygen and trigger denitrification due to higher porosity. Soils with potential for preferential flow paths, such as root channels in RG and RT elements, may require higher WFPS than cultivated counterparts to achieve the restriction in oxygen diffusion necessary to trigger denitrification.

In 2005, mean N_2O flux > 10 ng N_2O-N m^{-2} s^{-1} was again primarily associated with CV elements and BC elements (Table 6.6). As in 2004 mean fluxes > 10 ng N_2O-N m^{-2} s^{-1} were recorded first in CV elements on consecutive sampling dates from 19 May to 9 June. A second episode of high activity in CV elements occurred starting 11 July and ended 2 Aug. Mean flux > 10 ng N_2O-N m^{-2} s^{-1} began at BC elements on 8 Aug. and occurred consecutively until 20 Sep. During this period of activity in the BC elements the highest mean flux of 2005 (86.63 ng N_2O-N m^{-2} s^{-1}) was recorded. Overall, fewer negative mean fluxes were recorded in 2005 and most of these were associated with CX elements.

In 2005, WFPS generally remained above 60% through to June, for all elements, when it declined below 60%, first in the CX elements followed by CV, RG, and RT elements (Table 6.7). Mean WFPS remained high (> 90%) at BC elements until 8 Aug. and remained > 60% to 6 Sep.

Table 6.6: Mean N_2O flux and standard deviation (ng N_2O-N m^{-2} s^{-1}) from the landscape elements at St. Denis Wildlife Area in 2005. Fluxes > 10 ng N_2O-N m^{-2} s^{-1} are bolded.

Landscape Element		Date (month / day)												
		3/15	3/30	4/8	4/15	4/22	4/28	5/5	5/19	5/24	6/2	6/9	6/17	6/22
Cultivated														
Convex	mean	0.00	0.85	4.65	1.87	1.26	6.18	-0.62	1.32	-0.30	4.86	0.20	-0.19	8.66
	σ†	0.00	4.05	4.03	5.21	4.27	4.90	1.52	3.04	1.32	3.93	10.21	0.61	6.61
Concave	mean	0.00	1.73	3.13	1.09	1.00	3.65	3.17	**46.30**	**34.60**	**17.33**	**28.60**	2.67	2.77
	σ	0.00	3.33	4.13	3.15	3.64	5.11	4.18	134.60	78.40	16.95	61.29	5.29	3.01
Uncultivated														
Riparian Grass	mean	0.33	0.10	1.49	0.00	-0.20	-0.33	-0.18	4.49	3.53	9.19	6.25	7.46	1.99
	σ	1.04	0.32	2.14	0.00	1.06	2.89	1.74	8.17	9.75	16.76	12.33	19.98	8.17
Riparian Trees	mean	0.00	2.01	2.33	0.00	0.16	-0.65	0.00	1.01	0.36	5.96	2.24	3.87	0.76
	σ	0.00	4.35	2.59	0.00	1.13	2.62	0.00	1.79	1.14	5.92	5.92	7.87	4.62
Basin Center	mean	0.40	-0.42	2.16	0.00	0.09	1.18	1.43	0.73	0.00	8.31	3.01	2.18	-0.47
	σ	1.00	2.92	2.00	0.00	1.23	1.06	1.55	0.96	0.00	4.40	9.17	3.82	2.19

Landscape Elements		Date (month / day)											
		7/4	7/11	7/18	7/25	8/2	8/8	8/15	8/22	9/6	9/20	10/4	10/18
Cultivated													
Convex	mean	0.71	1.62	3.47	-2.00	3.58	-0.92	0.35	0.48	0.16	-0.15	-1.20	0.10
	σ	7.61	6.10	3.76	3.68	4.93	5.33	1.45	2.71	2.11	4.19	3.82	1.32
Concave	mean	2.78	**15.86**	6.65	**24.77**	**25.70**	5.83	6.79	1.21	3.26	-0.03	-2.67	1.45
	σ	8.08	31.93	6.58	52.17	44.58	14.15	13.27	3.61	2.66	3.98	4.13	2.87
Uncultivated													
Riparian Grass	mean	4.18	0.85	5.55	0.78	**12.30**	4.02	4.66	3.54	2.23	1.71	0.49	-0.10
	σ	3.27	7.19	5.32	10.45	15.53	7.87	6.78	5.98	4.31	3.39	4.04	2.50
Riparian Trees	mean	2.63	-1.08	4.72	0.87	8.01	4.40	6.60	8.05	8.00	2.65	-1.94	0.71
	σ	11.57	4.73	5.17	8.13	5.75	8.57	24.18	23.50	20.16	8.07	4.77	2.07
Basin Center	mean	7.74	5.06	3.69	0.80	8.75	**37.03**	**86.63**	**60.51**	**19.88**	**17.23**	0.57	2.08
	σ	9.47	5.71	3.98	4.20	8.42	62.95	140.58	99.74	33.27	31.02	4.37	3.26

† Standard Deviation

Table 6.7: Mean water-filled pore space and standard deviation (%) from the landscape elements at St. Denis Wildlife Area in 2005 (0-15 cm). Values > 60% are bolded.

Landscape Element		Date (month / day)											
		3/15	3/30	4/8	4/15	4/22	4/28	5/5	5/19	5/24	6/2	6/9	6/17	6/22
Cultivated														
Convex	mean			**63**	51	**62**	59	**66**	**83**	**65**	**62**	**71**	**85**	48
	σ†			18	19	18	4	20	14	08	16	21	12	04
Concave	mean			**92**	**89**	**87**	**79**	**82**	**84**	**78**	**63**	**72**	**89**	**68**
	σ			19	18	15	17	21	18	15	17	17	12	27
Uncultivated														
Riparian Grass	mean			**85**	**90**	**83**	**70**	**70**	**78**	**71**	**70**	56	**69**	**71**
	σ			27	15	17	26	26	20	22	22	15	18	25
Riparian Trees	mean			**87**	**77**	**80**	**82**	**80**	**78**	**78**	**70**	**80**	**75**	**70**
	σ			27	36	28	24	23	22	23	24	18	19	32
Basin Center	mean			**100**	**100**	**100**	**100**	**100**	**100**	**98**	**96**	**98**	**95**	**100**
	σ			0	0	0	0	0	0	5	14	7	11	0

Landscape Element		Date (month / day)											
		7/4	7/11	7/18	7/25	8/2	8/8	8/15	8/22	9/6	9/20	10/4	10/18
Cultivated													
Convex	mean	49	36	42	35	38	37	33	34	33	38	34	41
	σ	8	7	8	9	7	7	7	5	9	12	10	10
Concave	mean	43	42	56	38	37	36	35	34	36	34	32	34
	σ	25	21	24	5	8	6	5	8	10	6	13	14
Uncultivated													
Riparian Grass	mean	**65**	49	53	43	40	25	29	27	29	31	31	32
	σ	31	29	33	31	22	4	5	4	8	8	6	7
Riparian Trees	mean	**67**	52	**66**	56	41	42	42	42	43	34	34	26
	σ	35	33	36	38	31	31	31	31	31	24	25	2
Basin Center	mean	**100**	**100**	**92**	**93**	**93**	**64**	**66**	**67**	**63**	**64**	**67**	56
	σ	0	0	24	23	22	38	36	35	39	38	37	36

† Standard Deviation

In 2005 mean flux in RG and RT elements was > 10 ng N_2O-N m^{-2} s^{-1} only once (5 May) from Apr. until early June (Table 6.6), yet during this period WFPS ranged from 70% to 90% (Table 6.7). At CX elements the mean WFPS was also over 60% on several dates from Apr. until mid June yet the highest mean flux in this period was only 6.2 ng N_2O-N m^{-2} s^{-1}. The major flux activity in 2005 at BC and CV elements was again associated with the disappearance of water from the wetland units (Table 6.5). High mean fluxes from CV elements started on 19 May and lasted until 9 June. This coincided with the disappearance of water from pond 105a (observed, but not measured in 2005) and from pond 104, although the flux came primarily from pond 104 (Table 6.5) where again exposure of some of the sample locations occurred due to declining water levels. Intense rainfall in mid-June (Figure 6.3) prolonged standing water in pond 104, which minimized fluxes at the submerged locations, and fluxes ceased at the exposed locations. The result is that mean WFPS remained high, yet fluxes did not. The second period of high flux activity from CV elements occurred when water in pond 104 finally drained entirely and the previously water-covered locations drained to a WFPS that was conducive to high flux activity (Table 6.5). The magnitude of mean flux will be partially dependent on how locations within a single element class are distributed among these three states: water-covered, saturated, and unsaturated. Thus it is possible for mean WFPS to be below 60%, yet still be associated with a mean N_2O flux > 10 ng N_2O-N m^{-2} s^{-1} if a single location within the unit is at a WFPS high enough to trigger denitrification and produce a strong flux, like the period of mean flux activity from the CV elements in July and Aug.

As mean flux > 10 ng N_2O-N m^{-2} s^{-1} was ending at the CV elements, mean flux activity increased at the BC elements (8 Aug.). This coincided with drainage of water from ponds 103 and 118, which reached 0 cm by 16 Aug. (Table 6.5). This period of high fluxes lasted until 20 Sep. due to prolonged activity in pond 103. During this time water had nearly finished draining from pond 105, but for reasons unknown activity at this pond was limited (Table 6.5).

The release of N_2O from the BC elements at this time was much delayed compared to 2004, which was a direct result of the standing water remaining in the ponds much later into 2005. However, the fluxes were much stronger than in 2004

leading one to speculate that the prolonged flooding of these elements might be creating conditions that promote high emissions, such as the development of N_2 fixing algae that becomes a source of mineralizable N upon the drying of the wetland (R. McDougal, personal communication, 2005). Without flux data from spring of 2003 we can only speculate that the limited runoff and rapid drying of the ponds in that year resulted in reduced fluxes compared to 2004 and 2005. Certainly the fluxes that were recorded for BC elements in 2003 were quite limited, increased during 2004 as water was retained longer in the ponds, and finally peaked in 2005 as water in ponds was higher than in the preceding two years.

6.4.3 Soil Temperature

It is difficult to summarize the soil temperature data because collecting temperatures at two depths doubles the number of readings compared to WFPS or N_2O flux. Even using mean values, it is a challenge to show both changes from date to date over the period of sample and differences between landscape elements. As well, there are gaps in the data, usually during spring snowmelt period, due to snow cover or standing water preventing access to the buried thermocouples. For these reasons the data has been summarized as ranges in temperatures by depth and landscape element in each year for spring, summer and fall (Table 6.8).

As well, mean rank and Kendall's coefficient of concordance is presented to show the relative differences in soil temperature between the landscape units, by depth, in each year and the temporal continuity of this pattern.

Overall, the value of W for each depth in each year indicates that relative differences in mean soil temperature between landscape elements had a moderate to high degree of continuity indicating that the landscape pattern of temperatures was moderately stable through time. The mean rank indicates that there was a tendency for RT elements to be the lowest in mean soil temperature and for CX element to be the highest in mean soil temperature; however, differences in mean rank were such that CX and CV elements were similar as were RT and BC elements. Overall, differences across maximum or minimum temperatures of landscape elements within a specific year and season did not exceed 10.0 ºC, with the exception of the fall of 2005 at the 5-cm depth.

Table 6.8: Summary of soil temperature measurements at the 5- and 20-cm depths taken at St. Denis in 2003, 2004 and 2005. Data is organized by landscape element. Convex (CX), concave (CV), riparian grass (RG), riparian tree (RT) and basin center (BC). Mean rank is average of rank across all sample dates (excludes dates with missing data that prevents calculation of a mean soil temperature for each element). Kendall's W coefficient indicates strength of temporal continuity of ranks. Ranges of mean soil temperature are presented by season.

Year	Depth (cm)	LE§	Mean Rank	Kendall's W	Mean Minimum / Maximum ºC		
					Spring	Summer	Fall
2003	5	CX	4.0	0.47	‡	14.4 / 26.5	†
		CV	3.8			14.4 / 26.9	
		RG	3.5			13.3 / 25.9	4.2 / 11.6
		RT	2.0			12.1 / 23.2	4.5 / 11.1
		BC	1.7			12.2 / 21.4	3.9 / 10.8
	20	CX	4.0	0.56		13.5 / 20.5	9.3 / 13.4
		CV	4.2			13.7 / 20.2	9.4 / 13.7
		RG	3.3			12.2 / 21.9	6.6 / 11.9
		RT	1.7			11.3 / 19.3	6.7 / 11.2
		BC	1.8			11.3 / 18.4	6.2 / 11.2
2004	5	CX	4.4	0.55	-7.9 / 16.2	11.4 / 18.9	9.6 / 14.4
		CV	4.0		-6.3 / 16.5	11.3 / 19.4	5.3 / 14.2
		RG	2.7		-5.3 / 12.3	10.9 / 17.0	4.6 / 12.2
		RT	1.6		†	9.2 / 14.7	5.0 / 10.9
		BC	2.2		-4.8 / 12.6	10.8 / 16.3	4.2 / 11.9
	20	CX	4.3	0.48	-6.2 / 10.9	10.9 / 16.0	6.7 / 13.0
		CV	3.9		-6.1 / 10.8	10.6 / 15.8	6.5 / 12.1
		RG	2.7		-3.9 / 7.9	9.4 / 14.5	6.0 / 10.8
		RT	1.6		-2.8 / 6.9	8.2 / 13.0	6.1 / 9.9
		BC	2.5		-3.9 / 8.6	10.0 / 14.1	6.0 / 10.4
2005	5	CX	4.3	0.51	-4.9 / 11.8	15.4 / 24.3	3.1 / 19.0
		CV	3.5		-5.1 / 12.4	14.7 / 24.2	2.9 / 17.7
		RG	1.8		†	12.5 / 18.9	3.1 / 14.8
		RT	1.8		†	11.2 / 17.9	3.7 / 13.4
		BC	3.7		-3.9 / 11.6	13.8 / 20.3	2.8 / 14.5
	20	CX	4.8	0.67	-4.3 / 11.5	12.2 / 18.3	5.0 / 12.9
		CV	3.8		-4.4 / 10.8	11.8 / 18.1	5.1 / 12.7
		RG	2.1		†	10.2 / 15.7	4.7 / 11.8
		RT	1.6		†	8.8 / 14.5	5.3 / 11.2
		BC	2.7		-5.3 / 8.3	10.6 / 15.6	4.9 / 44.8

‡ Measurements did not begin until July of 2003.
† Range not reported if missing data prevented determination of reliable range (missing data at the beginning or end of a season.
§ Landscape Element.

Figure 6.4 has been included to show month to month differences in soil temperature, at the 5-cm depth, between elements during the spring snowmelt period for 2004 and 2005. The medians for the landscape elements in both years remained below 5 ºC for both Mar. and Apr., although in Apr. of both years, locations within the elements, particularly CX and CV elements were > 5 ºC. In Mar. of 2005 depth of snow at the RT elements prevented measurements from being taken and in Apr. of both years, soil temperatures at BC elements could not be obtained due to standing water at these locations.

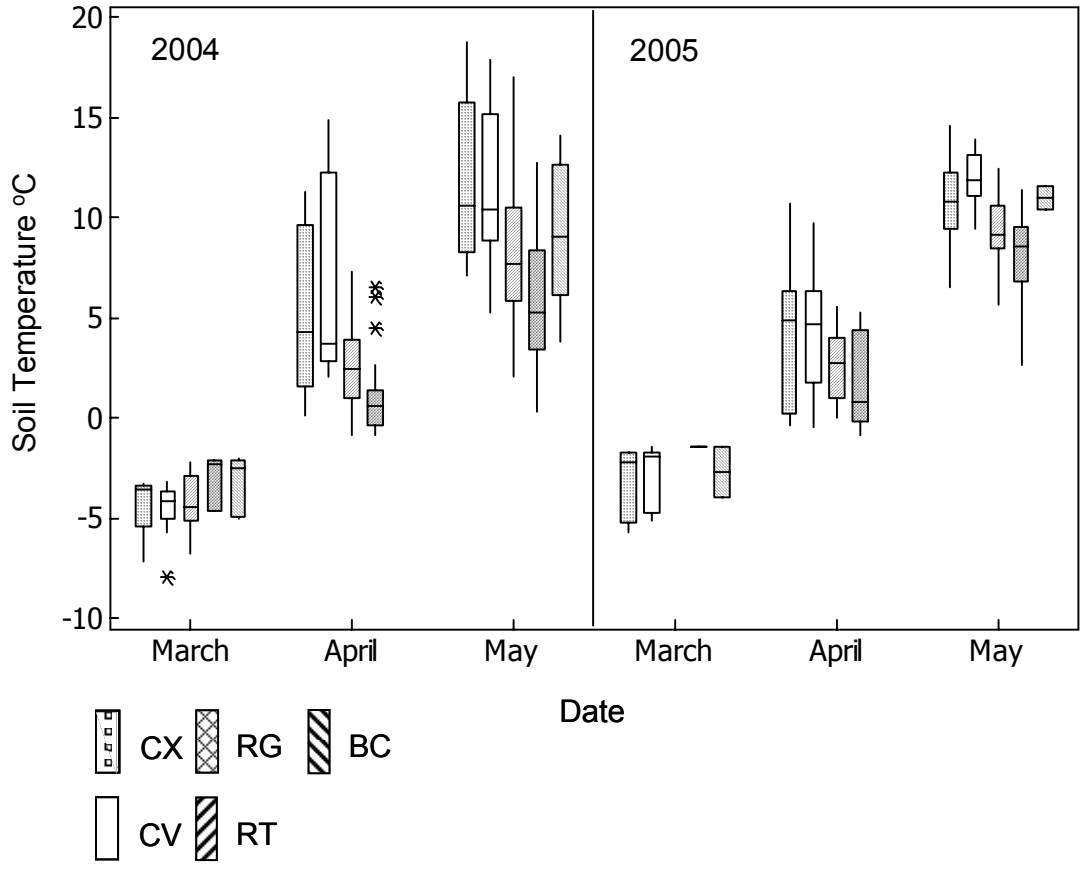

Figure 6.4: Box and whisker plot of soil temperatures, by landscape element at the 5-cm depth during the spring of 2004 and 2005 at the St. Denis Wildlife Area. Landscape elements are convex (CX), concave (CV), riparian grass (RG), riparian trees (RT) and basin center (BC). Box represents 1st (Q1) and 3rd (Q3) quartiles with median line (2nd quartile). Upper and lower whiskers represent Q3+1.5(Q3-Q1) and Q1-1.5(Q3-Q1), respectively. Asterisks represent values outside of whiskers.

6.4.4 Cumulative Nitrous Oxide Flux

In 2003, cumulative flux was highest at CV elements (1707.0 g N_2O-N ha^{-1} 108.5 d^{-1}) followed by CX elements (Table 6.9). The lowest cumulative mean flux was measured at BC elements (180.1 g N_2O-N ha^{-1} 108.5 d^{-1}). Cumulative mean flux was also highest for CV elements in 2004 (1953.5 g N_2O-N ha^{-1} 232.5 d^{-1}) (Table 6.10); however, the second highest cumulative flux was for BC elements (973.9 g N_2O-N ha^{-1} 232.5 d^{-1}).

In contrast to 2003, in 2004 CX elements had a negative cumulative flux (-20.2 g N_2O-N ha^{-1} 232.5 d^{-1}) having a positive cumulative flux at only one point in the year (12 Mar.). The RG and RT elements showed a negative cumulative flux until early and late July, respectively. For CV elements, a large increase in cumulative flux occurred in Apr., whereas large increases in cumulative flux occurred in BC elements in May and June. By comparison, cumulative flux in 2005 increased over the previous year with higher cumulative fluxes for all landscape elements except CV units (Table 6.11). Cumulative flux in the BC elements exceeded that for the CV elements (2098.7 and 1616.7 g N_2O-N ha^{-1} 231.5 d^{-1}, respectively). The CX, RG and RT elements increased in cumulative flux steadily over the period of emission sampling, whereas CV elements had large increases in cumulative flux in May and again in July. Cumulative flux for BC elements increased gradually, like that of the other wetland elements, until Aug. when cumulative flux increased rapidly and eventually exceeded that for CV elements.

The magnitude and timing of mean N_2O flux from the landscape elements at the St. Denis site indicate that CV and BC elements are most important in terms of overall yearly emissions. Together, these elements accounted for 58, 90 and 75% of cumulative emissions in 2003, 2004 and 2005, respectively (although most of the 2003 percentage was contributed by the CV elements alone). The CV and BC elements differed in their cumulative flux from year to year in that CV elements had similar cumulative flux each year (1707.0, 1953.5 and 1616.7 g N_2O-N ha^{-2} Xd^{-1} in 2003, 2004 and 2005, respectively) whereas the cumulative flux in BC elements increased each year from 180.1 to 973.9 and 2098.7 g N_2O-N ha^{-2} Xd^{-1}). Both CV and BC elements represent low elevation landforms, and hence are focal points for water redistribution in the landscape, and this was an important factor in these elements being important sources

Table 6.9: Mean cumulative N_2O flux (g N_2O-N ha^{-1} 108.5 d^{-1}) from the landscape elements at St. Denis Wildlife Area in 2003.

Landscape Element	Date (month / day)								
	7/3	7/8	7/17	7/31	8/8	8/29	9/12	9/26	10/10
Cultivated									
Convex	2.1	82.0	258.2	326.9	369.2	624.8	739.9	767.0	758.3
Concave	10.4	379.3	603.6	714.7	1035.3	1443.5	1693.8	1715.6	1707.0
Uncultivated									
Riparian Grass	8.9	14.0	0.5	65.9	191.1	337.2	308.5	337.0	339.3
Riparian Trees	0.2	7.0	23.8	113.7	73.3	252.6	228.2	271.8	275.3
Basin Center	2.2	-7.4	69.1	117.4	62.2	201.1	187.1	190.6	180.1

Table 6.10: Mean cumulative N_2O flux (g N_2O-N ha^{-1} 232.5 d^{-1}) from the landscape elements at St. Denis Wildlife Area in 2004.

Landscape Elements	Date (month / day)										
	3/5	3/12	3/23	4/8	4/15	4/21	5/6	5/14	5/28	6/8	6/16
Cultivated											
Convex	-11.4	26.5	-9.1	-5.0	-7.6	-19.6	-14.1	-1.8	-29.2	-29.2	-52.0
Concave	-14.9	1.8	-33.6	231.7	377.7	1225.9	1535.9	1625.5	1713.9	1734.7	1757.4
Uncultivated											
Riparian Grass	-0.1	-15.7	-33.5	-13.2	-20.3	-15.6	-14.0	0.0	-39.3	-39.3	-14.7
Riparian Trees	-2.1	-16.6	-32.8	-31.1	-29.8	-32.0	-28.5	-22.7	-37.3	-37.3	-50.7
Basin Center	-0.7	12.5	2.0	56.3	53.6	50.1	55.9	187.6	252.1	265.2	257.4

Landscape Elements	Date (month / day)									
	7/8	7/22	8/11	8/25	9/1	9/8	9/15	9/22	9/29	10/13
Uncultivated										
Convex	-46.6	-47.6	-61.3	-36.2	-36.7	-50.9	-45.8	-31.0	-22.6	-20.2
Concave	1782.5	1861.6	1877.3	1921.3	1923.1	1923.0	1925.3	1941.0	1945.9	1953.5
Uncultivated										
Riparian Grass	41.2	40.3	28.8	43.3	50.5	49.9	54.7	73.5	82.7	87.5
Riparian Trees	-2.9	65.7	181.3	217.8	232.0	234.2	250.8	279.9	286.3	290.8
Basin Center	557.6	620.6	740.3	847.4	859.8	874.6	891.1	955.1	968.7	973.9

Table 6.11: Mean cumulative N_2O flux (g N_2O-N ha^{-1} 231.5 d^{-1}) from the landscape elements at St. Denis Wildlife Area in 2005.

Landscape Elements	Date (month / day)										
	3/15	3/30	4/8	4/15	4/22	4/28	5/5	5/19	5/24	6/2	6/9
Cultivated											
Convex	0.0	8.8	41.0	52.3	59.3	94.0	88.4	99.3	97.4	131.0	132.3
Concave	0.0	17.9	39.6	46.2	51.8	72.3	101.0	481.1	690.3	810.1	995.4
Uncultivated											
Riparian Grass	4.3	5.3	15.6	15.6	14.5	12.6	11.0	47.9	69.2	132.7	173.2
Riparian Trees	0.0	20.8	36.9	36.9	37.8	34.2	34.2	42.5	44.7	85.9	100.4
Basin Center	5.2	0.8	15.8	15.8	16.3	22.9	35.9	41.9	41.9	99.3	118.8

Landscape Elements	Date (month / day)										
	6/17	6/22	7/4	7/11	7/18	7/25	8/2	8/8	8/15	8/22	9/6
Cultivated											
Convex	131.3	194.8	200.7	210.5	231.5	218.5	240.1	234.9	237.1	241.6	243. 6
Concave	1010.4	1030.8	1053.6	1149.5	1189.7	1350.2	1505.6	1538.4	1579.4	1590.9	1631.8
Uncultivated											
Riparian Grass	215.1	229.8	264.1	269.2	302.8	307.9	382.2	404.8	433.0	466.7	494.6
Riparian Trees	122.1	127.7	149.3	142.8	171.3	177.0	225.4	250.1	290.1	366.5	466.8
Basin Center	131.0	127.6	191.1	221.7	244.1	249.2	302.1	510.1	1034.0	1609.1	1858.2

Landscape Elements	Date (month / day)		
	9/20	10/4	10/18
Cultivated			
Convex	241.8	227.3	228.4
Concave	1631.5	1599.1	1616.7
Uncultivated			
Riparian Grass	515.2	521.2	519.9
Riparian Trees	498.9	475. 5	484.1
Basin Center	2066.7	2073.6	2098.7

of emission; however, the timing of precipitation events, spring snowmelt and recession of standing water are the factors that appear responsible for the timing of emissions from these elements.

The true contribution of N_2O flux from each landscape element is made clear by taking into account its aerial extent. As per Bedard-Haughn et al. (2006) the CX elements account for the largest portion of the area of the site (14.4 ha), and thus can have a large impact on the total emissions from the research site. For example, in 2003, 10.92 kg N_2O-N were produced by the CX elements, which is close to 35% of the total emissions produced from the site that year (Table 6.12). In 2004, CX elements were a net sink for N_2O-N reducing the total emissions (23.87 kg N_2O-N) by comparison to 2003 (31.92 kg N_2O-N). By contrast, the aerial extent of the BC elements (0.6 ha) contributed much less to the total emissions from the site (Table 6.12) even in 2005 when BC elements produced the highest cumulative emissions on a hectare basis (Table 6.11). Concave elements, with an aerial extent similar to the CX elements (11.8 ha), produced the largest portion of the total emissions in each year and in terms of annual emissions are the most important landscape elements, especially in 2004 and 2005 (Table 6.12). The RG and RT elements, on the other hand, have small aerial extents and were not major contributors to the total emissions in any year.

Table 6.12: Mean cumulative N_2O flux (g N_2O-N y^{-1}) and extent of area (ha) per landscape element per year from the St. Denis National Wildlife Area.

Landscape Elements	Area (ha)	Year 2003	2004	2005
Cultivated				
Convex	14.4	10920	-291	3289
Concave	11.8	20143	23051	19077
Uncultivated				
Riparian Grass	1.0	339	88	520
Riparian Trees	1.5	413	436	726
Basin Center	0.6	108	584	1259
Total	29.3	31923	23868	24871

6.4.5 Correlations

Pearson product moment correlation between soil N_2O flux and WFPS or soil temperature were notably poor. The correlation coefficient did not exceed 0.100 using

the data set, unaggregated. Using mean values there was marginal improvement in the coefficients; however the strongest correlation, that with soil temperature at the 5-cm depth was still only 0.201 ($p = 0.002$). Mean soil N_2O also was poorly correlated with other parameters such as landscape element, date and year. The strongest of these comparisons was with landscape element (0.304; $p=0.000$). A regression using all parameters explained only 17.2% of the variability in soil N_2O flux, whereas a regression for WFPS explained 57.8% of its variability. Neither, log transformation of the data, nor correlations with ranked data improved the results.

6.5 Discussion

There are no published N_2O flux measurements from uncultivated wetlands in the Canadian Prairie region. However, soil N_2O flux measurements from agricultural landscapes in the Canadian Prairie region are available. Corre et al. (1996) reported median values of soil nitrous oxide flux from a range of land uses in the Black soil zone of Saskatchewan. These median values ranged from approximately 0 to 3000 μg N_2O-N m^{-2} d^{-1} (35 ng N_2O-N m^{-2} s^{-1}). On an undulating, agricultural landscape Pennock et al. (2005) reported means from several crop types ranging from 11.7 to 32.2 ng N_2O-N m^{-2} s^{-1} for non-manured soil. Lemke et al. (1998) recorded mean N_2O flux values as high as 350 μg N_2O-N m^{-2} h^{-1} (97.2 ng N_2O-N m^{-2} s^{-1}) from the Parkland region of Alberta. Therefore, the range mean values of N_2O flux obtained from the St. Denis site (-3.6 to 93.5 ng N_2O-N m^{-2} s^{-1}) is reasonable considering the range of previously published data.

The pattern of flux in each year of the study reflects the concept of the event-based and background emission pattern (Brumme et al., 1999) that was discussed in Yates et al. (2006a) (Chapter 3). The N_2O emission events were triggered by both precipitation, as in 2003, and the recession of water from the ponds as in 2004 and 2005. Per hectare, wetland units (CV and BC) were the primary source areas for the emission events because precipitation and snow melt runoff concentrate in these positions allowing WFPS to reach levels that are known to trigger denitrification (Lemke et al. 1998; Davidson and Verchot, 2000). The background emission pattern was distributed over the CX, RG and RT elements. At this site, the background emissions can be a

significant contributor to total yearly emissions as in 2003 (Table 6.12), by virtue of the land area represented by the CX elements.

Brumme et al. (1999) describe the event-based pattern as consisting of extreme flux events that interrupt the continuous, low-level background pattern. So is the case at the St. Denis site. However, the timing of the events follow the recession of water from the ponds, and thus during 2004 and 2005, the spatial pattern of the flux events was dependent upon how much the ponds fill and in what order they dried out. In 2003 the flux events were dependent upon the CV positions and their response to precipitation. One can argue that the event-based pattern, even though it relied on the same units overall, was spatially different each year. Therefore, N_2O fluxes from this site have a long-term cycle and one or even two years of data is insufficient to describe this activity. In 2003 the ponds were dry through out the period of flux measurement. Pond water lasted until mid Aug. in 2004 and in 2005 there was a carry over of water to the spring of 2006 in at least one pond (Table 6.5). Excess water from 2005 creates the potential for even higher water levels in 2006.

Long-term water level data presented by van der Kamp et al. (1999) showed that levels in pond 120 ranged from zero to >135 cm (over-flow level) over a cycle as long as approximately 10 years. Over-flow levels in pond 120 would inundate locations that were in the RT and RG elements. Prolonged saturation of soils in these units may result in levels of emissions greater than that recorded in my study, and alter the spatial pattern of emissions once more. Thus, even three years worth of data collected at this site may not be enough to properly describe the N_2O flux activity.

Within the uncultivated wetlands, in terms of N_2O flux, it is clear that the BC elements stand out as a separate unit from the RG and RT elements. The cumulative emission from BC elements was 2.5 times higher than RG and RT elements combined in 2004 and 2 times higher in 2005. By contrast RG and RT elements were similar in cumulative emission in 2003 and 2005. In 2004 cumulative emission was higher in RT than RG elements by an order of magnitude. Mean fluxes for the two elements in 2004 were similar until the complete recession of pond 120 between 22 July and 11 Aug. when RT elements began producing higher mean fluxes. Thus, although there will be conditions, related to pond water levels, when the RG and RT units will behave different

from each other,the overall differences in flux between the two units do not warrant separate measurement. On the other hand, BC elements should be measured separately from other areas of the uncultivated wetlands at all times.

The relative importance of the landscape elements in terms of annual N_2O flux depends on the aerial extent of each element. The CV elements had high cumulative emissions and have a large aerial extent such that they contributed the majority of total emissions from the site in each year. Conversion of uncultivated wetlands to cultivated CV elements will result in a substantial increase in total yearly emissions from this site.

The level of activity and direction of flux at the CX elements was important to the magnitude of the total emissions from the site and management of these areas would effect the total yearly emissions. Conversely, the uncultivated wetland elements did not contribute much to the total site emissions, even though BC elements were high in cumulative emissions on a per hectare basis. Thus, the restoration of CV elements to an uncultivated wetland state may make a significant reduction in yearly emissions.

It is interesting that in 2005 the emission events from pond 103 and 118 were much stronger than from ponds 105 and 120. Such an event might not be expected from pond 120 as it maintained a substantial level of standing water past the end of the field season; however, there was no indication of a flux event from pond 105 even though the standing water in the pond had nearly disappeared. This suggests that there are differences between uncultivated wetlands in their response to conditions that lead to the production of soil N_2O. Therefore additional research is required to understand the reason for the difference between ponds such as 103 and 105.

Using the aerial extent of each element and its contribution to the total emissions over the three years of the study one can explore changes to total emissions by converting, the aerial extent and portion of emissions of one element to another. For example, using the data in Table 6.12, if the land area of the RG, RT and BC elements was converted to CV elements, the emissions from the site for the three year period would be 13% higher (data not shown). Conversely, if the land area of CV elements is proportioned over the uncultivated wetland elements, the reduction in emissions over the three years of the study would be approximately 60%.

Although conversion of CV elements to uncultivated wetland elements appears attractive, the effect of increasing the number of obstacles to farming operations and removing areas of the field that have the potential to be highly productive must be considered. It is possible that the best scenario is an 'all or nothing' situation where if a reduction in emissions are desired, the entire field is converted to a permanent grass cover management. Under these conditions, where the aerial extent of CX and CV elements are converted to a RG-like element, the total emissions over the three years of the study would be reduced by approximately 60%. The same level of emission reduction is achieved with what might be a less resource-intensive management system with the potential to sequester carbon. Another possible outcome of this management is the potential to reduce runoff to the uncultivated wetlands as described by van der Kamp et al. (1999; 2002). Drying out of these wetlands might reduce the number of emission events, but it may also seriously affect duck nesting habitat.

The trend toward highest and lowest mean soil temperatures at CX and RT elements, respectively, reflects the fact that the soil at CX elements are the most exposed and RT units are the most sheltered. However, differences between the mean rank and ranges of mean soil temperature for the landscape elements were often minimal between CX and CV elements and RT and among the vegetated wetland elements. Thus, the temporal continuity of the pattern of mean soil temperature in the landscape was present, but not strong. Accepting that minimum temperatures tend to occur early in the season on or about the same date (as do maximum temperatures, later in the season) then these temperature differences would not be expected to explain differences in N_2O flux though its control on the rate of microbial activity. It is most likely that soil temperature exerts a control on N_2O emission in the spring by generally reducing soil microbial activity and suppressing flux at the element that would be first to be exposed during snowmelt. On 12 Mar. 2004 the highest mean flux was from the CX elements (also the highest mean flux from the CX elements in that year). At this time soils were frozen at the 5-cm depth. At these elements, at this time, soils are first to be exposed during snowmelt because they tend to have the thinnest snow cover during winter. Although soil temperatures at the 5-cm depth were negative, the surface of the soil had thawed and was saturated from the melting of snow in place (i.e., the soil temperature measurements

do not represent the condition in the microbially active layer. The fact that fluxes were low when conditions were excellent for denitrification may be due to overall cool soil temperatures.

In 2004 mean soil N_2O flux > 10 ng N_2O-N m^{-2} s^{-1} began in Apr. at the CV elements when the median soil temperature at the 5-cm depth was still below 5 ºC. However, the variability in the data (Figure 6.4) suggests several locations, especially in CV positions, were well above 5 ºC. In 2005 mean soil N_2O flux > 10 ng N_2O-N m^{-2} s^{-1} did not begin until May. Median soil temperatures at this time were similar to what they were in 2004, but the inter-quartile ranges on the box plot indicates that fewer locations were > 5 ºC suggesting the cooler spring delayed the spring denitrification event. Thus, soil temperature probably does exert significant control on soil N_2O flux, at least during the spring. However, more detailed soil temperature measurements would be required to better explain the variation in flux.

6.6 Conclusions

The highest cumulative emissions over the three years of the study came from the CV and BC elements. The CV elements were an important source of soil N_2O in all three years whereas the BC units were important in 2004 and dominant in 2005. Precipitation events drove flux activity in 2003, primarily from the CV elements, suggesting that such events are generally of insufficient magnitude to trigger emission events in vegetated wetland units possibly because of the high porosity or lack of available N. Major emission events from vegetated wetlands occurred after flooding of BC elements and recession of standing water. The longer the duration of standing water at BC elements, the higher the emissions after recession.

The spatial and temporal pattern of emissions follow an event-based / background emission pattern with CV and BC elements the sources areas for the major N_2O flux events, with the CX, RG and RT elements contributing background emissions. Differences in pond water levels from year to year changed the spatial pattern of emissions. In 2003 the emission events were from CV elements and in 2004 / 2005 emission events were from both CV and BC elements; however, the former was important early in the season, whereas the latter assumed importance late in the season.

Taking aerial extent of landscape units into account, the CV elements were the most important source areas of N_2O in all three years whereas the RG, RT and BC elements were relatively unimportant, even with a high cumulative flux per hectare from BC elements in 2005. The magnitude of flux activity and direction of flux from the CX elements impacted the total cumulative flux across the site by virtue of the large aerial extent of this element. Management practices intended to reduce soil N_2O emissions at this site would be most effective if they are designed to decrease N_2O production from CV elements. Practices designed to reduce flux from CV elements may be effective, but not practical if they involve restoration to uncultivated wetlands; especially if some uncultivated wetlands are prone to emission events. Cultivation of what are currently uncultivated wetlands would likely increase the total cumulative N_2O emissions from the site.

High WFPS was associated with both high and low magnitude fluxes, and low WFPS was associated with low N_2O flux, suggesting that soil water content exerts some control on N_2O flux, but that other factors are also equally important. Mean soil temperature was generally highest for CX elements and lowest for RT elements, although the overall differences in soil temperature among the landscape elements was not likely to account for differences in emissions. Soil temperature has limited control on soil N_2O emission, except in spring when temperatures are primarily below 5 ºC; however the soil temperature measurements probably did not represent the conditions at the soil surface at that time. Correlations and regressions confirmed that WFPS and soil temperature had little relationship to soil N_2O emission during the period of this study.

For future measurement of fluxes from uncultivated wetlands in these terrains it is necessary to distinguish the BC as a unit separate from the tree or grass margins of the wetland. More research may be necessary to establish if RG and RT elements need be kept separate; however, the relatively low fluxes from these units may not warrant this. Certainly, N_2O emission research in these terrains requires at least three years data to account for the range in climatic conditions that lead to water level differences in the uncultivated wetlands. Additional research in this area should be directed at discovering the reasons for differences between uncultivated wetlands in soil N_2O flux.

7.0 SYNTHESIS AND CONCLUSIONS

7.1 Synthesis

One of the most commonly noted features of soil N_2O emissions in the literature is the high degree of variability in the spatial and temporal distribution of flux. This variability has been considered the primary reason for a general inability to model and estimate soil N_2O emissions with an acceptable degree of uncertainty. Because they are microbially mediated, the processes causing soil N_2O emissions and the process-level factors that control them are fairly well understood. However, the sensitivity of these processes to soil physical properties, such as moisture content and temperature that are in turn sensitive to climatic variables, makes extrapolation of process-level measurements to accurate estimates of emissions over larger scales difficult.

With multiple processes behind the production of soil N_2O and non-linear relationships between controlling variables and flux, N_2O emissions tend to be highly variable at small scales. Small-scale variability has been construed as short-range dependency, which has been considered the result of a random distribution. However, soil N_2O flux is any thing but randomly distributed as indicated by the commonly observed high skew in soil N_2O flux data sets and hence does not show the normal distribution one would attribute to randomly distributed data. It has been observed that skewed flux measurements are the result of hot spots of denitrification and these hot spots are the result of non-homogeneity in the distribution of soil properties. Given this, it is possible that in certain terrains where the distribution of soil properties is governed by a strong controlling factor such as topography the distribution and magnitude of fluxes may be predictable.

It was a goal of this study to define the spatial pattern of soil N_2O emissions in a Saskatchewan farm field with hummocky topography and assess the stability of the spatial pattern over time. Considering that hot spots of denitrification may be important to the spatial pattern, the study was designed (128-point transect) to take advantage of a

spatial analytical tool, wavelets, that could describe the point-to-point variation in fluxes, show us the relative contribution of hot spots to overall variability, and identify the contribution from specific locations and spatial scales. With repeated sampling the critical periods of emissions would be known and a better understanding of how to improve the modeling of emissions in these landscapes would be gained.

The initial stage was to examine the frequency distributions of data sets from repeated samplings of the transect. Each data set (128 flux measurements) exhibited some degree of skew. The degree of skew varied from extreme (reverse J-shaped distribution) to almost no skew at all (symmetrical distribution). The shape of distribution was closely related to the magnitude of the mean N_2O flux. This makes sense because extreme flux values skew the data and contribute a large part of the mean value. A reduction in the magnitude of flux associated with the extreme values will reduce the mean value and hence reduce the skew. Extreme fluxes occurred during the spring snow melt period and following intense precipitation events, when high WFPS restricts oxygen diffusion and probably triggers denitrification. Following such events, as WFPS declines, fluxes diminish in magnitude and the distribution shape shifts towards log normal and finally symmetrical distributions. Thus, not only does the distribution shape change, but this change is tied to weather and soil conditions. The distribution shape evolves over time and because the distribution shape is in a continuing state of transition, the shapes are usually statistically distinct from each other. Exceptions to this are the distributions that result from the events triggered in the spring and the precipitation events. At these times, the magnitude of the extreme values was similar.

It follows that changing distribution shapes, representing changes to the activity of hot spots of denitrification, implies that there may be changes to spatial pattern over time. Geostatistics indicated that the spatial dependency was not stable over time, supporting the idea of an evolving spatial pattern. However, random variability was high and a trend in the data did exist at least on one sampling day, even after using a geostatistical method to specifically address the extreme measurements. The implication is that the extreme values cannot be thought of as realizations of the true mean flux on that day and stationarity is compromised. One could conceive that we have two means

on days with extreme fluxes; one for the extreme values and the other for the more numerous, low magnitude values.

Such a concept fits well with the event-based / background emission pattern proposed by Brumme et al. (1999). The low flux values represent the general background emission pattern of the site and the extreme values represent the event-based pattern that is superimposed on the background pattern at certain times of the year.

We can take this emission pattern one step further and expose an evolution within the event-based pattern and understand its direct connection to landscape. This was done by viewing the wavelet spectrums for specific dates and comparing this to a landscape element segmentation of the transect locations. The high flux values on any specific date during the spring snow melt period in 2004 were associated with specific landscape elements. However, the landscape element of importance was different on each date and the progression from element to element was congruent with the pattern of spring snowmelt and water redistribution. Thus, although the spatial pattern is not stable, each pattern was still the result of landform and land use. Our ability to see the landscape pattern was only lost when the emissions declined to the background levels that characterize the random variability.

The wavelet analysis further explored the nature of the event-based pattern superimposed on the background emission pattern. The event-based pattern was characterized by local, non-repetitious peaks in wavelet variance. These features are non-scaleable and of comparatively short duration, but represent a large portion of the total variance. The background emissions appeared as a cyclic pattern, ranging in spatial scale from 20 to 60 meters. Variation within this scale range was probably due to the change in landscape elements as sources of high flux. The cyclic pattern was temporally persistent and represented the overall control of landscape on soil N_2O emissions across the site. Thus monitoring of emissions at this site and similar sites should incorporate the time of year and the landscape position into sampling design. By stratifying the landscape using landscape units that reflect the event-based and background emission patterns, at least during spring and probably intense precipitation events, one can use spatial scale to minimize the number of locations for a large area yet capture the contribution of extreme fluxes from the much smaller, localized areas.

Predicting emissions in this landscape may benefit from the same stratification. On a field scale, the statistical relationship between soil N_2O flux and factors such as WFPS and soil temperature is poor. However, the wavelet coherency analysis demonstrated that it is possible that over certain locations within the field, the relationship is stronger. Using wavelet coherency a strong, positive relationship between soil temperature and N_2O flux on 30 Mar. 2005 was found over a wide set of locations (20 to 100). This variation was related to the broad landform cycles along the transect represented by those locations with the strongest fluxes coming from CX elements. On 29 Apr. there was a strong local coherency feature in the wavelet coherency spectrum for WFPS and soil N_2O associated with a single CV element. On 23 June there was no significant relationship between soil N_2O and WFPS or soil temperature because fluxes dropped to a background pattern. Thus, positive predictive relationships do exist between soil N_2O flux and WFPS or soil temperature at the site and these relationships are tied to specific landscape elements; however the relationship is location and time dependent. Because the strong coherency was visible when strong flux occurred at cultivated landscape elements, there was also a land-use component to the location-and time-dependent pattern. When neither CX nor CV elements are emitting above a background level, no strong coherency between soil N_2O and other factors existed. Therefore, predictive relationships between soil N_2O flux and other factors are strong only when there is an event-based pattern of emissions.

Measurement of soil N_2O flux using the transect sampling design allowed the use of novel statistical methods and revealed the fluid spatial pattern of N_2O emissions and their relationship to the landscape. However, large transects are resource intensive. In the 50-point stratified design at the St. Denis site, locations were sampled weekly and biweekly for the finer temporal resolution needed for an accurate estimate of annual emissions.

In the 50-point stratified design the CV elements (that in this case included sample locations with CW elements) had a high cumulative flux over each year of the study. The more intensive 50-point samplings confirmed the role of these elements in the event-based pattern and, more importantly, demonstrated that the spring emission event in 2004 (that was sampled twice in Apr. using the transect) was continuous

through Apr. and into May, thus, confirming temporal continuity between the transect samplings. The CX elements, which were well represented by the transect, were briefly active in the spring, and otherwise remained at a background level of activity for the duration of the field seasons. The transect was able to capture the importance of the CX elements to the spatial pattern in early spring, information that would have been otherwise lost. However, the transect was unable to capture important events in the UW elements, which had been segmented into BC, RG and RT elements for the 50-point design. The event-based pattern also was manifest in the BC elements where late-season emission events occurred sporadically in 2004 and with more intensity and longer duration in 2005. Climatic conditions in 2004 did not allow for long periods of standing water in the wetland elements and thus the events occurred between transect samplings and transect sampling ended in 2005 before the major event in BC elements occurred. The result is that BC elements were more important than CV elements in terms of cumulative emissions in 2005, whereas the transect sampling did not show this. The RG and RT elements were generally low in cumulative emissions and did not respond to spring snow melt and precipitation events, unlike the CV and BC elements. The event-based response in the BC elements suggest that during the event period, the relationship between soil N_2O flux and controlling variables at these locations may be strong, although the relationship would be short lived and highly localized.

The cumulative flux presented by landscape element on an aerial basis provided a more realistic picture of the importance of different elements to the total yearly emissions from the research site. The CV elements had a large influence on the magnitude of yearly emissions due to their large aerial extent and high cumulative flux. The CX elements under certain conditions can be major contributors to yearly emissions as their aerial extent is similar to that of the CV elements, though they primarily showed a background level of activity and had both negative and positive annual flux.

The event-based emission pattern was a key determinant of the spatial distribution of soil N_2O flux, as well as the location-dependent distribution of coherency between flux and WFPS or soil temperature and their change over time. The driving force behind the event-based emission pattern was weather, particularly the fate of precipitation inputs at the site. The fate of precipitation (snow and rainfall) was

determined by the hydrology of the site and the concentration of water, primarily snow melt, in depressions. Rainfall played an important role in 2003, triggering the event-based emission pattern after a prolonged dry period. The concentration of snow melt runoff in cultivated and uncultivated ponds set the conditions for the subsequent emission events in 2004 and 2005 and these were triggered by the recession of water from the ponds.

The spatial pattern of soil N_2O emission and the relationship between controlling variables is very much a product of the state of the landscape at any given time and the state of the landscape (i.e., soil moisture content, soil temperature) is in constant evolution due to changing climatic variables. Given that climatic variables can be expected to follow a general seasonal pattern, the timing of emission events within the background pattern may be predictable and the magnitude of N_2O flux may be estimated through models based on long term soil variables and the inputs and movement of water in each season.

7.2 Implications for Up-scaling N_2O Emission Data

The up-scaling of soil N_2O emission data can take any number of forms; however, commonly extrapolations from small to large scales is done using a measure and multiply approach or estimation of flux using proxy variables in some sort of model (Schimel and Potter, 1995). The measure and multiply approach is simple and relies on direct measurement of flux from representative units within a region or area over which mean flux is wanted. A flux measurement is obtained and multiplied by the land area of the units represented by the measurement. This method produced a mean value of N_2O flux from the St. Denis site (Chapter 6); however, it is necessary, based on the results of this study, to make measurements at a landscape scale (i.e., the site has to be segmented into units based on landform and land use). Using a stratified sampling design based on landscape elements would be most important during the spring snowmelt period and following intense precipitation events, especially if the precipitation itself follows an extensive dry period. This would be necessary to capture the event-based pattern that was related to specific landscape elements. During extensive dry periods and in the fall when the emission pattern is at a background level, segmentation may not be necessary

as differences in flux between elements have disappeared. At this time measurements may be minimized by using the scale information provided by the wavelet analysis to keep sample spacing at a maximum.

To further minimize direct measurements, models could be employed to estimate N_2O flux within the site. Current models capable of estimating soil N_2O emission such as CENTURY-NGAS, DNDC, ExpertN and NASA CASA have in common the ability to simulate soil climate dynamics, plant growth, nutrient uptake and litterfall, decomposition of organic matter, and nitrogen mineralization and transformation (Frolking et al., 1998). Within each of these models is a function or algorithm that produces an estimate of soil N_2O flux dependent upon an estimate of the soil moisture. For example, in the CENTURY-NGAS model, the NGAS component estimates denitrification gas flux using a WFPS curve and WFPS estimates provided by the CENTURY component. ExpertN produces estimates of N_2O production using N transformation rates of nitrification and denitrification that are regulated by soil moisture and temperature (Kaharabata et al., 2003). These models have been used to produce estimates of daily emissions for sites or treatments within sites where the soil physical and climatic factors do not vary within the site. Essentially these models estimate daily flux at a field scale, which then can be aggregated into seasonal or year emissions.

At the St. Denis site, soil physical parameters and the distribution and fate of moisture inputs vary across the landscape due to differences in land use and landform. Thus, whereas you can apply a single set of soil physical and climatic parameters at a field scale at sites in the studies cited above, at St. Denis accurate modeling would require employment of these models at a landscape scale. Essentially, the landscape has to be segmented and model applied individually to the different elements. In addition to this there may not be temporal continuity to the application of a model. The results from the wavelet analysis indicate that there will be periods of time when a field-scale model may be applied, such as in late Mar. of 2004, because a correlation between soil N_2O and soil temperature was at that time found over a large area of the transect. There will also be periods of time when emissions can only be modeled at specific landscape elements, such as CW, because the relationship between soil N_2O and, in this case, WFPS was localized. At these times, in other areas of the landscape, the relationship

between N_2O and WFPS or soil temperature was poor and that modeling would not be successful in those areas of the field. Still, there may be periods of time when modeling will not be successful anywhere at the site because a significant relationship between soil N_2O and the other variables considered in this study was not found.

One approach to modeling under these conditions is to consider each landscape segment in isolation and model emissions strictly on input parameters specific to that unit. Regional estimates could be made by aggregating elemental mean values and adjusting based on their contribution in land area. This approach does not take into account the communication that occurs between elements in regards to re-distribution of water. A more thorough model would account for these and other transfers, but would require more detailed information on antecedent moisture and climatic conditions as well as distribution of snow. Either model could not be applied one dimensionally, but would require a framework built on a digital elevation model to estimate coverage and recession of standing water, which was highly important to emission events from the CW and BC elements.

7.3 Implications for Uncertainty in N_2O Emission Data

An early objective of this project was to quantify the uncertainty surrounding the emission measurements and draw a conclusion as to the appropriate measurement scale to minimize uncertainty in modeled or up-scaled estimates. As the project progressed, however, it became clear that the area of uncertainty analysis is very broad and a proper evaluation of the uncertainty in the data was a project unto itself and was beyond the scope of this study. It also became clear that this study provided an excellent opportunity to look at the root causes of uncertainty, so the effort was shifted in this direction. This lead to the description of the probability distributions and heavy emphasis on the evolution of spatial patterns and the relationship to soil and landscape attributes. However, it is still appropriate to make some comments on uncertainty in relation to the conclusions made in the previous chapters.

Process-level measurements of soil N_2O emissions contain a certain level of random variability (Schimel and Potter, 1995) and the transect measurements at St. Denis are no exception to this as shown by the semivariograms. Uncertainty in N_2O

emission data, at this level, leads to greater uncertainty when such measurements are extrapolated directly to the scales necessary to examine their relationship to climate change within ecosystems (10 to 100 km) (Schimel and Potter, 1995). Variability in the data from St. Denis also contains, on some days, a level of systematic variability that is also expressed in the semivariograms. The systematic variation will contribute to greater uncertainty at regional scales if measurements are directly extrapolated from the process scale. However, the wavelet analysis indicates that the systematic variability in the St. Denis flux data was to a large degree a result of the control that landscape has on the pattern of snowmelt and the redistribution of water.

The point-scale measurements aggregated at the field scale, revealed no useful relationships between soil N_2O flux and WFPS or soil temperature. At a landscape scale, strong relationships between N_2O flux and the other variables could be found at certain locations at certain times indicating that the landscape scale is what O'Neill (1988) would refer to as the coherent level or the level where predictive power is maximized. Groffman (1991) considered that up-scaling measurements of nitrification and denitrification would be improved if the landscape scale could be shown to be the coherent level for the multi-scale processes behind soil N_2O emissions. Aggregating process-scale measurements at the landscape scale should reduce propagation errors when extrapolating to higher scales. However, Whelan and Gandolfi (2002) point out that the use of distal factors, such as landform and land use, is dependent on that systematic component of the variability being dominant over the inherent random variability. If we go back to the results from St. Denis we again see that there were days where the systematic variation was not expressed over the random variation. It is of some consolation that on those days when random variation was high, and relationships between soil N_2O flux and WFPS or soil temperature were not significant, mean flux was generally low. Thus, if error is propagated directly to the field scale because we are unable to aggregate measurements with any effect at a landscape scale, then the uncertainty resulting from this propagation would be surrounding low flux estimates. On the days that fluxes are high, when the event-based pattern of emissions is in operation, then we have the ability to aggregate at the landscape scale and should expect lower uncertainty surrounding flux estimates.

7.4 Conclusions

The spatial and temporal variation in N_2O flux followed an event-based / background emission pattern. High flux events were triggered by precipitation events and the recession of water from wetlands following spring snowmelt. The emission events were characterized by reverse J-shaped distributions, high variance and high coherency at cultivated wetland elements. Spatial dependency was characterized by a high nugget:sill ratio on most sampling days, but decreased during an emission event. A trend in the data caused by extreme values was present on at least one day and proper spatial analysis for data of that nature required alternative methods not sensitive to stationarity.

To address problems with non-stationarity wavelet analysis was used. The local wavelet spectra showed that the spatial pattern of variance in soil N_2O flux was related to the landscape over a 20- to 60-m scale range. The spatial pattern changed as specific landscape elements became sources of peak N_2O flux and again as peak emissions moved to positions down-slope. This caused minor changes to the scale of variation; however, the spatial scale was generally temporally stable. The shift in peak flux between landscape elements was driven primarily by the pattern of snowmelt and the redistribution of water in the landscape. The extreme fluxes from specific landscape elements, were non-scalar, local features in the wavelet spectra that represented the event-based emission pattern superimposed on the background emission pattern.

Strong location-dependent positive relationships were found between soil N_2O flux and WFPS or soil temperature and related to specific landscape elements. The results indicate that models intended to estimate N_2O flux from these landscapes cannot rely on a single predictive relationship, but will have to incorporate predictive relationships localized at specific landscape elements depending on the time of year. At certain times predictive relationships cannot be used and up-scaled estimates will have to rely on direct measurement of emissions.

The highest cumulative emissions, on a per hectare basis, over the three years of the study came from the CV and BC elements. The CV elements were an important source of soil N_2O in all three years whereas the BC units were important in 2004 and

dominant in 2005. Major emission events from vegetated wetlands occurred after flooding of BC elements and recession of standing water. The difference in pond water levels from year to year changed the spatial pattern of the event-based / background emissions. On an aerial basis CV elements were most important to the annual emission from the site. Annual emission from the site would be decreased if management practices were used that decreased N_2O production from CV elements.

In fulfilling these objectives several issues in regards to up-scaling and uncertainty were addressed. Up-scaling flux measurements using a measure and multiply approach may be successful if measurements or estimates are aggregated at a landscape scale. It is important to stratify the landscape based on units that reflect the event-based / background emission pattern. The uncertainty in emission estimates can be minimized by using only models when and where strong predictive relationships exist such as when flux events are expected from depressions as standing water recedes or when background flux is expected to be strongest, overcoming the inherent random variability.

8.0 REFERENCES

Agriculture and Agri-Food Canada. 1998a. The health of our air: Towards sustainable agriculture in Canada. Publication 1981/E, Research Branch, Ottawa, ON.

Agriculture and Agri-Food Canada. 1998b. The Canadian System of Soil Classification. 3rd ed. Publication 1646. NRC Research Press. Ottawa, ON.

Ambus, P. 1998. Nitrous oxide production by denitrification and nitrification in temperate forest, grassland and agricultural soils. Eur. J. Soil Sci. 49:495-502.

Ambus, P., and S. Christensen. 1994. Measurement of N_2O emission from a fertilized grassland: an analysis of spatial variability. J. Geophys. Res. 99:16549-16555.

Anderson, O.E. and F.C. Boswell. 1964. The influence of low temperature and various concentrations of ammonium nitrate on nitrification in acid soils. Soil Sci. Soc. Am. J. 28:525-529.

Anthony, W.H., G.L. Hutchinson, and G.P. Livingston. 1995. Chamber measurement of soil-atmosphere gas exchange: linear vs. diffusion based models. Soil Sci. Soc. Am. J. 59: 1308-1310.

Asman, W.A.H., M.O. Andreae, R. Conrad, O.T. Denmead, I.N. Ganzeveld, W. Helder, T. Kaminski, M.A. Sofiev and S. Trumbore. 1999. Working group report: how can fluxes of trace gases be validated between different scales? p. 87-97 *In* A.F. Bouwman (ed). Approaches to Scaling a Trace Gas Fluxes in Ecosystems. Elsevier Science, New York, NY.

Bedard-Haughn, A., F. Jongbloed, J. Akkerman, A. Uijl, E. de Jong, T. Yates, and D.Pennock. 2006. The effects of erosional and management history on soil organic carbon stores in ephemeral wetlands of hummocky agricultural landscapes. Geoderma. (in press).

Blöschl, G., and M. Sivapalan. 1995. Scale issues in hydrological modeling: a review. Hydrol. Proc. 9:251-290.

Boone, R.D. 1994. Light-fraction soil organic matter: origin and contribution to net nitrogen mineralization. Soil Biol. Biochem. 26:1459-1468.

Bowman, R.A. and D.D. Focht. 1974. The influence of glucose and nitrate concentration upon denitrification rates in sandy soils. Soil Biol. Biochem. 6:297-301.

Broadbent, F.E., and F. Clark. 1965. Denitrification. p. 344-359 *In* W. V. Bartholomew and F. E. Clark (ed). Soil Nitrogen. American Society of Agronomy, Madison, WI.

Broadbent, F.E., and B.F. Stojanovic. 1951. The effect of partial pressure of oxygen on some soil nitrogen transformations. Soil Sci. Soc. Am. Proc. 16:359-363.

Brumme, R., W. Borken, and S. Finke. 1999. Hierarchical control on nitrous oxide emission in forest ecosystems. Global Biogeochem. Cycles 13:1137-1148.

Burford, J.R., and J.M. Bremner. 1975. Relationships between the denitrification capacities of soils and total, water-soluble and readily decomposable soil organic matter. Soil Biol. Biochem. 7:389-394.

Butterbach-Bahl, K., M. Kesik, P. Miehle, H. Papen, and C. Li. 2004. Quantifying the regional source strength of N-trace gases across agricultural and forest ecosystems with process based models. Plant Soil. 260:311-329.

Cabrera, M.L. 1993. Modeling the flush of nitrogen mineralization caused by drying and rewetting soils. Soil Sci. Soc. Am. J. 57:63-66.

Cambardella, C.A., T.B. Moorman, J.M. Novak, T.B. Parkin, D.L. Karlen, and A.E. Konopka. 1994. Field-scale variability of soil properties in central Iowa soils. Soil Sci. Soc. Am. J. 58:1501-1511.

Castignetti, D., and T.C. Hollocher. 1982. Nitrogen redox metabolism of a heterotrophic, nitrifying and denitrifying Alcaligenes sp. from soil. Appl. Environ. Microbiol. 44:923-928.

Cicerone, R.J. 1987. Changes in stratospheric ozone. Science 237:35-41.

Clausnitzer, V., J.W. Hopmans, and J.L. Starr. 1998. Parameter uncertainty analysis of common infiltration models. Soil Sci. Soc. Am. J. 62:1477-1487.

Corre, M.D., C. van Kessel, and D.J. Pennock. 1996. Landscape and seasonal patterns of nitrous oxide emissions in a semiarid region. Soil Sci. Soc. Am. J. 60:1806-1815.

Corre, M.D., D.J. Pennock, C. van Kessel, and D.K. Elliott. 1999. Estimation of annual nitrous oxide emissions from a transitional grassland-forest region in Saskatchewan, Canada. Biogeochemistry. 44:29-49.

Cressie, N.A.C. 1985. Fitting variogram models by weighted least squares. J. Int. Assoc. Math. Geol. 17, 563-586.

Cressie, N.A.C. 1993. Statistics for spatial data. Revised edition. John Wiley and Sons, New York, NY.

Davidson, E.A., and L.V. Verchot. 2000. Testing the hole in the pipe model of nitric oxide emissions from soils using the TRAGNET database. Global Biogeochem. Cycles 14:1035-1043.

Del Grosso, S.J., W.J. Parton, A.R. Mosier, D.S. Ojima, A.E. Kulmala, and S. Phongpan. 2000. General model for N_2O and N_2 gas emissions from soils due to denitrification. Global Biogeochem. Cycles 14:1045-1060.

Derwent, R.G., A.R. Mosier, S. Bogdanov, J.H. Duyzer, V. Garcon, S. Houweling, M.A. Sofiev, H. Denier van der Gon, F. Wania, and R. Wanninkhof. 1999. Working group report: How should the uncertainties in the results of scaling be investigated and decreased? p. 299-313 *In* A. F. Bouwman (ed). Approaches to Scaling a Trace Gas Fluxes in Ecosystems. Elsevier Science, New York, NY.

Downie, N.M., and R.W. Heath. 1974. Basic Statistical Methods, 4th ed. Harper and Row, New York, NY.

Drury, C.F., T.O. Oloya, D.J. McKenney, E.G. Gregorich, C.S. Tan, and C.L. van Luyk. 1998. Long-term effects of fertilization and rotation on denitrification and soil carbon. Soil Sci. Soc. of Am. J. 62:1572-1579.

Ebdon, D. 1985. Statistics in Geography. 2nd ed. Basil Blackwell Ltd. Oxford. UK

Environment Canada, 2005a**.** Monthly data report for 2003. [Online] Available at http://www.climate.weatheroffice.ec.gc.ca/climateData/canada_e.html (verified 27 June 2005).

Environment Canada, 2005b**.** Canadian climate normals, 1971-2000. [Online] Available at http://www.climate.weatheroffice.ec.gc.ca/climate_normals/index_e.html (verified 27 June 2005).

Environment Canada, 2005c**.** Daily climate data [Online] Available at http://www.climate.weatheroffice.ec.gc.ca/climateData/dailydata_e.html (verified 9 Nov 2005).

FAO and IFA. 2001. Global estimates of gaseous emissions of NH_3, NO and N_2O from agricultural land. International Fertilizer Industry Association and Food and Agriculture Organization of the United Nations, Rome.

Firestone, M.K., M.S. Smith, R.B. Firestone, and J.M. Tiedje. 1979. The influence of ntirate, nitrite, and oxygen on the composition of gaseous products of denitrification in soil. Soil Sci. Soc. Am. J. 43:1140-1144.

Firestone, M.K., R.B. Firestone, and J.M. Tiedje. 1980. Nitrous oxide from soil denitrification: factors controlling its biological production. Science 208:749-751.

Fitzpatrick, E.A. 1986. An Introduction to Soil Science. 2nd ed. Longham Scienitific and Technical. Burnt Mill, Essex.

Folorunso, O.A., and D.E. Rolston. 1985. Spatial and spectral relationships between field-measured denitrification gas fluxes and soil properties. Soil Sci. Soc. Am. J. 49:1087-1093.

Folorunso, O.A., and D.E. Rolston. 1984. Spatial variability of field-measured denitrification gas fluxes. Soil Sci. Soc. Am. J. 48:1214-1219.

Frolking, S.E., A.R. Mosier, D.S. Ojima, C. Li, W.J. Parton, C.S. Potter, E. Priesack, R. Stenger, C. Haberbosch, P. Dörsch, H. Flessa, and K.A. Smith. 1998. Comparison of N_2O emissions from soils at three temperate agricultural sites: simulations of year-round measurements by four models. Nutr. Cycl. Agroecosys. 52:77-105.

Gianello, C., and J. M. Bremner. 1986. A comparison of chemical methods of assessing potentially available organic nitrogen in soil. Commun. Soil Sci. Plant Anal. 17:215-236.

Goovaerts, P., and C.N. Chiang. 1993. Temporal persistence of spatial patterns for mineralizable nitrogen and selected soil properties. Soil Sci. Soc. Am. J. 57:372-381.

Goovaerts, P. 1997. Geostatistics For Natural Resource Evaluation. Oxford University Press, New York, NY.

Granger, R.J., D.M. Gray, and G.E. Dyck. 1984. Snowmelt infiltration into frozen Prairie soils. Can. J. Earth Sci. 21:669-677.

Graps, A. 1995. An introduction to wavelets. IEEE Comput. Sci. Eng. 2:1-18.

Grinsted, A.J., C. Moore, and S. Jevrejeva. 2004. Application of the cross wavelet transform and wavelet coherence to geophysical time series. Nonlinear Proc. Geoph. 11: 561-566.

Groffman, P.M. 1984. Nitrification and denitrification in conventional and no-tillage soil. Soil Sci. Soc. Am J. 49:329-334.

Groffman, P.M. 1991. Ecology of nitrification and denitrification in soil evaluated at scales relevant to atmospheric chemistry. p. 201-217 *In* W.B. Whitman and J. Rogers (ed). Microbial Production and Consumption of Greenhouse Gases: Methane, Nitrogen Oxides and Halomethanes. Am. Soc. Microbiol. Washington, D.C.

Groffman, P.M., R. Brumme, K. Butterbach-Bahl, K.E. Dobbie, A.M. Mosier, D. Ojima, H. Papen, W.J. Parton, K.A. Smith, and C. Wagner-Riddle. 2000. Evaluating annual nitrous oxide fluxes at the ecosystem scale. Global Biogeochem. Cycles 14:1061-1070.

Hayashi, M., G. van der Kamp, and D.L. Rudolph. 1998a. Water and solute transfer between a prairie wetland and adjacent uplands, 1. Water balance. J. Hydrol. 207:42-55.

Hayashi, M., G. van der Kamp, and D.L. Rudolph. 1998b. Water and solute transfer between a prairie wetland and adjacent uplands, 2. Chloride cycle. J. Hydrol. 207:56-67.

Hayashi, M., G. van der Kamp, and R. Schmidt. 2003. Focused infiltration of snowmelt water in partially frozen soil under small depressions. J. Hydrol. 270:214-229.

Hogan, J.M., and F.M. Conly. 2002. St. Denis National Wildlife Area land Cover Classification: 1997. Technical Report Series No. 384, Canadian Wildlife Service, Prairie and Northern Region.

Hutchinson, G.L., and A.R. Mosier. 1981. Improved soil cover method for field measurement of nitrous oxide fluxes. Soil Sci. Soc. Am. J. 45:311-316.

International Atomic Energy Agency. 1992. Manual on measurement of methane and nitrous oxide emissions from agriculture. IAEA-TECDOC-674. INIS Clearinghouse, Vienna.

IPCC. 2001. Climate change 2001: The scientific basis. Contribution of Working Group I to the Third Assessment Report of the Intergovernmental Panel on Climate Change. Cambridge University Press, Cambridge, UK.

Izaurralde, R.C., R.L. Lemke, T. W. Goddard, B. McConkey, and Z. Zhang. 2004. Nitrous oxide emissions from agricultural toposequences in Alberta and Saskatchewan. Soil Sci. Soc. Am. J. 68:1285-1294.

Kachanoski, R.G., and E. de Jong. 1988. Scale dependence and the temporal persistence of spatial patterns of soil water storage. Water Resour. Res. 24, 85-91.

Kaharabatta, S.K., C.F. Drury, E. Priesack, R.L. Desjardins, D.J. McKenney, C.S. Tan and D. Reynolds. 2003. Comparing measured and Expert-N predicted N_2O emissions from conventional till and no till corn treatments. Nutr. Cycl. Agroecosys. 66:107-118.

Khalil, M.A.K., and R.A. Rasmussen. 1992. The global sources of nitrous oxide. J. Geophys. Res. 97:14,651-14,660.

Kliewer, B.A., and J.W. Gilliam. 1995. Water table management effects on denitrification and nitrous oxide evolution. Soil Sci. Soc. Am. J. 59:1694-1701.

Knowles, R. 1981. Denitrification. p. 323-369 *In* J.N. Ladd and E.A. Paul (ed). Soil Biochemistry Vol. 5. Marcel Dekker, Inc., New York, NY.

Koops, J.G., M.L. van Beusichem and O. Oenema. 1997. Nitrogen loss from grassland on peat soils through nitrous oxide production. Plant Soil 188:119-130.

Kravechenko, A.N., D.G. Bullock, and C.W. Boast. 2000. Joint multifractal analysis of crop yield and terrain slope. Agron. J. 92, 1279-1290.

Kumar, P., and E. Foufoula-Georgiou. 1997. Wavelet analysis for geophysical applications. Rev. Geophys. 35:385-412.

Lakshman, G. 1971. The Water Budget of Shallow Permanent or Intermittent natural Reservoirs as it Affects Economy and Wildlife. Saskatchewan Research Council. Progress Report No. 6.

Lapitan, R. L., Wanninkhof, R., and A.R. Mosier. 1999. Methods for stable gas flux determination in aquatic and terrestrial systems. p. 29-66 *In* A.F. Bouwman (ed). Approaches to Scaling a Trace Gas Fluxes in Ecosystems. Elsevier Science, New York, NY.

Lark, R.M., A.E. Milne, T.M. Addiscott, K.W.T. Goulding, C.P. Webster and S. O'Flaherty. 2004. Analyzing spatially intermittent variation of nitrous oxide emissions from soil with wavelets and the implications for sampling. Eur. J. of Soil Sci. 55:601-610.

Lau, K.-M., and H. Weng. 1995. Climate signal detection using wavelet transform: How to make a time series sing. Bull. Am. Meteorol. Soc. 76:2391-2402.

Lemke, R.L., R.C. Izaurralde, and M. Nyborg. 1998. Seasonal distribution of nitrous oxide emissions from soils in the parkland region. Soil Sci. Soc. Am. J. 62:1320-1326.

Lemke, R.L., R.C. Izaurralde, M. Nyborg, and E.D. Solberg. 1999. Tillage and N source influence soil-emitted nitrous oxide in the Alberta Parkland region. Can. J. Soil Sci. 79:15-24.

Letey, J., N. Valoras, A. Hadas, and D.D. Focht. 1980. Effect of air-filled porosity, nitrate concentration, and time on the ratio of N_2O/N_2 evolution during denitrification. J. Environ. Qual. 9:227-231.

Lindsay, R.W., D.B. Percival, and D.A. Rothrock. 1996. The discrete wavelet transform and the scale analysis of the surface properties of sea ice. IEEE Trans. on Geosci. and Remote Sens. 34:771-787.

Linn, D.M., and J.W.Doran. 1984. Effect of water-filled pore space on carbon dioxide and nitrous oxide production in tilled and nontilled soils. Soil Sci. Soc. Am. J. 48:1267-1272.

Lissey, A. 1968. Surficial mapping of groundwater flow systems with application to the Oak River Basin, Manitoba. Ph.D. Thesis, University of Saskatchewan, Saskatoon.

Maag, M., and F.P.Vinther. 1999. Effect of temperature and water on gaseous emissions from soils treated with animal slurry. Soil Sci. Soc. Am. J. 63:858-865.

MacKenzie, A.F., M.X. Fan, and F. Cadrin. 1997. Nitrous oxide emission as affected by tillage, corn-soybean-alfalfa rotations and nitrogen fertilization. Can. J. Soil Sci. 77:145-152.

Mathsoft Engineering and Education Inc. 2002. Mathsoft™ Mathcad® 11 User's Guide. Mathsoft Engineering and Educ. Inc. Cambridge, MA.

McKenney, D.J., C.F. Drury, and S.W. Wang. 2001. Effects of oxygen of denitrification inhibition, repression, and de-repression, in soil columns. Soil Sci. Soc. Am. J. 65:126-132.

Meyboom, P. 1966. Unsteady groundwater flow near a willow ring in hummocky moraine. J. Hyrdol. 4:38-62.

Meyers, S., B. Kelley, and J. O'Brien. 1993. An introduction to wavelet analysis in oceanography and meterology: with application to the dispersion of Yanai waves. Mon. Wea. Rev. 121:2855-2866.

Miller, J.J., D.F. Acton, and R.J. St. Arnaud. 1985. The effect of groundwater formation in a morainal landscape in Saskatchewan. Can. J. Soil Sci. 65:293-307.

Minitab Inc. 2003. Meet MINITAB® Release 14 for Windows®. Minitab Inc., State College, PA.

Mosier, A.R., M. Stillwell, W.J. Parton, and R.G. Woodmansee. 1981. Nitrous oxide emissions from a native shortgrass prairie. Soil Sci. Soc. Am. J. 45:617-619.

Müller, C., R. J. Stevens, R.J. Laughlin, and H.-J. Jäger. 2004. Microbial processes and the site of N_2O production in a temperate grassland soil. Soil Biol. Biochem. 36:453-461.

Myrold, D.D., and J.M. Tiedje. 1985. Diffusional constraints on denitrification in soil. Soil Sci. Soc. Am. J. 49:651-657.

Nyborg, M., J.W. Laidlaw, E.D. Solberg, and S.S. Malhi. 1997. Denitrification and nitrous oxide emissions from a black chernozemic soil during spring thaw in Alberta. Can. J. Soil Sci. 77:153-160.

O'Neill, R.V. 1988. Hierarchy theory and global change. p. 29-46 *In* T. Rosswall, R. Woodmansee, and P.G. Risser (ed). Scales and Global Change: Spatial and

Temporal Variability in Biospheric and Geospheric Processes. John Wiley and Sons, Inc., New York, NY.

Pardo-Igúzquiza, E., and F.J. Rodríguez-Tovar. 2000. The permutation test as a non-parametric method for testing the statistical significance of power spectrum estimation in cyclostratigraphic research. Earth Planetary Sci. Lett. 181:175:189

Pardo-Igúzquiza, E., and F.J. Rodríguez-Tovar. 2005. MAXENPER: a program for maximum entropy spectral estimation with assessment of statistical significance by the permutation test. Comput. Geosci. 31:555-567.

Parkin, T.B. 1987. Soil microsites as a source of denitrification activity. Soil Sci. Soc. Am. J. 51:1194-1199.

Parsons, D.F., M. Hayashi, and G. van der Kamp. 2004. Infiltration and solute transport under a seasonal wetland: Bromide tracer experiments in Saskatoon, Canada. Hydrol. Proc. 18:2011-2027.

Parton, W.J., A.R. Mosier, and D.S. Schimel. 1988. Rates and pathways of nitrous oxide production in a shortgrass steppe. Biogeochemistry. 6:45-58.

Pennock, D.J., C. van Kessel, R.E. Farrell, and R.A. Sutherland. 1992. Landscape-scale variations in denitrification. Soil Sci. Soc. Am. J. 56:770-776.

Pennock, D., R. Farrell, R. Desjardins, E. Pattey and J.I. MacPherson. 2005. Upscaling chamber-based measurements of N_2O emissions at snowmelt. Can. J. Soil Sci. 85:113-125.

Percival, D.P. 1995. On estimation of the wavelet variance. Biometrika. 82:619-631.

Poth, M. and D.D. Focht. 1985. ^{15}N kinetic analysis of N_2O production by Nitrosomonas europaea: an examination of nitrifier denitrification. Appl. Environ. Microbiol. 49:1134-1141.

Press, W.H., S.A Teukolsky, W.T. Vetterling, and B.P. Flannery. 1992. Numerical recipes in C. The art of scientific computing. 2nd ed. Cambridge University Press, New York.

Renault, P., and P. Stengel. 1994. Modeling oxygen diffusion in aggregated soils: I. anaerobiosis inside the aggregate. Soil Sci. Soc. Am. J. 58:1017-1023.

Renault, P., and J. Sierra. 1994. Modeling oxygen diffusion in aggregated soils: II. anaerobiosis in topsoil layers. Soil Sci. Soc. Am. J. 58:1023-1030.

Richardson, J.L., J.L. Arndt, and J.A. Montgomery. 2001. Hydrology of wetland and related soils. p. 35-84 *In* J.L. Richardson and M.J. Vepraskas (ed). Wetland Soils – Genesis, Hydrology, Landscapes and Classification. CRC press Boca Raton, FL.

Robertson, G.P. 1989. Nitrification and denitrification in humid tropical ecosystems: potential controls on nitrogen retention. p. 55-69 *In* J. Procter (ed). Mineral nutrients in tropical forest and savanna ecosystems. Br. Ecol. Soc. Spec. Publ. no. 9. Blackwell Scientific, Oxford, UK.

Robertson, G.P., and J.M. Tiedje. 1987. Nitrous oxide sources in aerobic soils: nitrification, denitrification and other biological processes. Soil Biol. Biochem. 19:187-193.

Rodhe, H. 1990. A comparison of the contribution of various gases to the greenhouse effect. Science 248:1217-1219.

Rosenberry, D.O., and T.C. Winter. 1997. Dyamics of water-table fluctuations in an upland between two prairie-potholes in North Dakota. J. Hyrdol. 191:266-289.

Rozas, H.R.S., H.E. Echeverria, and L.E. Picone. 2001. Denitrification in maize under no-tillage: effect of nitrogen rate and application time. Soil Sci. Soc. Am. J. 65:1314-1323.

Schimel, D.S., and C.S. Potter. 1995. Process modeling and spatial extrapolation. p. 358-383 *In* P.E. Matson and R.C. Harris (ed). Biogenic Trace gases: Measuring Emissions from Soil and Water. Blackwell Science, University Press, Cambridge, UK.

Schimel, D.S., and N.S. Panikov. 1999. Simulation models of terrestrial trace gas fluxes at soil microsites to global scales. p. 187-202 *In* A.F. Bowman (ed). Approaches to Scaling a Trace Gas Fluxes in Ecosystems. Elsevier Science, New York, NY.

Schmidt, E.L., and L.W. Belser. 1994. Autotrophic Nitrifying Bacteria. p. 159-177 *In* R.W. Weaver, J.S Angle, and D.S. Bottomley (ed). Methods of Soil Analysis, Part 2. Microbiological and Biochemical Properties, SSSA Book Series, no. 5. Soil Sci. Soc. Am., Madison, WI.

Sexstone, A.J., T.B. Parkin, and J.M. Tiedje. 1985. Temporal response of soil denitrification rates to rainfall and irrigation. Soil Sci. Soc. Am. J. 49:99-103.

Shjeflo, J. B. 1968. Evapotranspiration and the Water Budget of Prairie Potholes in North Dakota. Geological Survey Professional Paper 585-B. U.S. Department of the Interior. Washington.

Si, B.C. 2002. Spatial and statistical similarities of local soil water fluxes. Soil Sci. Soc. Am. J. 66:753-759.

Si, B.C. 2003. Scale and location dependent soil hydraulic properties in non-level landscapes. p. 163-178 *In* Y. Pachepski et al. (ed). Scaling in soil physics. CRC Press, Boca Raton, FL.

Si, B.C., and R.E. Farrell. 2004. Scale-dependent relationship between wheat yield and topographic indices: a wavelet approach. Soil Sci. Soc. Am. J. 68:577-587.

Si, B.C., and Zeleke. 2005. Wavelet coherency analysis to relate saturated hydraulic properties to soil physical properties. Water Resour. Res. Vol. 41, W11424, DOI; 10.1029 / 2005WR004118.

Skiba, U., K.A. Smith, and D. Fowler. 1993. Nitrification and denitrification as sources of nitric oxide and nitrous oxide in a sandy loam soil. Soil Biol. Biochem. 25:1527-1536.

Smith, W.N., R.L. Desjardins, B. Grant, C. Li, R. Lemke, P. Rochette, M.D. Corre, and D. Pennock. 2002. Testing the DNDC model using N_2O emissions at two experimental sites in Canada. Can. J. Soil Sci. 82:365-374.

Stanford, G., Vander Pol, R.A., and Stanislaw, D. 1975. Denitrification rates in relation to total and extractable soil carbon. Soil Sci. Soc. Am. J. 39:284-289.

Stevens, R.J., and R.J. Laughlin. 1998. Measurement of nitrous oxide and di-nitrogen emissions from agricultural soils. Nut. Cycl. Agroecosys. 52:131-139.

Tiedje, J.M. 1982. Denitrification. p. 1011-1026 *In* A.L. Page, R.H. Miller, and D.R. Keeney (ed). Methods of Soil Analysis, Part 2 Microbiological and Biochemical Properties, Agron. Monogr. no. 9. ASA-SSSA, Madison, WI.

Tiedje, J.M. 1988. Ecology of denitrification and dissimilatory nitrate reduction to ammonium. p 179-244 *In* A. J. B. Zehnder (ed). Biology of Anaerobic Microorganisms. John Wiley and Sons, Inc., Toronto, ON.

Tiedje, J.M. 1994. Denitrifiers. p. 245-267 *In* R.W. Weaver, J.S Angle, and D.S. Bottomley (ed). Methods of Soil Analysis, Part 2 Microbiological and Biochemical Properties, SSSA Book Series, no. 5. Soil Sci. Soc. Am.,Madison, WI.

Topp, G.C., and P.A. Ferre. 2002. The soil solution phase. p. 417-545 *In* J.H. Dane and G.C. Topp (ed). Methods of Soil Analysis Part 4 Physical Methods. SSSA Book Series, no 5. Soil Sci. Soc. Am., Madison, WI.

Torrence, T., and G.P. Compo. 1998. A practical guide to wavelet analysis. Bull. Am. Meteorol. Soc. 79:61-78.

Torrence, C. and P.J. Webster. 1999. Interdecadal changes in the ENSO-monsoon system. J. Climate. 12, 2679-2690.

Trangmar, B.B., R.S. Yost, and G. Uehara. 1985. Application of geostatistics to spatial studies of soil properties. Adv. Agron. 38:45-94.

van Bochove, E., D. Prevost, and F. Pelletier. 2000. Effects of freeze-thaw and soil structure on nitrous oxide produced in a clay soil. Soil Sci. Soc. Am. J. 64:1638-1643.

Van Cleemput, O., and W.H. Patrick, Jr. 1974. Nitrate and nitrite reduction in flooded gamma-irraditated soil under controlled pH and redox potential conditons. Soil Biol. Biochem. 6:85-88.

Van Cleemput, O., W.H. Patrick, Jr., and R.C. McIlhenny. 1976. Nitrite decomposition in flooded soil under different pH and redox potential conditions. Soil Sci. Soc. Am. J. 40:55-60.

van der Kamp, G., and M. Hayashi. 1998. The groundwater recharge function of small welands in the semi-arid northern prairies. Great Plains Res. 8:39-56.

van der Kamp, G., W.J. Stolte, and R.B. Clark. 1999. Drying out of small prairie wetlands after conversion of their catchments from cultivation to permanent brome grass. Hydrol. Sci. J. 44:387-397.

van der Kamp, G., M. Hayashi, and D. Gallen. 2002. Comparing the hydrology of grassed and cultivated catchments in the semi-arid Canadian Prairies. Hydrol. Process. 17:559-575.

Veldkamp, E., M. Keller, and M. Nunez. 1998. Effects of pasture management on N_2O and NO emissions from soils in the humid tropics of Costa Rica. Global Biogeochem. Cycles 12:71-79.

Veldkamp, E., and A.M. Weitz. 1994. Uncertainty analysis of δ^{13} C method in soil organic matter studies. Soil Biol. Biochem. 26:153-160.

Velthof, G.L., and J.W. van Groenigen, G. Gebauer, S. Pietrzak, S.C. Jarvis, M. Pinto, W. Corré, and O. Oenema. 2000. Temporal stability of spatial patterns of nitrous oxide fluxes from sloping grassland. J. Environ. Qual. 29:1397-1407.

Walley, F., and T. Yates, J.-W. van Groenigen, and C. van Kessel. 2002. Relationships between soil nitrogen availability indices, yield, and nitrogen accumulation in wheat. Soil Sci. Soc. Am. J. 66:1549-1561.

Whelan, M.J., and C. Gandolfi. 2002. Modelling of spatial controls on denitrification at the landscape scale. Hydrol. Proc. 16:1434-1450.

Williams, R.G.B. 1984. Introduction to statistics for geographers and earth scientists. Macmillan, London.

Wrage, N., G.L. Velthof, M.L. van Beusichem, and O. Oenema. 2001. Role of nitrifier denitrification in the production of nitrous oxide. Soil Biol. Biochem. 33:1723-1732

Yates, T.T, B.C. Si, R.E. Farrell, and D.J. Pennock. 2006a. Probability distribution and spatial dependence of nitrous oxide emission: temporal change in a hummocky terrain. Soil Sci. Soc. of Am. J. (in press).

Yates, T.T, B.C. Si, R.E. Farrell, and D.J. Pennock. 2006b. Wavelet spectra of nitrous oxide emission from hummocky terrain during spring snowmelt. Soil Sci. Soc. of Am. J. (in press).

Yoshida, T., and M. Alexander. 1970. Nitrous oxide formation by Nitrosomonas europaea and heterotrophic microorganisms. Soil Sci. Soc. Am. Proc. 34:880-882.

Yu, P., T.C. Yang, and S.J. Chen. 2001. Comparison of uncertainty analysis methods for a distributed rainfall-runoff model. J. Hydrol. 244:43-59.

Zebarth, B.J., E. de Jong, and J.L. Henry. 1989. Water flow in a hummocky landscape in central Saskatchewan, Canada, II. Saturated flow and groundwater recharge. J. Hydrol. 110:181-198.

APPENDIX A

Permission to publish and republish as given to the Soil Science Society of America for chapters 3.0 and 4.0.